PRESSURE-IMPULSE DIAGRAMS USING FINITE ELEMENT ANALYSIS FOR REINFORCED CONCRETE COLUMNS SUBJECTED TO BLAST LOADING

A THESIS IN
Civil Engineering

Submitted to the Faculty of the University of
Missouri-Kansas City in partial fulfillment of
the requirements for the degree of
MASTER OF SCIENCE

by

Rasekh Rahim Zadeh

University of Missouri-Kansas City

2011

PRESSURE-IMPULSE DIAGRAMS USING FINITE ELEMENT ANALYSIS FOR REINFORCED CONCRETE COLUMNS SUBJECTED TO BLAST LOADING

Rasekh Rahim Zadeh, Candidate for the Master of Science Degree,

University of Missouri- Kansas City

ABSTRACT

Reinforced concrete is one of the prime building materials widely used to construct protective structures. One of the purposes of this project is to study the non-linear response of reinforced concrete structures when subjected to impact and blast loading. The study is conducted at two levels: material level and structural level.

At the material level, the strength enhancement of three material models of LS-DYNA subjected to high strain rates is studied. The effects of strain rate and lateral inertial confinement on the strength enhancement are investigated. Recommendations are made to improve the accuracy of the results of future numerical simulations for reinforced concrete structures subjected to loads having high strain rates.

At the structural level, Pressure-Impulse diagrams for reinforced concrete columns that have four configurations of transverse reinforcement are developed. Finite element modeling in LS-DYNA is used to analyze the structures and calculate the damage level for each blast event.

The developed Pressure-Impulse diagrams are used to study the effect of confinement on the reduction of damage level at impulsive, dynamic, and quasi-static loading conditions.

APROVAL PAGE

The faculty listed below, appointed by the Dean of the School of Computing and Engineering have examined a thesis titled “Pressure-Impulse Diagrams Using Finite Element Analysis for Reinforced Concrete Columns Subjected to Blast Loading,” presented by Rasekh Rahim Zadeh, candidate for Master of Science in Civil Engineering, and certify that in their opinion it is worthy of acceptance.

Supervisory Committee

Ganesh Thiagarajan, Ph.D., P.E., Committee Chair
Department of Civil and Mechanical Engineering

Ceki Halmen, Ph.D.
Department of Civil and Mechanical Engineering

ZhiQiang Chen, PhD.
Department of Civil and Mechanical Engineering

TABLE OF CONTENTS

LIST OF ILLUSTRATIONS

Figure Page

LIST OF TABLES

Table Page

ACKNOWLEDGEMENTS

This is a great opportunity to express my deep and sincere gratitude to my advisor, Dr. Ganesh Thiagarajan, for his continuous guidance, support, and motivation during the last two years. I would also like to thank Dr. Ceki Halmen and Dr. Zhiqiang Chen for serving on the graduate committee.

I would like to mention my lab mates Dr. Yun Kai Lu, Anirudha Kadambi, Sampath Bhashyam, Jitesh Nalagotla, and Gunjan Shetye for the fun and memorable moments that we cherished together at the Computational Mechanics lab.

I owe my loving thanks to my parents, Mahmoud Rahim Zadeh and Kheironnesa Rahimi for their encouragement, patience, and understanding throughout my studies abroad. I would also like to thank my family members and friends for their loving support.

I gratefully acknowledge the financial support provided by the National Science Foundation through award Number 0748085.

CHAPTER 1

INTRODUCTION

The non-linear response of concrete when subjected to extreme dynamic loads such as blast and impact is an important consideration for analysis and design of protective structures. As a result of very rapid loading of structures during impact and blast loading, structural materials are subjected to very high strain rates. High strain rates causes enhancement in both compressive and tensile strength of structural materials in addition to change in the post yield behavior. This change in the response needs to be reproduced in the materials' constitutive models that have been developed or under development.

In the larger scale than the material level, the response of structural members of protective structures subjected to extreme shock waves experienced during an explosion needs to be calculated with high level of accuracy too. Pressure-impulse diagrams are a type of response spectra developed for structures subjected to blast loading. These diagrams are developed by combining the applied pressure and impulse associated with an explosion and the maximum structural response due to the explosion. They are iso-damage curves that give the damage level of a specific structure under a combined pressure and impulse condition. Since the structural response is needed to be calculated for the development of pressure-impulse diagrams, structural analysis by using finite element modeling can be utilized because of its power to take into account the nonlinear material behavior and the different modes of structural failure. Once the pressure-impulse diagrams are developed for different structural members, they are compared together and the most effective structural configuration that can better resist explosion waves can be selected.

1.1. Problem Statement

LS-DYNA, as a finite element program capable of performing non-linear dynamic analysis, has several material models for concrete that were developed by researchers for different applications. This software program is used extensively in research projects to simulate the blast loading of structures and the structural response. LS-DYNA has several constitutive models to represent concrete. Choosing the material model that generate the closest numerical results in respect to experimental results or calibrating material models requires understanding the response of these concrete material models when subjected to high strain rates.

The concrete strength enhancement at high rates of loading originates from two phenomena: strain rate and lateral inertia confinement which latter is a function of the size of structure. In concrete material models of LS-DYNA, the effect of strain rate can be controlled through a parameter included in the material models; however, the effect of the size of the structure on the strength enhancement cannot be controlled directly. In real structures, the effect of structure size on the strength enhancement can be significant. Thus, this question arises that how much strength enhancement is generated in large structures due to both the strain rate and the lateral inertia confinement effects. Another question is that should the strain rate effect be included in the simulations if the dynamic increase factors (DIF) proposed by design guidelines are to be followed.

No literature was found that studies the strength enhancement caused by the strain rate effect and the lateral inertia confinement while they are differentiated. As LS-DYNA has several concrete material models, a comparison between their responses to high rates of

loading can help in better selection of the model for future studies. Hence, three concrete material models of the library of LS-DYNA are selected to study the effect of high strain rate loading on their behavior.

Pressure-impulse diagrams provide a reliable method for evaluation of the response of a structural member subjected to different types of blast loading. The generation of pressure-impulse diagrams by simulating both the explosion and the structure in LS-DYNA requires the correct positioning of explosives with respect to the structure. In addition, it needs to study if making some changes like change in the ratio of transverse reinforcement can improve the structural behavior during blast loading, and if so, can pressure-impulse diagrams reflect the change. For these reasons, the development of pressure-impulse diagrams for four types of reinforced concrete columns was included in this research project.

1.2. Objective of the Study

This study has the following three objectives:

1) High rates of loading associated with impact and blast affects the non-linear response of reinforced concrete structures. This research specifically investigates the effect of strain rate and the size of structure on the strength enhancement of three material models of LS-DYNA that are widely used to model concrete. Understanding these effects will help to improve the constitutive material models or build new models which yield numerical results with high level of accuracy in respect to the experimental results.

2) The mesh size affects the accuracy of the results obtained from a finite element analysis. In this study the mesh sensitivity of three concrete material models of LS-DYNA subjected to three ranges of strain rate is investigated. The results help in selection of appropriate mesh size in respect to the strain rate associated with the loading.
3) This research studies the development of pressure-impulse diagrams for reinforced concrete columns by using finite element analysis. In addition, the effect of change in transverse reinforcement on the damage level of four types of columns is studied by comparing pressure-impulse diagrams.

1.3. Scope of the Study

In order to accomplish the objectives outlined above, the following tasks are performed:

1. Generate finite element model of three sizes of cylinders meshed into three element sizes
2. Apply boundary conditions to cylinders as velocity loads with various intensities of rate of loading
3. Exclusion of the strain rate effect from the three material models and study the effect of lateral inertia confinement
4. Determine the rates of loading at which the effect of lateral inertia confinement is significant
5. Inclusion of the strain rate effect and study the strength enhancement in the three material models due to the strain rate effect only

6. Inclusion of the strain rate effect in the simulations at which the effect of lateral inertia confinement is significant and study the combined effect of strain rate and the lateral inertia confinement
7. Subject the cylinders with different mesh sizes to a range of rates of loading and study the sensitivity of each material model to mesh size at different strain rates
8. Generate the finite element model of columns with four configurations of transverse reinforcement
9. Subject the columns to explosions with different standoff distances and charge weights or pressure loads and generate pressure-impulse diagrams by using the maximum structural response for a given applied pressure and impulse
10. Compare the pressure-impulse diagrams for four types of columns and study the effect of confinement on the reduction of damage level

1.4. Thesis Organization

This thesis is organized into the following three chapters:

- Chapter 2: Discusses the effect of strain rate and lateral inertia confinement on the strength enhancement of concrete cylinders made of three material models of LS-DYNA and subjected to high strain dynamic velocity loading.
- Chapter 3: Discusses the use of finite element analysis to develop pressure-impulse diagrams for reinforced concrete columns with four types of transverse reinforcement configuration.

- Chapter 4: Discusses the conclusions from the previous three chapters and presents recommendations for future research.

CHAPTER 2

EFFECT OF RATE OF LOADING ON THE STRENGTH ENHANCEMNT OF CONCRETE MATERIAL MODELS

During an explosion or an impact event, structural materials experience very high pressure shock waves in a very short period of time. This type of load event subjects the structural materials to very high rates of loading. The high rate of loading affects the response of structures to the dynamic loads compared to structural response when subjected to the similar static loads. Concrete as a visco-plastic structural material demonstrates strain-rate dependent characteristics. This behavior must be reproduced in the material models used to simulate concrete subjected to high rates of loadings.

LS-DYNA (LS-DYNA 2007) is a finite element software program which is used to simulate the response of structures to blast and impact loading. It contains several material models that can be used to represent concrete. In this research three different types of material models from LS-DYNA material library are used to investigate their response to dynamic loads with high rates of loading. The effect of strain rate, lateral inertia confinement, and mesh size are studied in this research.

2.1. Literature Review

Each loading condition has its unique rate of loading. The strain rate for structures subjected to creep is about $10^{-7} s^{-1}$. For quasi-static loading, the strain rate is approximately $10^{-5} s^{-1}$. During an earthquake, structures can be subjected to maximum rate

of $10^{-2}\,s^{-1}$. However, impact and blast loads subject structures to significant loads applied at a very short period of time which produces strain rates between 1 and $1000\,s^{-1}$ (Bischoff and Perry 1991). Hentz et al. (2004) also presents the following ranges of strain rates for different types of loading: 10^{-8} to 10^{-7} s^{-1} for creep, 10^{-6} to 10^{-5} s^{-1} for quasi-static loading, $10^{-4}$to 10^{-1} s^{-1} for vehicle and plane impact, 10 to 10^{2} s^{-1} for missile impact, 10^{-4} to 10^{1} s^{-1} for earthquake and induced shocks, and 10^{-2} to 10^{3} s^{-1} and higher for blast loading (Hentz et al. 2004).

The rate of loading has a significant influence on the response of visco-plastic structural materials including concrete. High rates of loading affect material properties including compressive and tensile strength, modulus of elasticity, ductility, and Poisson's ratio (Bischoff and Perry 1991) .

Based on the work performed by Curione (1958) and ASCE (1985) referenced in Bischoff and Perry (1991), the design compressive strength of concrete can increase about 25 to 30% percent during dynamic loading of concrete. Bischoff and Perry (1991) compiled the work of many researchers which showed that the compressive strength of concrete increases as much as 85 to 100 percent during impact loading. But there was a wide variation in results which increased as the strain rate increased (Bischoff and Perry 1991).

Ross et al. (1995) conducted both experimental and numerical studies on the effects of strain rate on concrete strength. Concrete specimens were initially tested in a standard material test machine at strain rates of approximately 10^{-7} to 10^{-3} s^{-1}. The lowest strain rate of 10^{-7} s^{-1} referred to as the static data was used as the basis for normalizing higher strain-rate data. Higher strain-rate tests from 1 to 1000 s^{-1} were conducted using Split Hopkinson Pressure Bar (SHPB) test. Concrete strength as the function of strain rate was determined

experimentally for both tension and compression. Based on their experiments, the concrete compressive strength enhancement was between 200 to 300 percent at strain rates between 100 to 1000 s^{-1} (Ross et al. 1995).

Grote et al. (1999) studied the effect of strain rate on the dynamic behavior of mortar at intermediate strain rates by using a series of SHPBs. The compressive strength of two mortar specimens was 44.8 and 47.3 MPa. The specimens were subjected to strain rates ranged from 250 to 1700 s^{-1}. Significant compressive strength enhancement was observed in the experiments. For instance, specimens subjected to strain rate of 250, 1000, and 1700 s^{-1} reached the maximum compressive strength of 75, 110, and 180 MPa respectively. This strength enhancement shows an increase of 63, 139, and 291 percent for the mentioned strain rates respectively (Grote et al. 2001).

The rate of loading affects the response of concrete to dynamic loading. As concrete is a heterogeneous material with inherent microcracks, discontinuities and voids that are initially present in the material, its behavior during static uniaxial loading is affected by the propagation of internal microcracks, which are tensile in nature and primarily oriented in the axial direction. During rapid loading, the time available for microcrack development or propagation is reduced. Hence, the strain rate dependent behavior of microcracking can influence the response when concrete is subjected to the very high rates of loading that occur during impact (Bischoff and Perry 1991).

In analysis and design of blast resistant structures, materials' strength enhancement due to rate of loading is taken into account by using Dynamic Increase factor (DIF) which is the ratio of dynamic to static strength. According to Malvar and Crawford (1998), DIF

depends on the strain rate and is calculated using equations based on Comite' Euro-International du Beton:

$$DIF = \frac{f'_{cd}}{f'_{cs}} = \left(\frac{\dot{\varepsilon}_d}{\dot{\varepsilon}_s} \right)^{1.026\alpha_s} \quad \text{for} \left| \dot{\varepsilon}_d \right| \le 30 s^{-1}$$

$$DIF = \frac{f'_{cd}}{f'_{cs}} = \gamma_s \left(\frac{\dot{\varepsilon}_d}{\dot{\varepsilon}_s} \right)^{1/3} \quad \text{for} \left| \dot{\varepsilon}_d \right| > 30 s^{-1}$$

$$\text{Where } \alpha_s = \frac{1}{5 + 9\frac{f'_{cs}}{f'_0}} \qquad \text{and} \qquad \log \gamma_s = 6.156\alpha_s - 2$$

In the above equations, f'_{cs} is the quasi-static unconfined compressive strength, f'_{cd} is the dynamic unconfined compressive strength, f'_0=10MPa, $\dot{\varepsilon}_d$ is the strain rate, and $\dot{\varepsilon}_s = 30 \times 10^{-6} s^{-1}$ (Malvar and Crawford 1998).

The strength enhancement in concrete due to rate of loading occurs as a result of two phenomena: strain rate effect, and lateral inertia confinement.

Rossi (1997) explains the physical mechanism involved in strain rate effects in concrete. The physical mechanism called Stefan Effect occurs when a thin film of a viscous liquid is trapped between two perfectly plane plates that are moved apart at a displacement

rate $\dot{h}$, the film exerts a return force on the plates that is proportional to the velocity of separation. This mechanism is reflected in this equation:

$$F = \frac{3\eta V^2}{2\pi h^5}.\dot{h}$$

Where F is the return force, η is the velocity of the liquid, h is the initial distance between the two plates, $\dot{h}$ is the velocity of separation of the two plates, and V is the volume of the liquid.

The presence of water in the concrete pores underlies a mechanism of this type when the solid matrix, which is regarded as a network of plates, is subjected to tensile strain. When the loading rate is increased in a uniaxial tensile test, the Stefan effect delays the creation of microcracks, and the propagation of the initial microcracks. Thus, the Stefan effect delays the localization of microcracks. After the localization, the Stefan Effect tends to oppose the propagation of the macrocracks (Rossi 1997).

Lateral inertia confinement also affects the strength enhancement of concrete at high rates of loading. According to Bischoff and Perry (1991), an elastic material loaded in compression will expand in the transverse direction as a result of Poisson's ratio effect. However, a cylinder loaded rapidly in the axial direction will not be able to expand instantaneously in the lateral direction because of inertial restraint, causing it to be initially in a state of uniaxial strain with corresponding lateral stresses that will act as a form of confinement (Bischoff and Perry 1991). As concrete is sensitive to lateral confining pressure, even a small lateral confining pressure of 10 percent of the uniaxial compressive strength, can cause a 50 percent increase in the failure strength (Kotsovos 1987). Since the lateral unloading velocity of brittle failure is considerably less than the axial elastic wave

velocity, unloading could be sufficiently delayed for the increased compressive strength of the confined central core. Thus, due to insufficient unloading time, a cylindrical specimen will have a greater load-carrying capacity and thus an apparent strain-rate effect due to the inertia forces (Bischoff and Perry 1991). The inertia forces have the consequence of opposing both the onset of microcracks and their propagation, thereby delaying microcrack localization. Inertia also acts after the stage of crack localization, opposing the propagation of the macrocracks.(Rossi 1997)

The rate of loading at which the lateral inertia confinement effect becomes significant is different from the rate of loading at which the strain rate effect causes strength enhancement. Even though the two effects act simultaneously, the Stefan effect and inertia forces are activated with different intensities according to the loading rate imposed on the specimen. For strain rates less than or equal $1s^{-1}$, an increase in material strength is related to viscous phenomena due to the presence of free water in the nanopores of concrete hydrates. For strain rates equal to or greater than 10 s^{-1}, inertia forces are mainly responsible for increasing strength (Rossi 1997). Malvern et al.(1985) also conducted compression tests on concrete by using SHPB test and concluded that the inertial confinement is negligible for strain rates less than $100s^{-1}$ (Malvern et al. 1985).

2.2. Methods and Materials

2.2.1. Material Models

LS-DYNA is a finite element modeling software which contains several material models that can be used to represent concrete. The material models are material Type 5 (soil and crushable foam), material Type 14 (soil and crushable foam failure), material Type 16 (pseudo tensor), material Type 25 (geological cap model), material Type 72R3 (concrete damage REL3), material Type 84 (Winfrith Concrete), and material Type 96 (brittle damage) (Bao and Li 2010). Another material model which can be used is material Type 159 (continuous surface cap model). (Yaramada 2010).

Based on the work done by Yaramada (2010), three material models are selected from the library of LS-DYNA in order to study the response of concrete to high rates of loading. They are material Type 159 (Continuous Surface Cap Model, CSCM), material Type 84 (Winfrith Concrete), and material Type 72R3 (Concrete Damage REL3).

Material type 159 (continuous surface cap model) was developed to predict the dynamic performance—both elastic deformation and failure—of concrete used in safety structures when involved in a collision with a motor vehicle (Murray et al. 2007). This model is a cap model with a smooth or continuous intersection between the failure surface and the hardening cap. This surface uses a multiplicative formulation to combine the shear surface with the hardening compaction surface smoothly and continuously. The smooth intersection eliminates the numerical complexity of treating a compressive corner region between the failure surface and the cap. This type of model is often referred to as a smooth cap model or as a continuous surface cap model (Murray 2007). The continuous surface cap

model is available for solid elements in LS-DYNA. The user has the option of inputting the user-defined material properties, or requesting default material properties for normal strength concrete (LS-DYNA 2007).

In this research, the following material parameters are introduced to LS-DYNA to generate default material properties for normal weight concrete. The modeled concrete has the unconfined compressive strength of 46 MPa, maximum aggregate size of 19mm, and mass density of $2.21\times10^{-9}\frac{Mg}{mm^3}$. The erosion parameter was set to 1.1 in order for the material to erode when the maximum principal strain of concrete exceeds 0.1.

For CSCM material model, LS-DYNA provides a parameter called IRATE to either initiate or cancel the strain rate effects. By setting the IRATE parameter to 1, strain rate effects are considered in the simulations, while setting the parameter to 0 cancels the strain rate effects.

Material Type 84 (Winfrith Concrete) which includes rate effects is a smeared crack (sometimes known as pseudo crack), smeared rebar model, implemented in the 8-node single integration point continuum element. This model was developed by Broadhouse and Neilson and Broadhouse over many years and has been validated against experiments (LS-DYNA 2007).

For this research, the mass density is set to $2.32\times10^{-9}\frac{Mg}{mm^3}$, the initial tangent modulus of concrete to 31,877 MPa, the Poisson's ratio to 0.2, and the uniaxial compressive and tensile strength are set to 46 and 4.75 MPa respectively. In addition, the maximum radius of aggregates is 9.5 mm and the fracture energy (energy per unit area dissipated in opening crack) which is read from the output of CSCM Concrete models is $0.0922\frac{N.mm}{mm^2}$.

The strain rate effect is incorporated in the Winfrith Concrete model through a parameter called RATE. The strain rate effect is included in the material model if the RATE parameter is set to zero, and it is excluded if the RATE parameter is set to one.

Material Type 72R3 (Concrete Damage REL3) (LS-DYNA 2007) is a three-invariant model, uses three shear failure surfaces, includes damage and strain-rate effects, and has origin based on the Pseudo-Tensor Model (Material Type 16). The most significant user improvement by Release III is a model parameter generation capability, based solely on the unconfined compression strength of the concrete (LS-DYNA 2007). This material model consists of three shear failure surfaces: the initial yield surface, the maximum yield surface, and the residual yield surface. During initial loading, the deviatoric stresses are elastic until the initial yield surface is reached. Then, the stresses can increase further until they reach the maximum yield surface. Beyond the maximum yield surface, the response can soften to the residual surface or be perfectly plastic (Malvar et al. 1997).

For this research, the mass density of concrete is set to $2.32\times10^{-9}\,\frac{Mg}{mm^3}$, the Poisson's ratio to 0.2, the uniaxial compressive and tensile strength to 45.4 MPa and 4.75 MPa respectively, and the maximum aggregate size to 19 mm. Since simulations are done with both IRATE effects off and on, the value of the compressive strength for this material is selected as 45.4 MPa in order to allow the usage of the effective strain rates published in LS-DYNA Keyword Manual.

The Concrete Damage REL 3 material model provides no direct way to turn the strain rate effect on or off. Instead, user should define and include the strength enhancement versus strain rate curve in the program. To consider the effect of the strain rate on the simulations, the LS-DYNA's predefined strength enhancement curve for concrete with

unconfined compressive strength of 45.4 MPa is used (LS-DYNA 2007). To cancel the strain rate effect, all the enhancement factors are set to 1 in the defined curve. Tables 2-1 and 2-.2 shows the curves used for the simulations.

Table 2-1 Tensile strength enhancement versus strain rate for Concrete Damage REL3 (LS-DYNA 2007)

Strain Rate (1/sec)	-3.E+04	-3.E+02	-1.E+02	-3.E+01	-1.E+01	-3.E+00	-1.E+00	-1.E-01	-1.E-02	-1.E-03	-1.E-04	-1.E-05	0.E+00
Strength Enhancement	9.7	9.7	6.72	4.5	3.12	2.09	1.45	1.36	1.28	1.2	1.13	1.06	1

Table 2-2 Compressive strength enhancement versus strain rate for Concrete Damage REL3 (LS-DYNA 2007)

Strain Rate (1/sec)	0.E+00	3.E-05	1.E-04	1.E-03	1.E-02	1.E-01	1.E+00	3.E+00	1.E+01	3.E+01	1.E+02	3.E+02	3.E+04
Strength Enhancement	1	1	1.03	1.08	1.14	1.2	1.26	1.29	1.33	1.36	2.04	2.94	2.94

2.2.2. Model Size

Lateral inertial confinement is one of the causes of the strength enhancement at high rates of loading which is studied in this research. Lateral inertia confinement is a function of both strain rate and the size of the specimens. To study the effect of the specimen size on the lateral inertia confinement and subsequently on the response of concrete material models, three different sizes of cylinder are selected for the simulation: 1) 101.6 x 203.2 mm (4 x 8 in.) 2) 203.2 x 406.4 mm (8 x 16 in.) 3) 406.4 x 812.8 mm (16 x 32 in.). Figure 2-1 illustrates the three cylinder sizes.

2.2.3. Mesh Size

Cylinders are modeled and meshed using constant stress 8 node hexahedron solid elements. Based on the dimension of the cylinders, three different mesh sizes are selected: coarse mesh size with a mesh seed dimension of 25.4 mm (1 in.), medium mesh size with seed dimension of 12.7 mm (1/2 in.) , and fine mesh size with seed dimension of 6.35 mm (1/4 in.). The responses of 101.6 x 203.2 mm (4 x 8 in.) cylinders are studied by using all the three different mesh sizes. For the 203.2 x 406.4 mm (8 x 16 in.) cylinders, both coarse and medium mesh sizes are used while for the 406.4 x 812.8 mm (16 x 32 in.) cylinders, only the coarse mesh size is utilized in order to keep the problem size manageable.

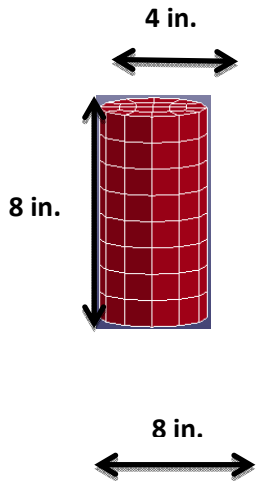

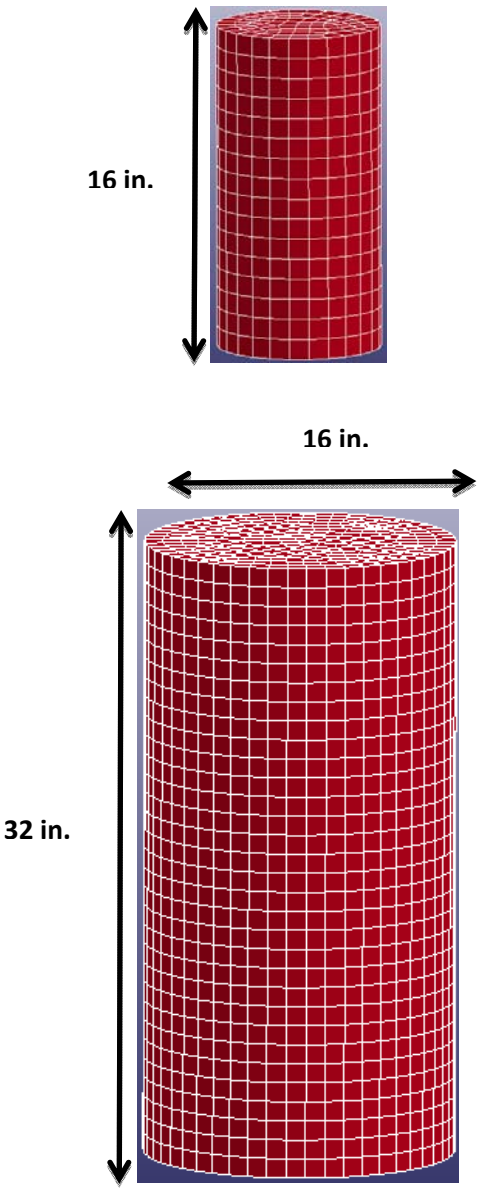

Figure 2-1: Three sizes of cylinders with coarse mesh size

2.2.4. Boundary Condition and Loads

The bottom and top nodes of the cylinders are restrained against translation in all directions except for the top nodes which are released to have translation in the direction of the applied load. The applied restraint will create a fixed condition at both sides of the

cylinders because all the nodes are restrained for translation. Although solid elements do not have rotational degrees of freedom, restraining translation for all the nodes at each side simulates a fixed support condition.

Concrete models are subjected to five dynamic compressive velocity loads with the following rates of loading: 0.0125, 1, 5, 10, 100, and 200 s^{-1}. The wide range of rate of loading values covers the loading rates occur during earthquake, impact and blast. It allows studying and differentiating the effect of strain rate and lateral inertia confinement. Table 2-3 presents the dynamic velocity loads associated with each simulation. The boundary condition and loading are illustrated in Figure 2-2.

Table 2-3 Velocity loads in mm/sec associated with each loading condition and model size

		Cylinder Size (mm)		
		101.6 x 203.2 mm (4 x 8 in.)	203.2 x 406.4 mm (8 x 16 in.)	406.4 x 812.8 mm (16 x 32 in.)
Loading Rate (s^{-1})	**0.0125**	2.54	5.08	No Simulations
	1	203.2	406.4	812.8
	5	1016	2032	No Simulations
	10	2032	4064	8128
	100	20320	40640	81280
	200	40640	81280	162560

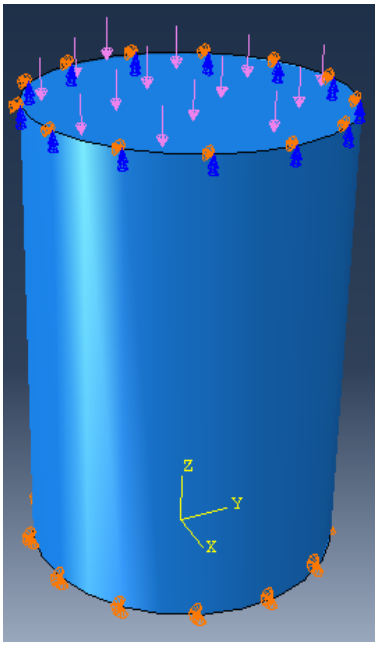

Figure 2-2: Boundary condition and loading of cylinders

2.2.5 Stress-Strain Calculation Procedure

Various elements within a model respond differently to the dynamic load. To have a stress-strain curves which better represents the whole model, the response of all the elements at the mid-height plain of the cylinder is considered for reporting the stress and strain values. By using the Section Force function of LS-DYNA and by introducing the nodes and elements at the mid-height section, the total force and displacement of the section is calculated. The engineering stress is then calculated by dividing the force by the area of the initial cross section. The strain is also quantified as the displacement of the mid-height section divided by the half height of the cylinders. Finally, the stress-strain curves are drawn using these values.

2.3. Effect of Structure Size and Lateral Inertia Confinement on the Response of Concrete Material Models

Lateral inertia confinement is a function of both the rate of loading and the structure size. The threshold at which the effect of lateral inertia confinement significantly affects the material response is at loading with the rate of 100 s^{-1} (Malvern et al. 1985).

In order to study the effect of lateral inertia confinement at high rates of loading and its relationships with the rate of loading and the model size, all the three sizes of cylinder models are subjected to strain loads in the range of 1 to 200 s^{-1}. As mentioned earlier, all the material models have the capability to include or exclude the effects of strain rate on the non-linear response of concrete. In order to differentiate between the effects of strain rate and lateral inertia confinement on the strength enhancement, the strain rate effect is excluded from the simulations by the means explained at the material definition part. This exclusion provides a means to study the lateral inertia confinement independently.

2.3.1. Effect of Lateral Inertia Confinement on the Response of Structures Using Material Model Type 159 (CSCM Concrete)

Cylinder of sizes 101.6 x 203.2 mm (4 x 8 in.), 203.2 x 406.4 mm (8 x 16 in.), and 406.4 x 812.8 mm (16 x 32 in.) modeled with the Continuous Surface Cap Model are subjected to loading rates of 1, 10, 100, and 200 s^{-1}. The IRATE parameter of the material model is set to zero which denotes the exclusion of the strain rate effects from the simulations. As observed from Figures 2-2 through 2-5, there is almost no increase in the strength of the models subjected to strain rates of 1, and 10 s^{-1} as a result of the lateral inertia

confinement because the models can just reach the unconfined strength of concrete (46 MPa). However, for rates of loading of 100 and 200 s^{-1}, the compressive strength of concrete significantly increases.

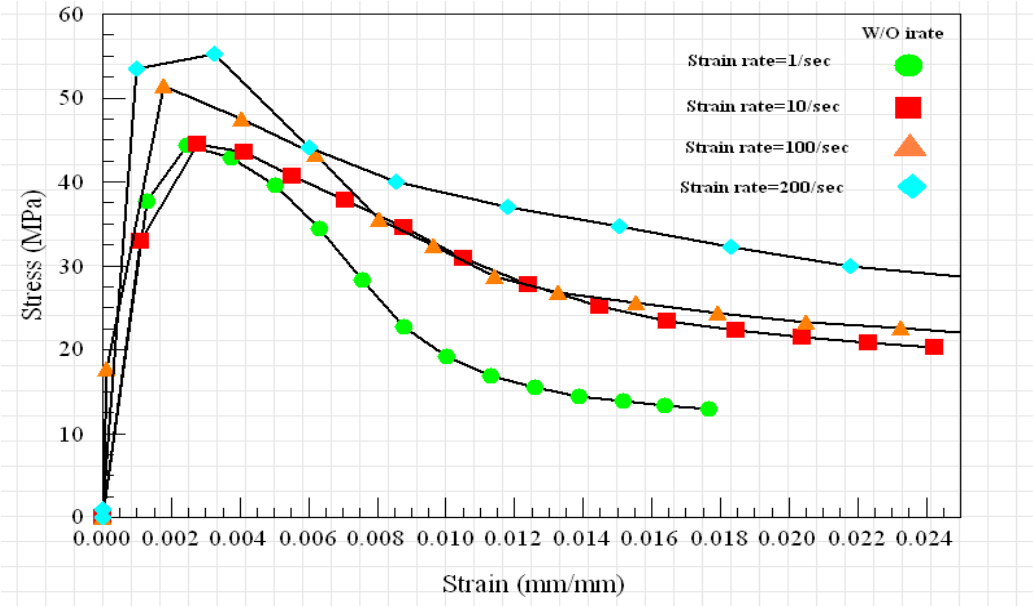

Figure 2-3: Effect of lateral inertia confinement on the response of 101.6 x 203.2 mm (4 x 8 in.) CSCM concrete cylinder models

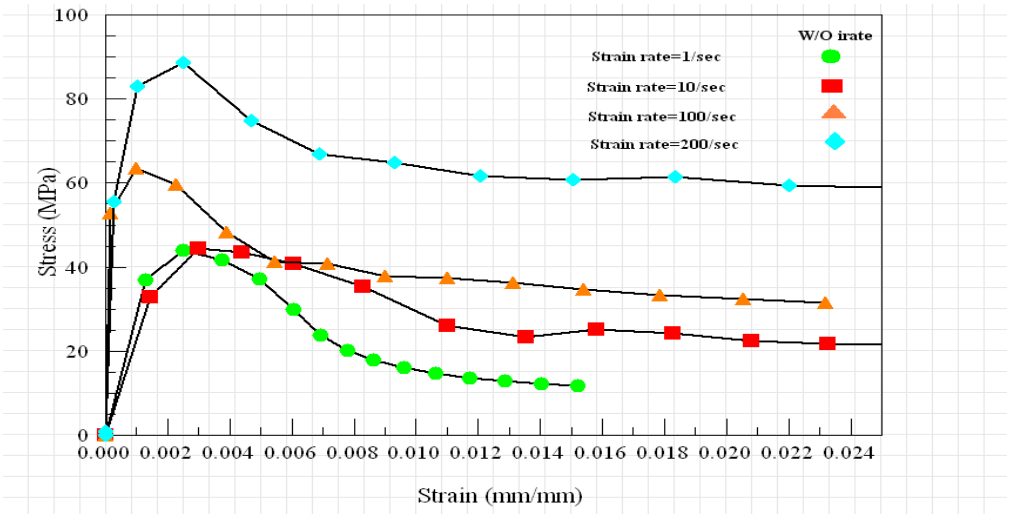

Figure 2-4: Effect of lateral inertia confinement on the response of 203.2 x 406.4 mm (8 x 16 in.) CSCM concrete cylinder models

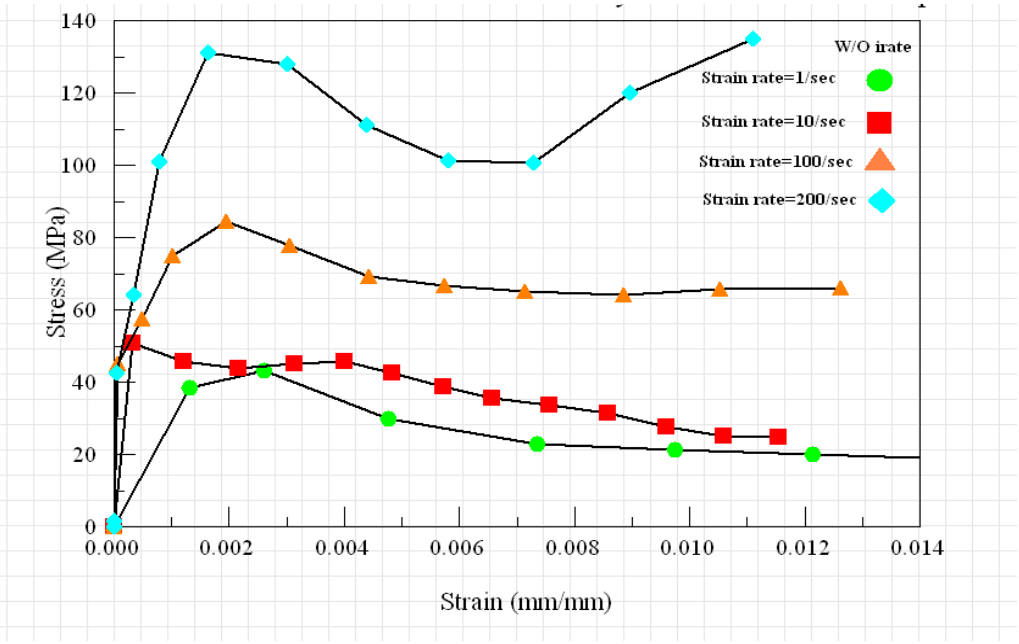

Figure 2-5: Effect of lateral inertia confinement on the response of 406.4 x 812.8 mm (16 x 32 in.) CSCM concrete cylinder models

As seen in Figures 2-3 through 2-5 and Table 2-4, concrete models made of CSCM concrete material model, when subjected to higher strain rates demonstrate higher values for the compressive strength. For instance, as the loading rate increases from 100 to 200 s^{-1}, the strength of 203.2 x 406.4 mm (8 x 16 in.) cylinder models made of 46 MPa concrete increases to 63.5 and 88.7 MPa. This represents the strength enhancement of 38% to 93% for 100 and 200 s^{-1} strain rates respectively.

In addition to the effect of loading rate on the lateral inertia confinement, the size of the structure greatly influences the strength of the models at higher rates of loading. From Table 2-4, it is observed that the strength enhancement is higher as the size of the cylinder increases. For example, while 101.6 x 203.2 mm (4 x 8 in.) cylinder shows only 20% strength enhancement at the strain rate of 200 s^{-1}, the strength enhancement is 93% and

178% for 203.2 x 406.4 mm (8 x 16 in.) and 406.4 x 812.8 mm (16 x 32 in.) cylinders respectively.

Table 2-4 Effect of rate of loading and model size on the lateral inertia confinement effect for CSCM material models

Material Type 159 (CSCM)						
	101.6 x 203.2 mm (4 x 8 in.) Cylinders		203.2 x 406.4 mm (8 x 16 in.) Cylinders		406.4 x 812.8 mm (16 x 32 in.) Cylinders	
Strain Rate (1/sec)	Peak Stress (MPa)	% Increase	Peak Stress (MPa)	% Increase	Peak Stress (MPa)	% Increase
100	51.5	12%	63.5	38%	84.5	84%
200	55.2	20%	88.7	93%	128	178%

2.3.2. Effect of Lateral Inertia Confinement on the Response of Structures Using Material Model Type 84 (Winfrith Concrete)

Concrete Cylinders of sizes 101.6 x 203.2 mm (4 x 8 in.), 203.2 x 406.4 mm (8 x 16 in.), and 406.4 x 812.8 mm (16 x 32 in.) modeled with Winfrith Concrete material model are subjected to loading rates of 1, 10, 100, and 200 s^{-1}. The strain rate effects are excluded from simulations by setting the IRATE parameter of the material model to one. As observed from Figures 2-6 through 2-8, similar to the CSCM models, there is almost no strength enhancement in the 46 MPa-Concrete structures subjected to strain rates of 1, and 10 s^{-1} as a result of the lateral inertia confinement. However, the effect of inertial confinement is noticeable at 100 and 200 s^{-1} rates of loading.

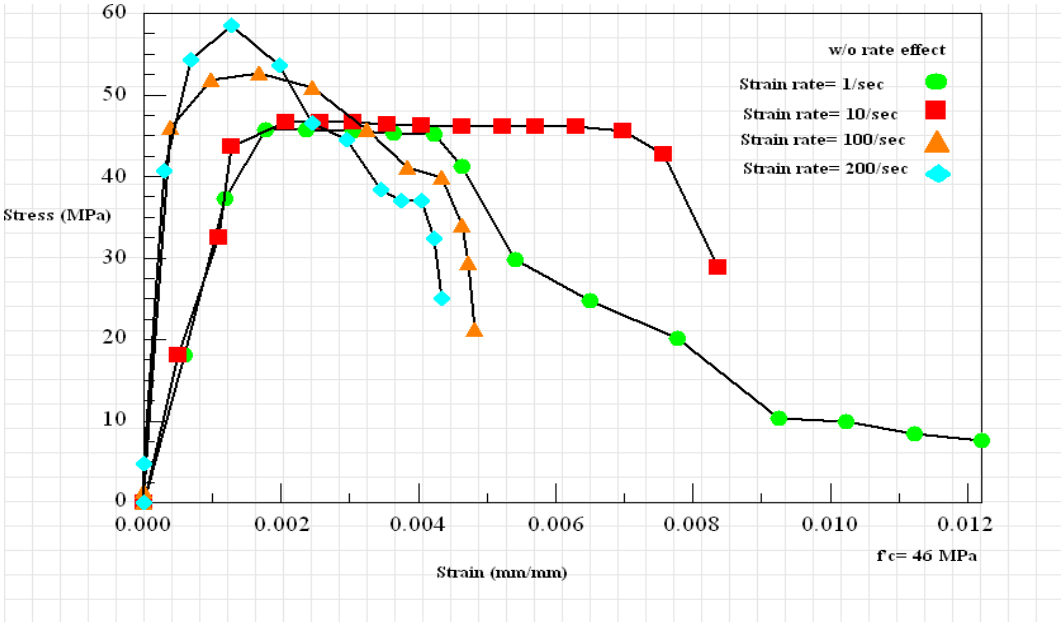

Figure 2-6: Effect of lateral inertia confinement on the response of 101.6 x 203.2 mm (4 x 8 in.) Winfrith Concrete cylinder models

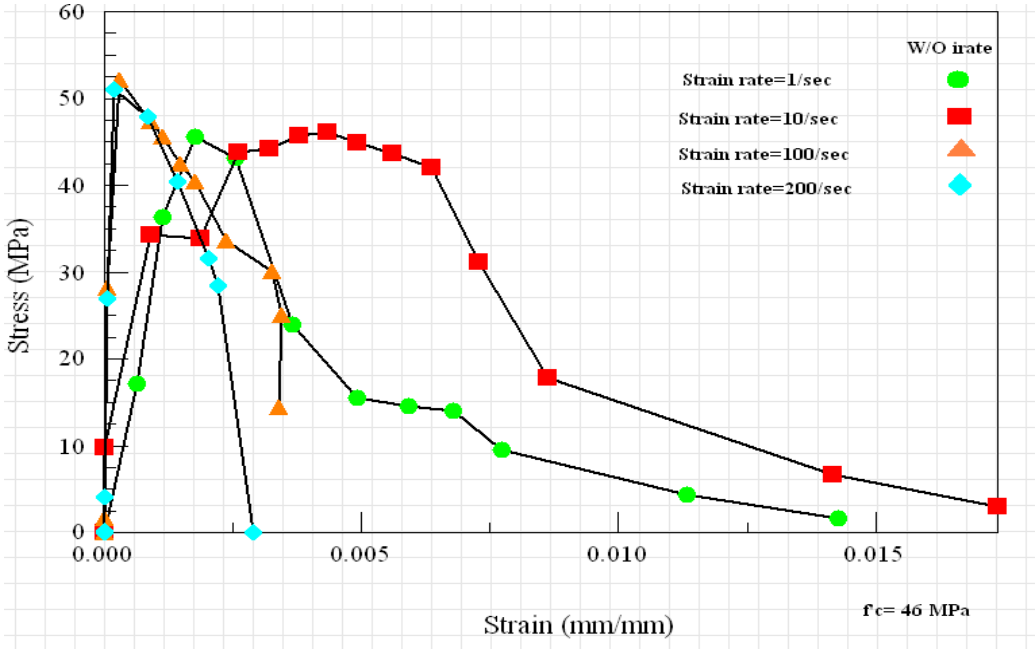

Figure 2-7: Effect of lateral inertia confinement on the response of 203.2 x 406.4 mm (8 x 16 in.) Winfrith Concrete cylinder models

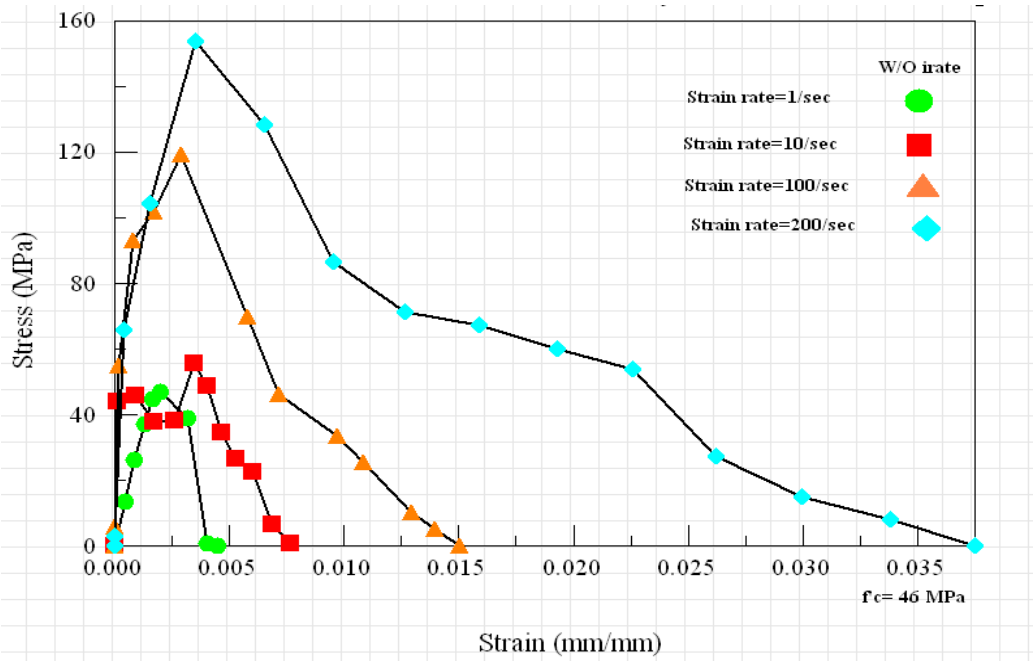

Figure 2-8: Effect of lateral inertia confinement on the response of 406.4 x 812.8 mm (16 x 32 in.) Winfrith Concrete cylinder models

At high rates of loading of 100 and 200 s^{-1}, significant increase occurs in the strength of the material as a result of the lateral inertia confinement. This trend is observable for both101.6 x 203.2 mm (4 x 8 in.) and 406.4 x 812.8 mm (16 x 32 in.) model sizes made of the Winfrith Concrete material model except for the $8in \times 16in$ cylinders.

The effect of the structure size on the lateral inertia confinement is also noticeable. As seen in Table 2-5, 101.6 x 203.2 mm (4 x 8 in.) cylinder shows only 27% increase in strength at the loading rate of 200 s^{-1}, while the 406.4 x 812.8 mm (16 x 32 in.) cylinders show 235% increase in the strength at the same loading rate.

Table 2-5 Effect of strain rate and model size on the lateral inertia confinement effect for Winfrith Concrete material models

Material Type 84 (Winfrith Concrete)						
	101.6 x 203.2 mm (4 x 8 in.) Cylinders		203.2 x 406.4 mm (8 x 16 in.) Cylinders		406.4 x 812.8 mm (16 x 32 in.) Cylinders	
Strain Rate (1/sec)	Peak Stress (MPa)	% Increase	Peak Stress (MPa)	% Increase	Peak Stress (MPa)	% Increase
100	52.7	15%	52.1	13%	119.1	159%
200	58.5	27%	51	11%	153.9	235%

2.3.3. Effect of Lateral Inertia Confinement on the Response of Structures Using Material Model Type 72R3 (Concrete Damage REL3)

Concrete cylinders of sizes 101.6 x 203.2 mm (4 x 8 in.), 203.2 x 406.4 mm (8 x 16 in.), and 406.4 x 812.8 mm (16 x 32 in.) modeled with Concrete Damage Rel3 material model are subjected to loading rates of 1, 10, 100, and 200 s^{-1}. The strain rate effects are excluded from simulations by equating all the coefficients in the strength enhancement versus strain rate curve to 1.0. As observed in Figures 2-9 through 2-11, similar to the CSCM and Winfrith Concrete models, there is almost no strength enhancement in the 45.4 MPa-Concrete structures subjected to strain rates of 1, and 10 s^{-1} as a result of the lateral inertia confinement. However, noticeable strength enhancement is observed at 100 and 200 s^{-1} rates of loading.

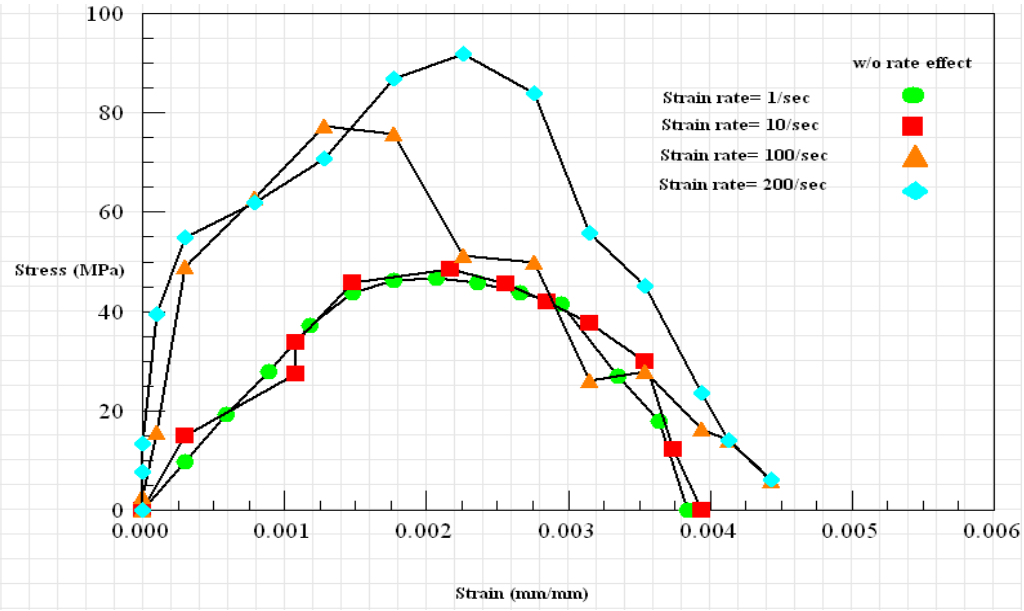

Figure 2-9: Effect of lateral inertia confinement on the response of 101.6 x 203.2 mm (4 x 8 in.) Concrete Damage REL 3 cylinder models

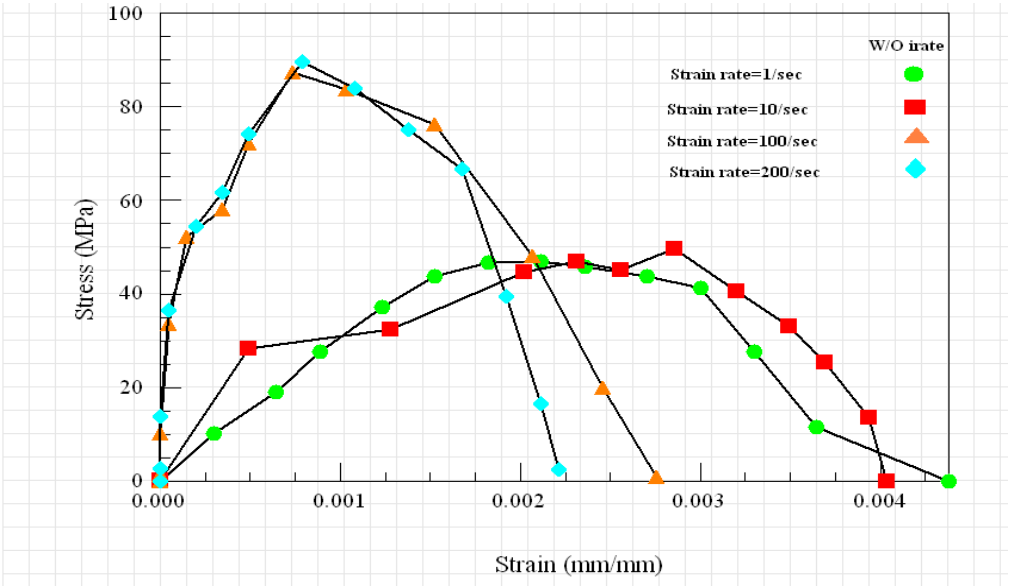

Figure 2-10: Effect of lateral inertia confinement on the response of 203.2 x 406.4 mm (8 x 16 in.) Concrete Damage REL 3 cylinder models

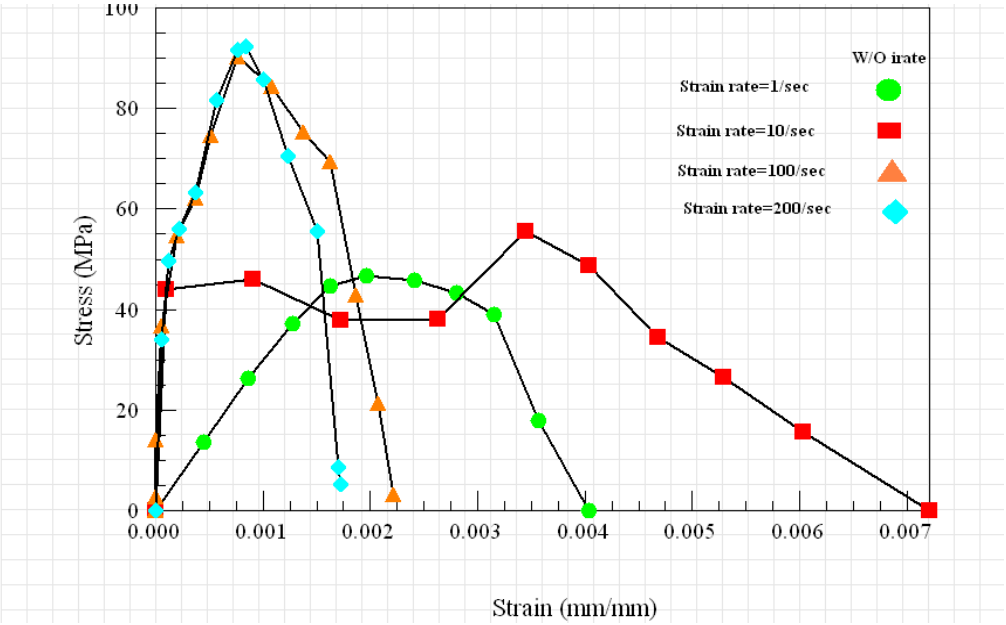

Figure 2-11: Effect of lateral inertia confinement on the response of 406.4 x 812.8 mm (16 x 32 in.) Concrete Damage REL 3 cylinder models

Although 101.6 x 203.2 mm (4 x 8 in.) cylinders show strength enhancement as the rate of loading increases from 100 to 200s^{-1}, no significant strength enhancement is observed for 203.2 x 406.4 mm (8 x 16 in.) and 406.4 x 812.8 mm (16 x 32 in.) cylinders as a result of increase in the rate of loading.

The effect of the model size on the lateral inertia confinement is also different for material Type 72R3 from the two previous material models. As observed from Table 2-6, the rise in the strength of the material as a result of an increase in the model size is not significant. For instance, for 101.6 x 203.2 mm (4 x 8 in.) cylinders subjected to dynamic load with strain rate of 200 s^{-1}, the strength is 91.9 MPa, and as the size increases to 406.4 x 812.8 mm (16 x 32 in.), the compressive strength reaches 101 MPa. So the effect of model size on the lateral inertia confinement and subsequently on the strength enhancement of concrete is not significant for material Type 72R3.

Table 2-6 Effect of strain rate and model size on the lateral inertia confinement effect for Concrete Damage REL3 material models

Material Type 72R3 (Concrete Damage REL3)						
Strain Rate (1/sec)	101.6 x 203.2 mm (4 x 8 in.) Cylinders		203.2 x 406.4 mm (8 x 16 in.) Cylinders		406.4 x 812.8 mm (16 x 32 in.) Cylinders	
	Peak Stress (MPa)	% Increase	Peak Stress (MPa)	% Increase	Peak Stress (MPa)	% Increase
100	77.4	68%	89.7	95%	90.2	96%
200	91.9	100%	87.3	90%	92.4	101%

2.4. Effect of Strain Rate on the Response of Concrete Material Models

In the study of the lateral inertia confinement effect in the previous section, the strain rate effect was excluded from simulations. In this part, the effect of strain rate is studied by turning on the strain rate parameters of the material models. According to the results of the previous section, the lateral inertia confinement effect does not have any significant effect on the strength enhancement of concrete models when the loading rate is 10 s^{-1} or lower. Therefore, the response of concrete is studied for the loading rates of 0.0125, 1, and 5 s^{-1} in order to exclude the effect of lateral inertia confinement.

2.4.1. Effect of Strain Rate on the Response of Structures Using Material Model Type 159 (CSCM Concrete)

For strain rates of 0.0125, 1, and 5 s^{-1}, the simulations are done with both the strain rate effect off and on conditions. When the strain rate effect is excluded, as seen in Figures 2-12 and 2-13, the strength of all the models with different rates of loading is the same and is about the unconfined strength of concrete (46 MPa). However, with inclusion of the strain rate effect in the simulations, the models demonstrate strength enhancement which increases as the rate of loading increases. For instance, for 101.6 x 203.2 mm (4 x 8 in.) cylinders, the inclusion of strain rate effect in the simulations causes the compressive strength to rise to 51.1, 63.5, and 74.1 MPa as the rate of loading rises to 0.0125, 1, and 5s^{-1} respectively.

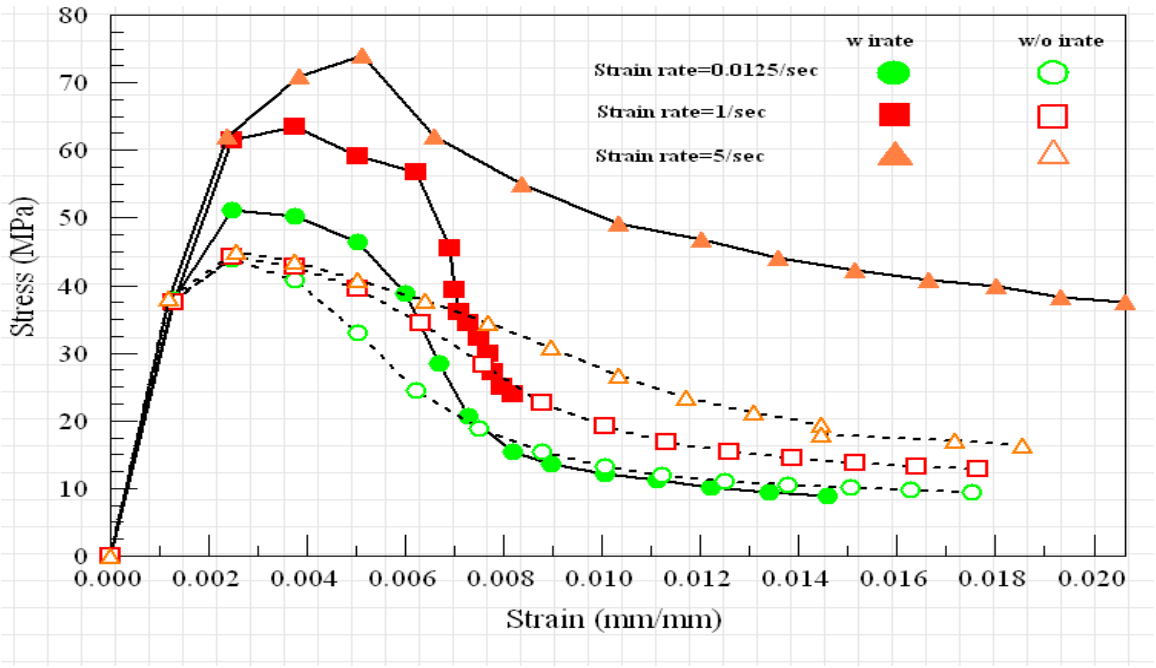

Figure 2-12: Effect of strain rate on the response of 101.6 x 203.2 mm (4 x 8 in.) CSCM concrete cylinder models

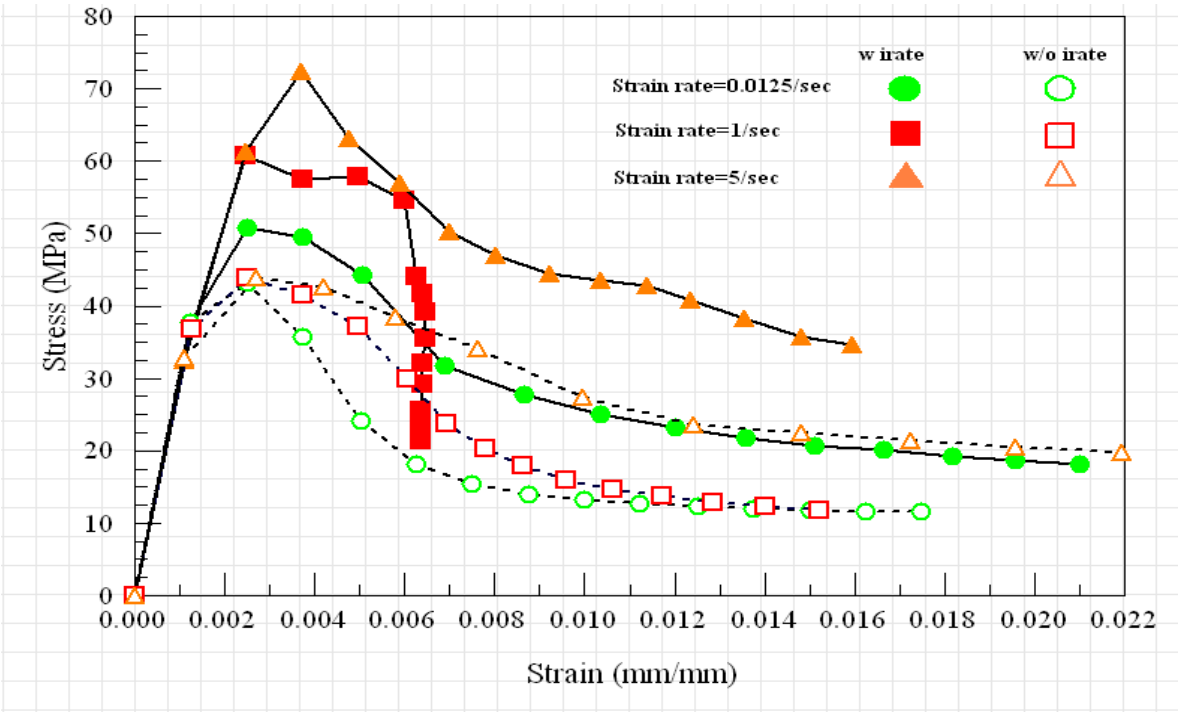

Figure 2-13: Effect of strain rate on the response of 203.2 x 406.4 mm (8 x 16 in.) CSCM concrete cylinder models

A comparison of the response of 101.6 x 203.2 mm (4 x 8 in.) and 203.2 x 406.4 mm (8 x 16 in.) cylinders as presented in Table 2-7 indicates that the size of model has no significant effect on the strength enhancement due to the strain rate effect. For 203.2 x 406.4 mm (8 x 16 in.) cylinders, the compressive strength rises to 50.8, 60.8, and 72.4 MPa for loading rates of 0.0125, 1, and $5s^{-1}$ respectively. These values are very close to strength enhancement in 101.6 x 203.2 mm (4 x 8 in.) cylinders for the similar rates of loadings.

Table 2-7 Effect of strain rate on the response of 101.6 x 203.2 mm (4 x 8 in.) and 203.2 x 406.4 mm (8 x 16 in.) models made of CSCM Concrete material model

Strain Rate (1/Sec)	101.6 x 203.2 mm (4 x 8 in.) Cylinders		203.2 x 406.4 mm (8 x 16 in.) Cylinders	
	Peak Stress (MPa)	% Increase	Peak Stress (MPa)	% Increase
0.0125	51.1	11%	50.8	10%
1	63.5	38%	60.8	32%
5	74.1	61%	72.4	57%

2.4.2. Effect of Strain Rate on the Response of Structures Using Material Model Type 84 (Winfrith Concrete)

To study the effect of strain rate on the strength enhancement of the models made of Winfrith Concrete, cylinders are subjected to velocity loads with 0.0125, 1 and 5 s^{-1} rate of loading. These rates of loading were selected because Winfrith Concrete material model did not show any strength enhancement due to the lateral inertia confinement effect for the rates of loading less than $10s^{-1}$. Using these rates of loading, the strain rate effect can be studied independently.

As observed from Figures 2-14 and 2-15, similar to CSCM Concrete models, Winfrith Concrete models experienced no strength enhancement when the IRATE effect was off in the models. As the IRATE turned on for the 101.6 x 203.2 mm (4 x 8 in.) cylinders, the strain rate effect caused the compressive strength to increase to 54, 61.5, and 65.8 MPa for loading rates of 0.0125, 1, and $5s^{-1}$ respectively. This shows the dependency of the maximum compressive strength to the rate of loading in Winfirth Concrete models.

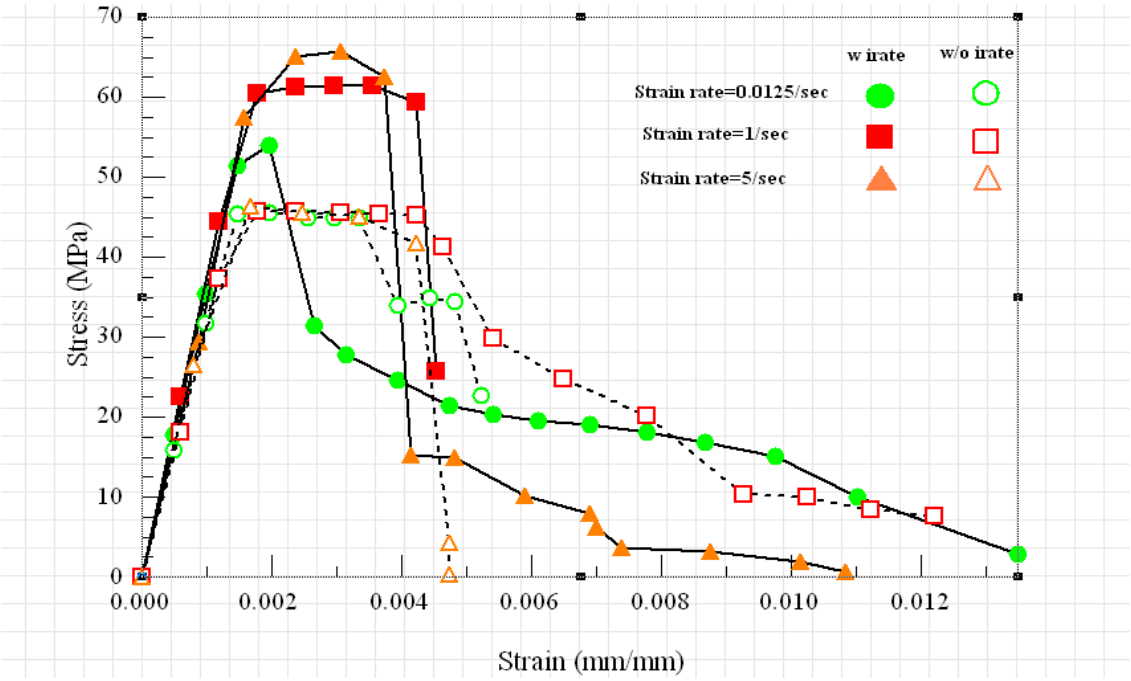

Figure 2-14: Effect of strain rate on the response of 101.6 x 203.2 mm (4 x 8 in.) Winfrith Concrete cylinder models

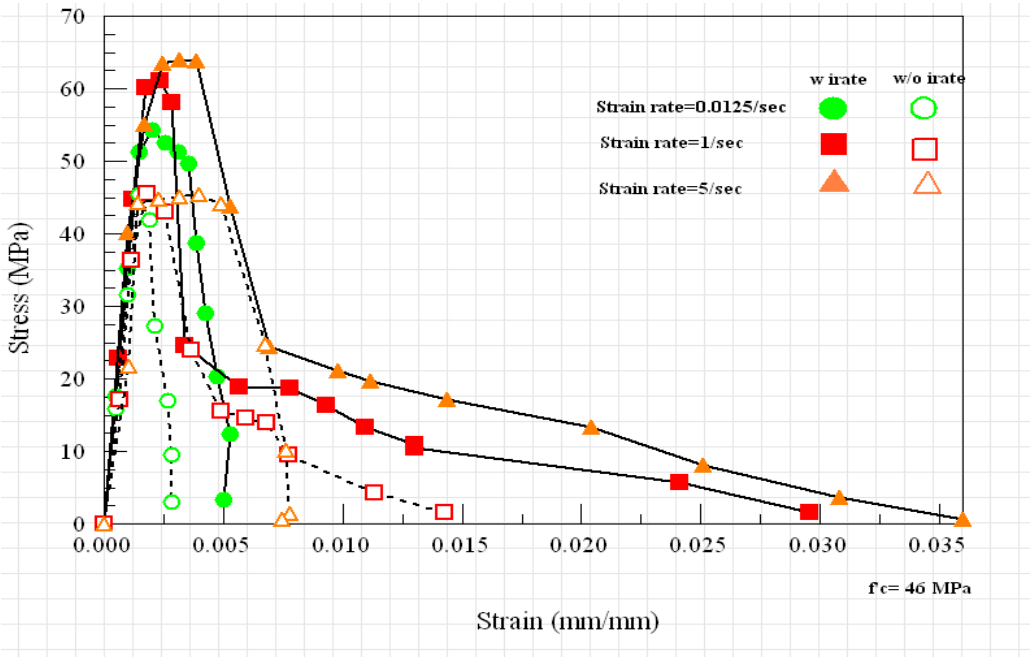

Figure 2-15: Effect of strain rate on the response of 203.2 x 406.4 mm (8 x 16 in.) Winfrith Concrete cylinder models

The size of model has no significant influence on the strength enhancement due to the strain rate effect as seen in Table 2-8, 203.2 x 406.4 mm (8 x 16 in.) cylinders reach the maximum compressive strength of 54.3, 61.1, and 64 MPa for loading rates of 0.0125, 1, and 5 s-1 respectively. These strength enhancement values are approximately the same as those of101.6 x 203.2 mm (4 x 8 in.) cylinders.

Table 2-8 Effect of strain rate on the response of 101.6 x 203.2 mm (4 x 8 in.) and 203.2 x 406.4 mm (8 x 16 in.) models made of Winfrith Concrete material model

Strain Rate (1/Sec)	101.6 x 203.2 mm (4 x 8 in.) Cylinders		203.2 x 406.4 mm (8 x 16 in.) Cylinders	
	Peak Stress (MPa)	% Increase	Peak Stress (MPa)	% Increase
0.0125	54	17%	54.3	18%
1	61.5	34%	61.1	33%
5	65.8	43%	64	39%

2.4.3. Effect of Strain Rate on the Response of Structures Using Material Model Type 72R3 (Concrete Damage REL3)

Similar to the methods used for the two other material models, structures made of Concrete Damage REL3 are subjected to rates of loading of 0.0125, 1, and 5 s^{-1} while the strength enhancement versus strain rate curve provided in LS-DYNA Manual for concrete with unconfined compressive strength of 45.4 MPa is used to activate the effect of strain rate on the response of the material model. The coefficients changed to 1.0 to deactivate the effect of strain rate.

No strength enhancement was observed while the strain rate effect was excluded for this material model. However, for101.6 x 203.2 mm (4 x 8 in.) cylinders strength of concrete

enhanced to 54.3, 59.6, and 62.8 MPa for loading rates of 0.0125, 1, and $5s^{-1}$ as observed in Figures 2-16 and 2-17.

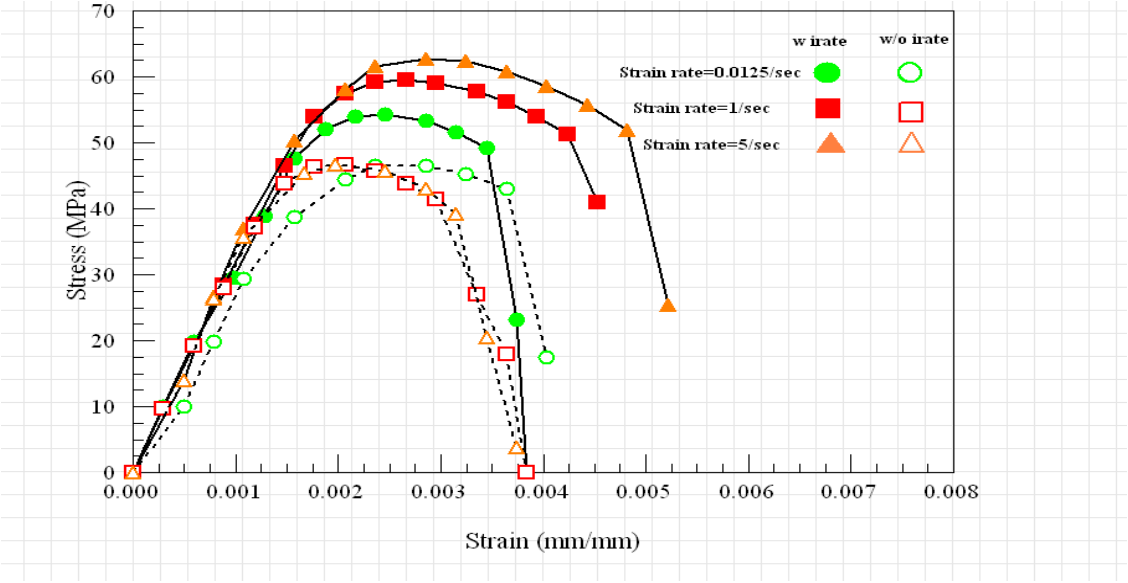

Figure 2-16: Effect of strain rate on the response of 101.6 x 203.2 mm (4 x 8 in.) Concrete Damage REL 3 cylinder models

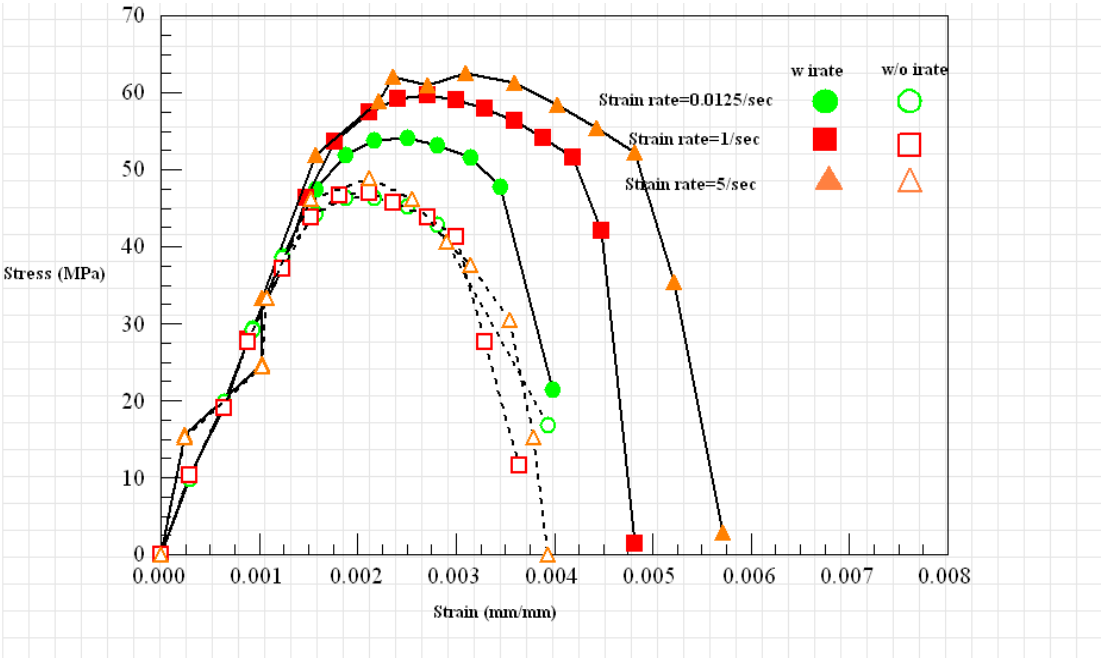

Figure 2-17: Effect of strain rate on the response of 203.2 x 406.4 mm (8 x 16 in.) Concrete Damage REL3 cylinder models

No effect from the size of structure on the strength enhancement due to the strain rate effect observed in the simulations. 203.2 x 406.4 mm (8 x 16 in.) cylinders experienced maximum compressive stress of 54.2, 59.6, and 62.5 MPa for loading rates of 0.0125, 1, and $5s^{-1}$. As Table 2-9 shows, these values are similar to maximum stress values in 101.6 x 203.2 mm (4 x 8 in.) cylinders.

Table 2-9 Effect of strain rate on the response of 101.6 x 203.2 mm (4 x 8 in.) and 203.2 x 406.4 mm (8 x 16 in.) models made of Concrete Damage REL3 material model

Strain Rate (1/Sec)	101.6 x 203.2 mm (4 x 8 in.) Cylinders		203.2 x 406.4 mm (8 x 16 in.) Cylinders	
	Peak Stress (MPa)	% Increase	Peak Stress (MPa)	% Increase
0.0125	54.3	18%	54.2	18%
1	59.6	30%	59.6	30%
5	62.8	37%	62.5	36%

2.5. Combined Effect of Lateral Inertia Confinement and Strain Rate on the Response of Concrete Material Models

In this research project, wide range of loading rates was selected to study the effect of both the lateral inertia confinement and the strain rate on the response of three concrete material models.

As discussed in 2.3, the effect of lateral inertia confinement on the strength enhancement of concrete material models is noticeable only for high rates of loading of 100 and 200 s^{-1}. No strength enhancement due to lateral inertia confinement was observed for the

remaining three rates of loading (0.0125, 1, 5, and 10s^{-1}). On the other hand, the strain rate effect is significant for all ranges of rates of loading.

In section 2.3, the effect of strain rate was excluded from the simulations in order to focus on the study of the lateral inertia confinement effect. In this section, the combined effect of both lateral inertia confinement and strain rate is studied by including the strain rate effect in the simulations of structures subjected to velocity loads with 100 and 200 s^{-1} rates of loading.

2.5.1. Combined Effect of Lateral Inertia Confinement and Strain Rate on the Response of Material Model Type 159 (CSCM Concrete)

As discussed in 2.3, the effect of lateral inertia confinement enhanced the strength of concrete models at high rates of loading of 100 and 200 s^{-1}. Inclusion of strain rate effect further enhances the strength of concrete models as observed in Figures 2-18 through 2-20. The strength enhancement as a result of strain rate effect inclusion is 50% to 70% of the enhanced strength due to the lateral inertia confinement. Tables 2-10 through 2-12 compare the strength enhancement for three sizes of cylinder models with and without the strain rate effect. As observed from the tables, the size of model has on direct effect on the strength enhancement due to the strain rate effect because the increase percent for all the model sizes is in the range of 50 to 70 percent. However, larger models experience higher strength enhancement levels because their initial strength enhancement due to the lateral inertia effect is higher.

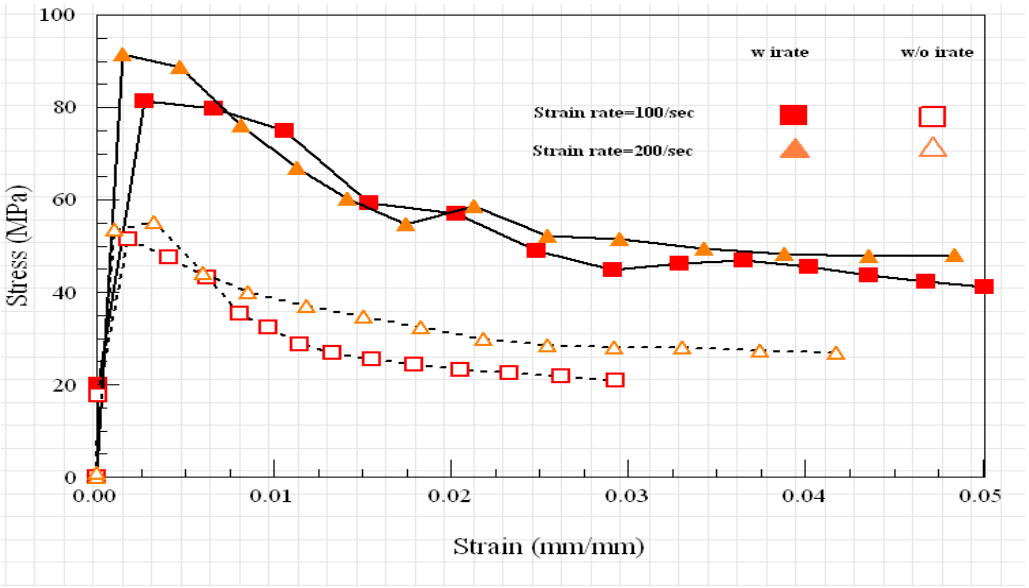

Figure 2-18: Combined effect of lateral inertia confinement and strain rate on the response of 101.6 x 203.2 mm (4 x 8 in.) CSCM concrete cylinder models

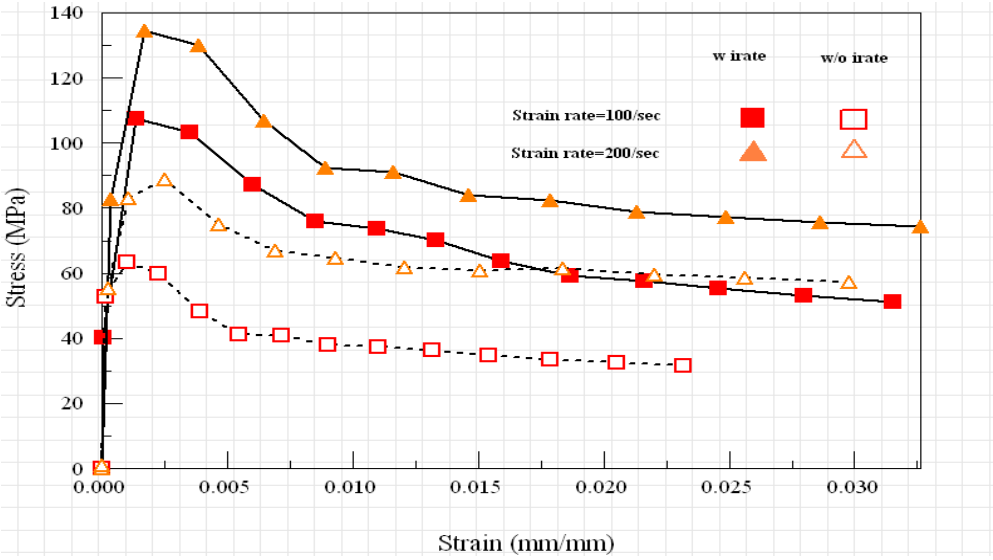

Figure 2-19: Combined effect of lateral inertia confinement and strain rate on the response of 203.2 x 406.4 mm (8 x 16 in.) CSCM concrete cylinder models

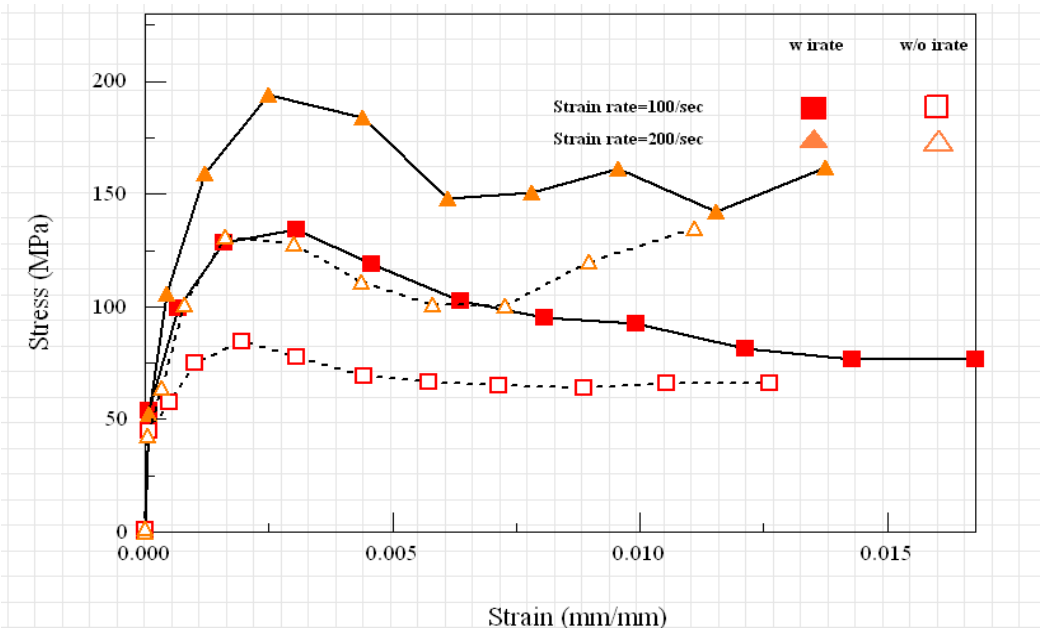

Figure 2-20: Combined effect of lateral inertia confinement and strain rate on the response of 406.4 x 812.8 mm (16 x 32 in.)CSCM concrete cylinder models

Table 2-10 Combined effect of lateral inertia confinement and strain rate effects on the strength enhancement of 101.6 x 203.2 mm (4 x 8 in.) cylinders of CSCM Concrete

	Effect of Lateral Inertia Confinement		Combined effect of Lateral Inertia Confinement& Strain Rate		Effect of Strain Rate inclusion
Rate of loading (1/sec)	Peak Stress (MPa)	% Increase	Peak Stress (MPa)	% Increase	% Increase
100	51.5	12%	81.3	77%	58%
200	55.2	20%	91.6	99%	66%

Table 2-11 Combined effect of lateral inertia confinement and strain rate effects on the strength enhancement of 203.2 x 406.4 mm (8 x 16 in.) cylinders of CSCM Concrete

	Effect of Lateral Inertia Confinement		Combined effect of Lateral Inertia Confinement& Strain Rate		Effect of Strain Rate inclusion
Rate of loading (1/sec)	Peak Stress (MPa)	% Increase	Peak Stress (MPa)	% Increase	% Increase
100	63.5	38%	107.5	134%	69%
200	88.7	93%	134.6	193%	52%

Table 2-12 Combined effect of lateral inertia confinement and strain rate effects on the strength enhancement of 406.4 x 812.8 mm (16 x 32 in.) cylinders of CSCM Concrete

	Effect of Lateral Inertia Confinement		Combined effect of Lateral Inertia Confinement& Strain Rate		Effect of Strain Rate inclusion
Rate of loading (1/sec)	Peak Stress (MPa)	% Increase	Peak Stress (MPa)	% Increase	% Increase
100	84.5	84%	134.4	192%	59%
200	128	178%	194.1	322%	52%

2.5.2. Combined Effect of Lateral Inertia Confinement and Strain Rate on the Response of Material Model Type 84 (Winfrith Concrete)

When both the lateral inertia confinement and strain rate effects are included in the simulations, models made of Winfrith Concrete show significant strength enhancement as observed in Figures 2-21 through 2-23. The strength enhancement as a result of strain rate effect inclusion is not uniform in this material model. As seen in Tables 2-13 through 2-15, the effect of strain rate on the strength enhancement is much higher than the effect of lateral

inertia confinement. For instance, for 203.2 x 406.4 mm (8 x 16 in.) cylinder models, while the lateral inertia effect causes 13% strength enhancement, the strain rate effect further enhances the strength to 104% of the initial enhanced strength. The range of strength increase as a result of strain rate effect is between 72% to 162% for the three sizes of cylinders and the two rates of loadings in models of Winfrith Concrete.

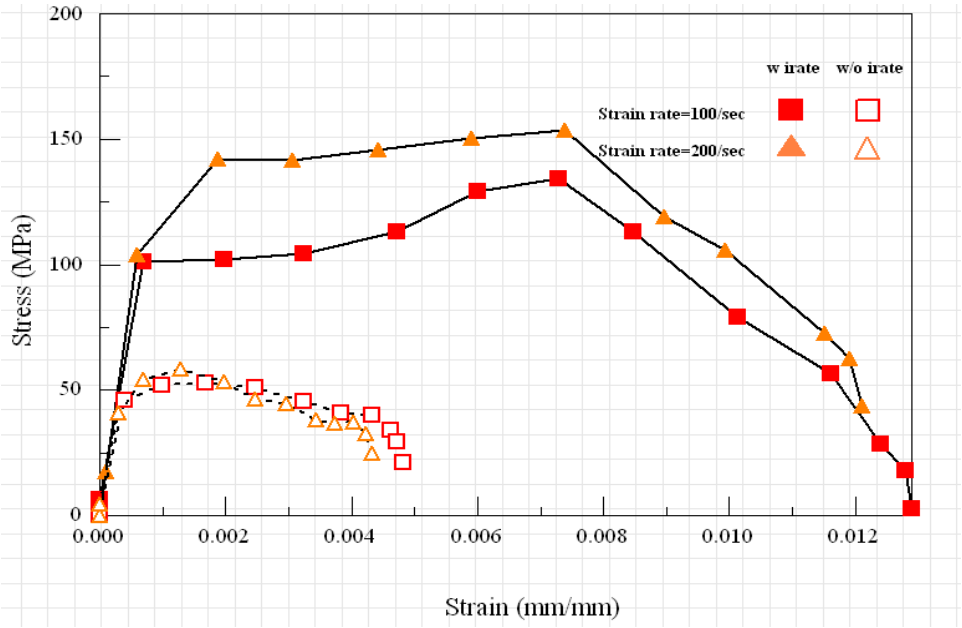

Figure 2-21: Combined effect of lateral inertia confinement and strain rate on the response of 101.6 x 203.2 mm (4 x 8 in.) Winfrith Concrete cylinder models

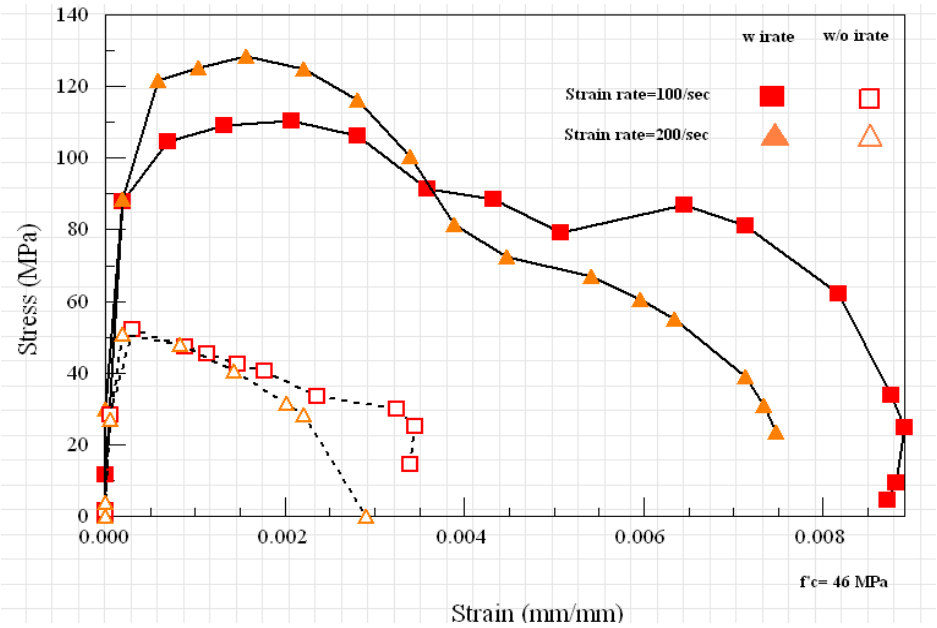

Figure 2-22: Combined effect of lateral inertia confinement and strain rate on the response of 203.2 x 406.4 mm (8 x 16 in.) Winfrith Concrete cylinder models

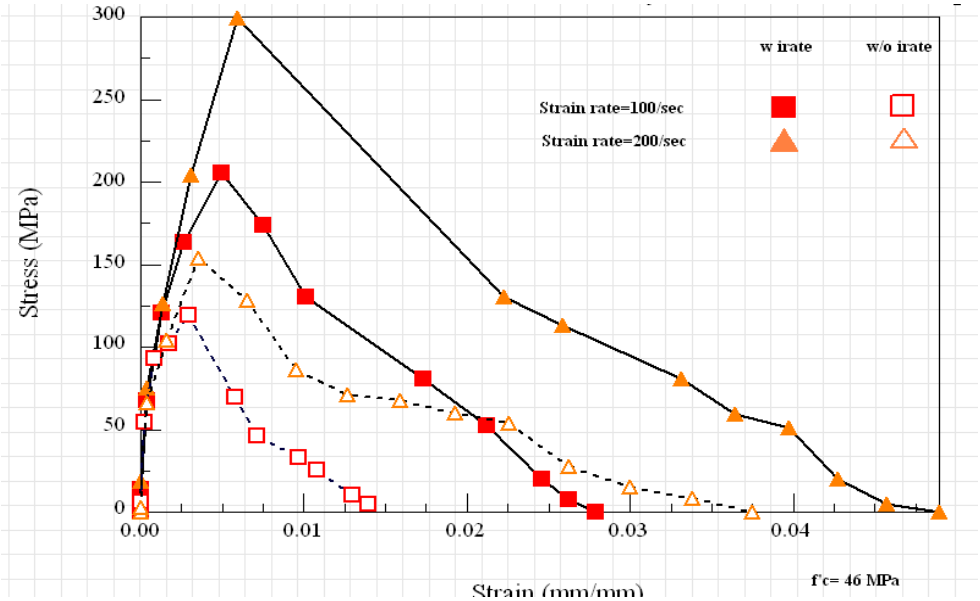

Figure 2-23: Combined effect of lateral inertia confinement and strain rate on the response of 406.4 x 812.8 mm (16 x 32 in.) Winfrith Concrete cylinder models

Table 2-13 Combined effect of lateral inertia confinement and strain rate effects on the strength enhancement of 101.6 x 203.2 mm (4 x 8 in.) cylinders of Winfrith Concrete

	Effect of Lateral Inertia Confinement		Combined effect of Lateral Inertia Confinement& Strain Rate		Effect of Strain Rate inclusion
Rate of loading (1/sec)	Peak Stress (MPa)	% Increase	Peak Stress (MPa)	% Increase	% Increase
100	52.7	15%	134.3	192%	155%
200	58.5	27%	153.4	233%	162%

Table 2-14 Combined effect of lateral inertia confinement and strain rate effects on the strength enhancement of 203.2 x 406.4 mm (8 x 16 in.) cylinders of Winfrith Concrete

	Effect of Lateral Inertia Confinement		Combined effect of Lateral Inertia Confinement& Strain Rate		Effect of Strain Rate inclusion
Rate of loading (1/sec)	Peak Stress (MPa)	% Increase	Peak Stress (MPa)	% Increase	% Increase
100	52.1	13%	106.1	131%	104%
200	51	11%	128.3	179%	152%

Table 2-15 Combined effect of lateral inertia confinement and strain rate effects on the strength enhancement of 406.4 x 812.8 mm (16 x 32 in.) cylinders of Winfrith Concrete

	Effect of Lateral Inertia Confinement		Combined effect of Lateral Inertia Confinement& Strain Rate		Effect of Strain Rate inclusion
Rate of loading (1/sec)	Peak Stress (MPa)	% Increase	Peak Stress (MPa)	% Increase	% Increase
100	119.1	159%	205.3	346%	72%
200	153.9	235%	299.2	550%	94%

2.5.3. Combined Effect of Lateral Inertia Confinement and Strain Rate on the Response of Material Model Type 72R3 (Concrete Damage REL3)

Figures 2-24 through 2-26 show the strength enhancement due to the strain rate effect in models made of Concrete Damage REL3 material models. The strength enhancement as a result of strain rate effect ranges from 19% to 62% of the initial enhanced strength as observed in Tables 2-16 through 2-18.

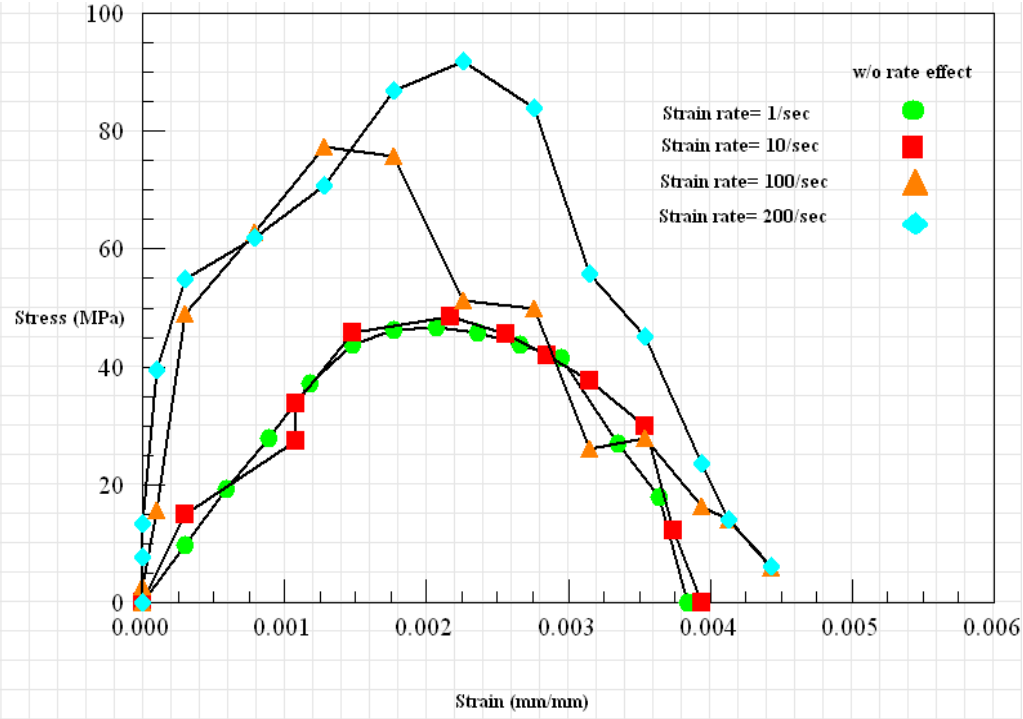

Figure 2-24: Effect of lateral inertia confinement on the response of 101.6 x 203.2 mm (4 x 8 in.) Concrete Damage REL 3 cylinder models

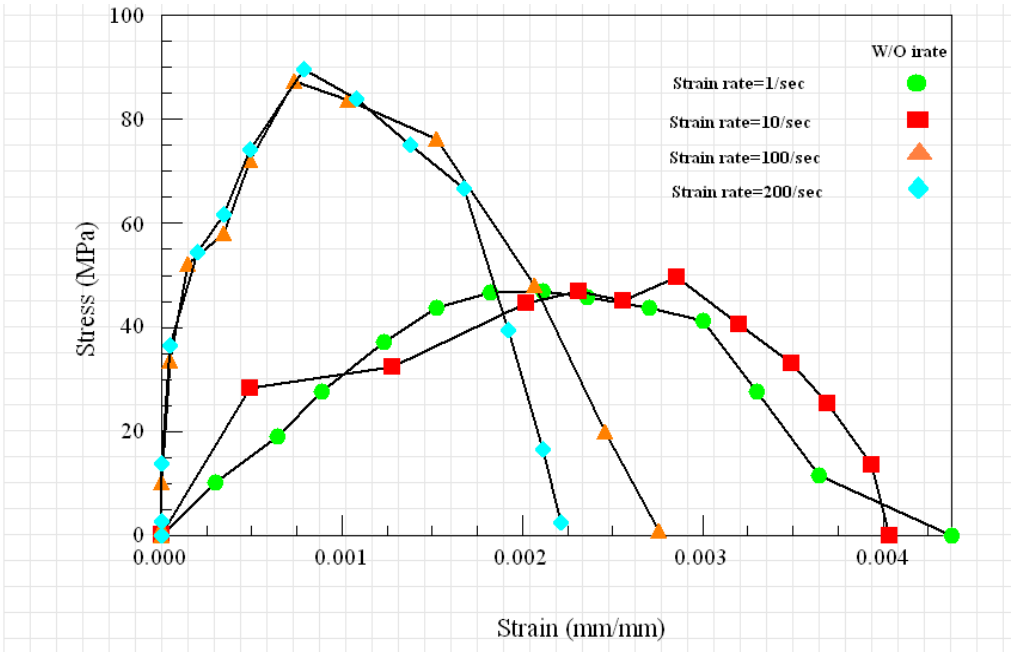

Figure 2-25: Effect of lateral inertia confinement on the response of 203.2 x 406.4 mm (8 x 16 in.) Concrete Damage REL 3 cylinder models

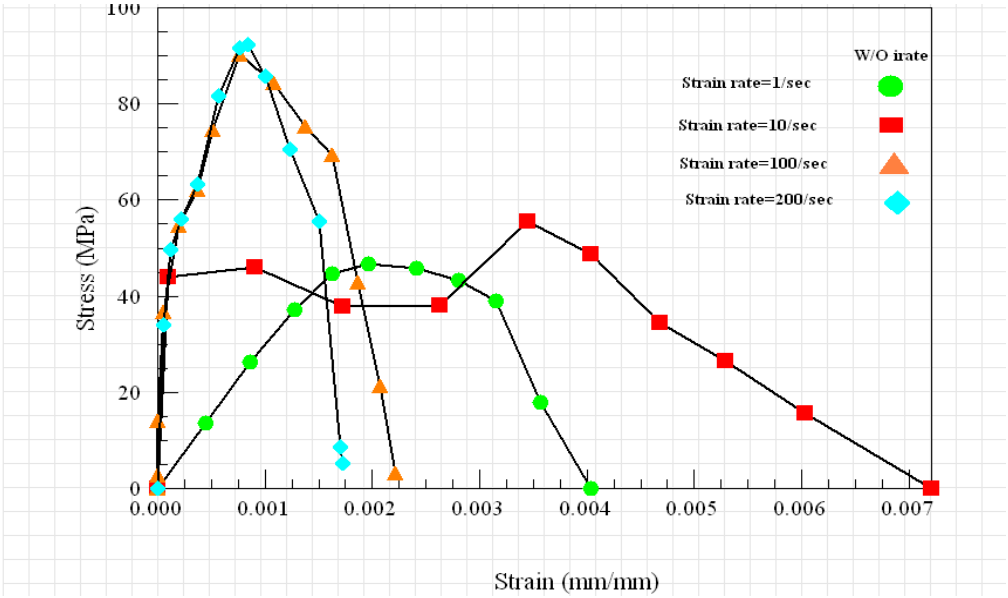

Figure 2-26: Effect of lateral inertia confinement on the response of 406.4 x 812.8 mm (16 x 32 in.) Concrete Damage REL 3 cylinder models

Table 2-16 Combined effect of lateral inertia confinement and strain rate effects on the strength enhancement of 101.6 x 203.2 mm (4 x 8 in.) cylinders of Concrete Damage REL3

	Effect of Lateral Inertia Confinement		Combined effect of Lateral Inertia Confinement& Strain Rate		Effect of Strain Rate inclusion
Rate of loading (1/sec)	Peak Stress (MPa)	% Increase	Peak Stress (MPa)	% Increase	% Increase
100	77.4	68%	123.2	168%	59%
200	91.9	100%	149	224%	62%

Table 2-17 Combined effect of lateral inertia confinement and strain rate effects on the strength enhancement of 203.2 x 406.4 mm (8 x 16 in.) cylinders of Concrete Damage REL3

	Effect of Lateral Inertia Confinement		Combined effect of Lateral Inertia Confinement& Strain Rate		Effect of Strain Rate inclusion
Rate of loading (1/sec)	Peak Stress (MPa)	% Increase	Peak Stress (MPa)	% Increase	% Increase
100	89.7	95%	130.5	184%	45%
200	87.3	90%	119.9	161%	37%

Table 2-18 Combined effect of lateral inertia confinement and strain rate effects on the strength enhancement of 406.4 x 812.8 mm (16 x 32 in.) cylinders of Concrete Damage REL3

	Effect of Lateral Inertia Confinement		Combined effect of Lateral Inertia Confinement& Strain Rate		Effect of Strain Rate Inclusion
Rate of loading (1/sec)	Peak Stress (MPa)	% Increase	Peak Stress (MPa)	% Increase	% Increase
100	90.2	96%	118.5	158%	31%
200	92.4	101%	110.2	150%	19%

2.6. Mesh Sensitivity of Concrete Material Models

In simulations using finite element modeling, the size of mesh is an important factor in the level of the accuracy of the results. While the coarse mesh may yield less accurate results, the fine mesh may increase the computational cost.

The sensitivity of the three material models to mesh size is studied for 101.6 x 203.2 mm (4 x 8 in.) cylinders meshed using three different sizes of hexahedral elements: 25.4 mm (1 in.), 12.7 mm (1/2 in.), and 6.35 mm (1/4 in.).

2.6.1. Mesh Sensitivity of Material Model Type 159 (CSCM CONCRETE)

The mesh sensitivity of the concrete models made of CSCM Concrete material and subjected to three rates of loading of 0.0125, 1, and 200 s^{-1} is shown in Figures 2-27 through 2-29. From the graphs, it is observed that the size of mesh has influence on the prediction of the maximum stress for all the three ranges of rates of loading. However, CSCM Concrete shows less mesh sensitivity at higher rates of loading. As seen in Figure 2-29, at 200 s^{-1} rate of loading, the maximum stress and the softening part of the stress-strain curve are very close for the models meshed with different sizes.

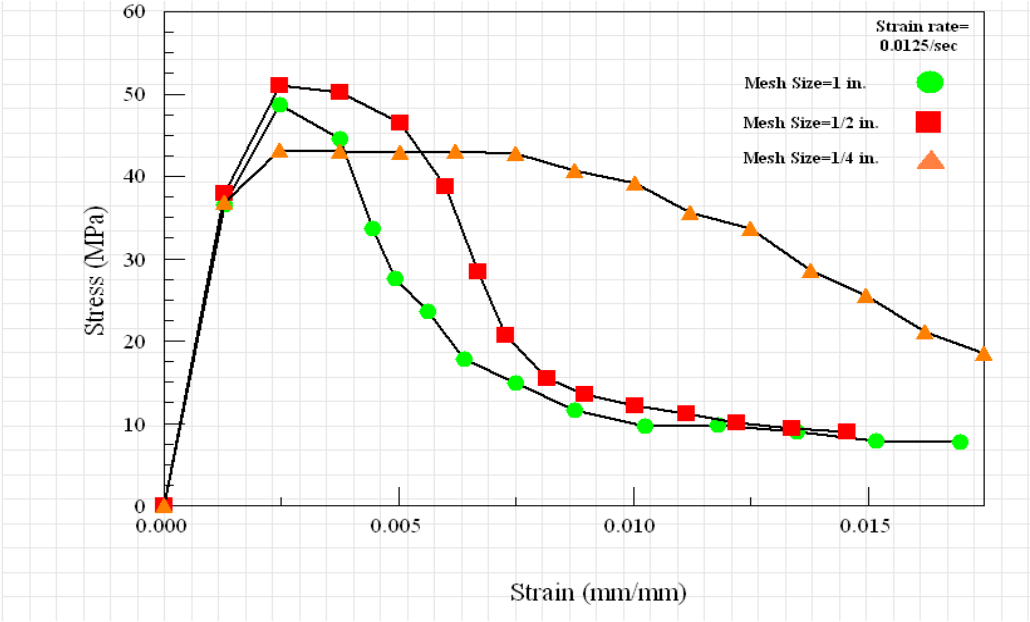

Figure 2-27: Mesh size effect on the response of 101.6 x 203.2 mm (4 x 8 in.) cylinders made of CSCM Concrete material model subjected to rate of loading of 0.0125/sec

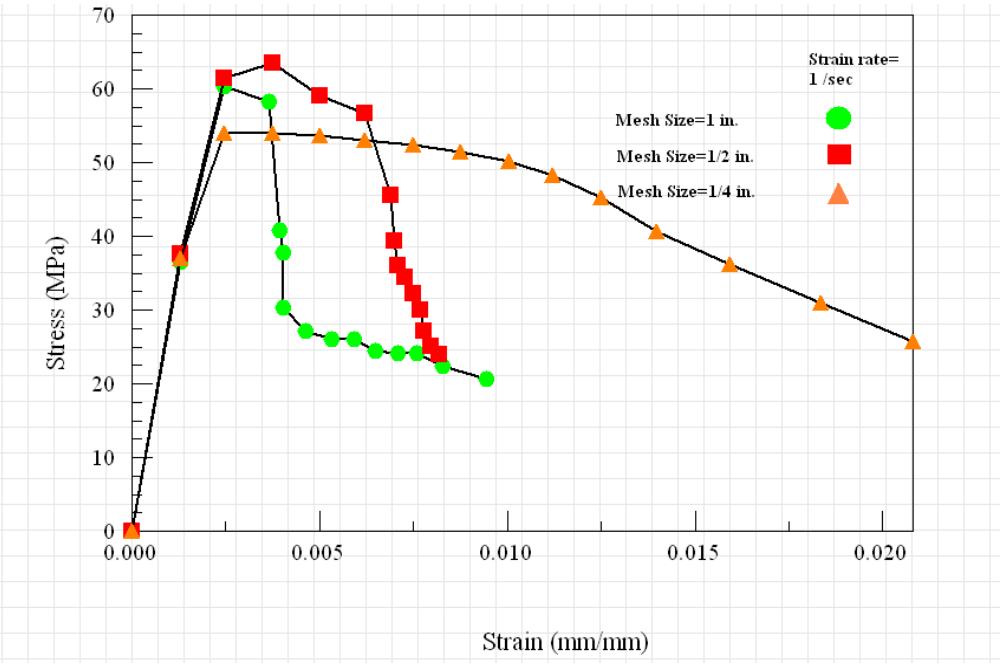

Figure 2-28: Mesh size effect on the response of 101.6 x 203.2 mm (4 x 8 in.) cylinders made of CSCM Concrete material model subjected to rate of loading of 1/sec

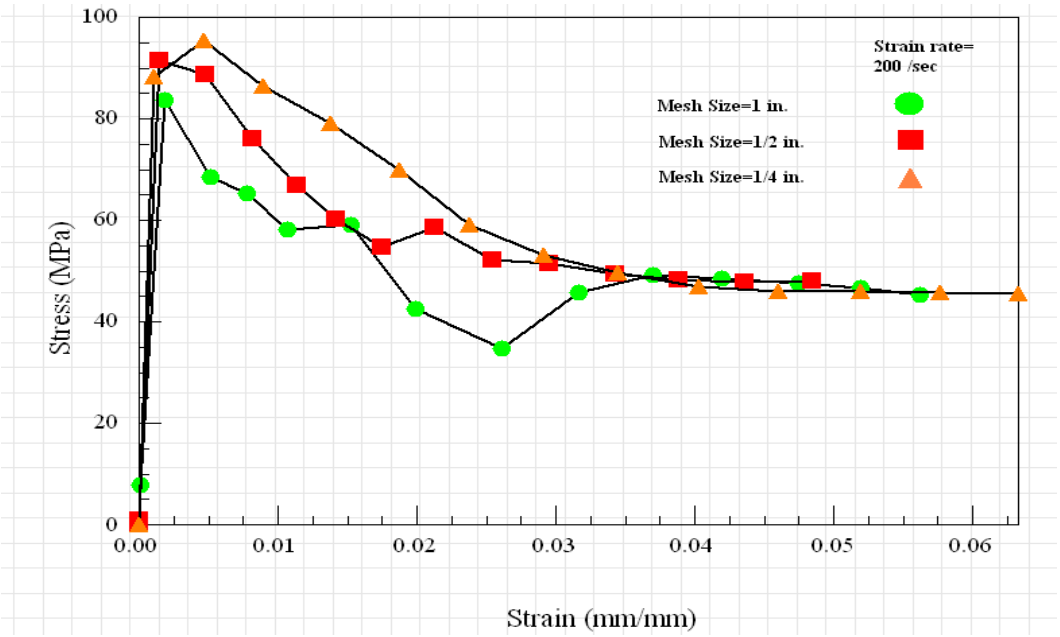

Figure 2-29: Mesh size effect on the response of 101.6 x 203.2 mm (4 x 8 in.) cylinders made of CSCM Concrete material model subjected to rate of loading of 200/sec

2.6.2. Mesh Sensitivity of Material Model Type 84(Winfrith Concrete)

Figures 2-30 through 2-32 shows the mesh sensitivity of models made of Winfrith Concrete material model at three rates of loading. Winfrith Concrete material model shows mesh sensitivity for all the rates of loading; however, the deviation is higher at high rates of loading.

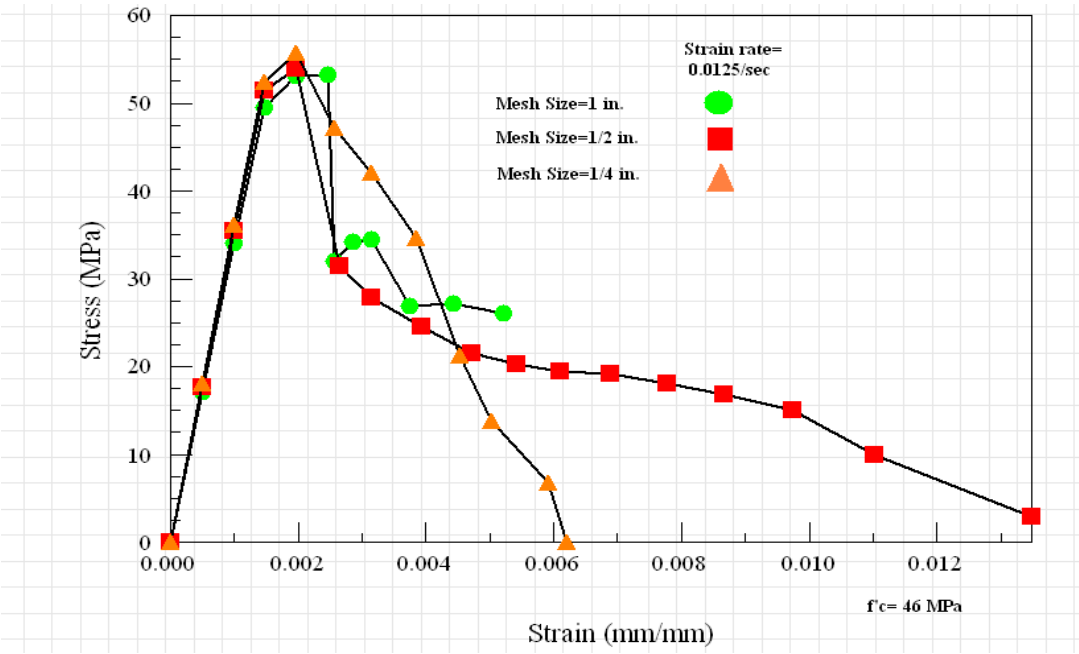

Figure 2-30: Mesh size effect on the response of 101.6 x 203.2 mm (4 x 8 in.) cylinders made of Winfrith Concrete material model subjected to strain rate of 0.0125/sec

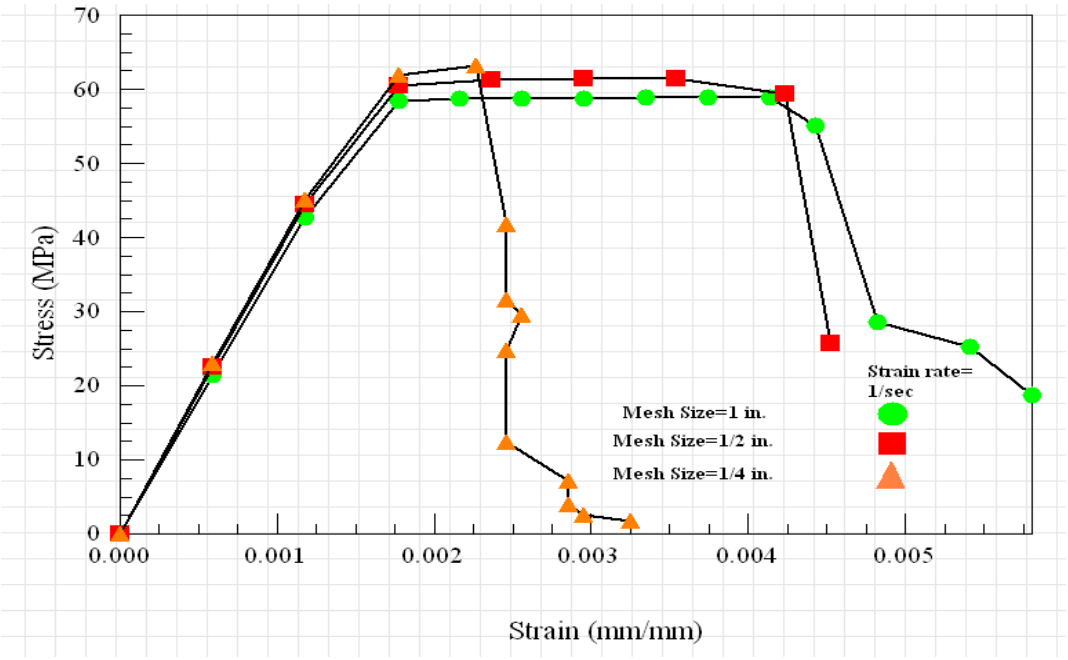

Figure 2-31: Mesh size effect on the response of 101.6 x 203.2 mm (4 x 8 in.) cylinders made of Winfrith Concrete material model subjected to strain rate of 1/sec

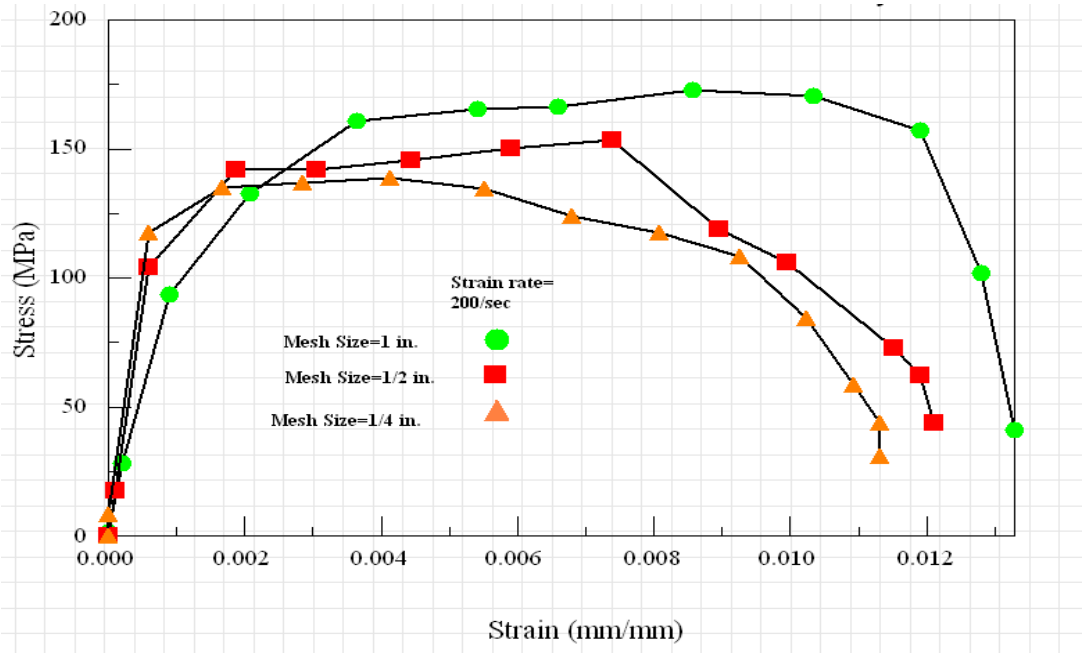

Figure 2-32: Mesh size effect on the response of 101.6 x 203.2 mm (4 x 8 in.) cylinders made of Winfrith Concrete material model subjected to strain rate of 200/sec

2.6.3. Mesh Sensitivity of Material Model Type 72R3 (Concrete Damage REL3)

Mesh sensitivity of models made of Concrete Damage REL3 at three rates of loading of 0.0125, 1, and 200s^{-1} are shown in Figures 2-33 through 2-35. The mesh sensitivity is very low for the low rates of loading; however, significant mesh sensitivity is observed at high rate of loading of 200 s^{-1}.

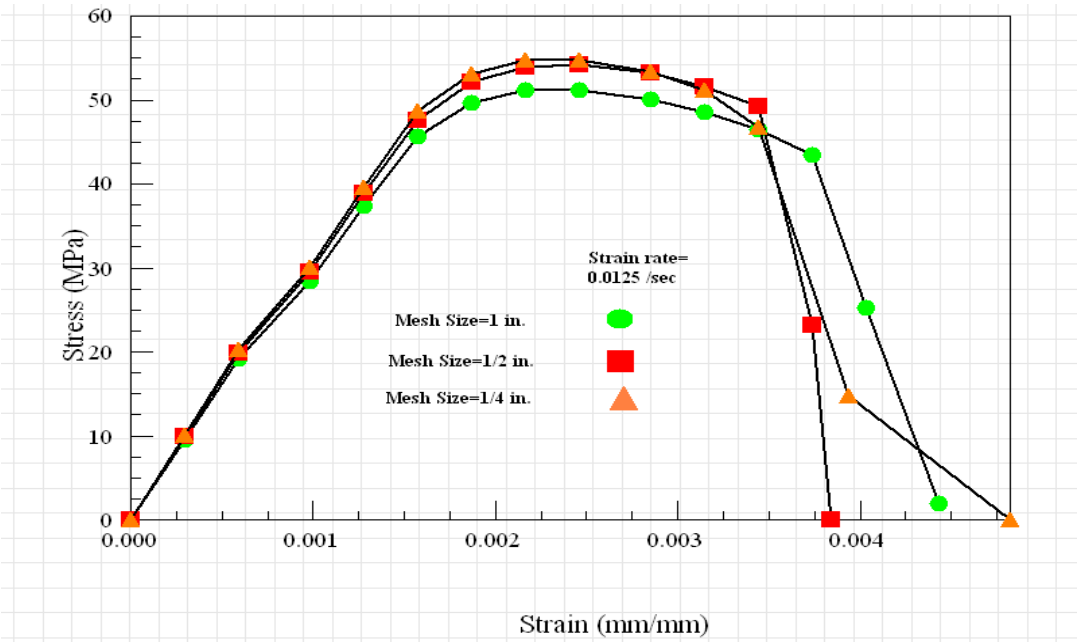

Figure 2-33: Mesh size effect on the response of 101.6 x 203.2 mm (4 x 8 in.) cylinders made of Concrete Damage REL3 material model subjected to strain rate of 0.0125/sec

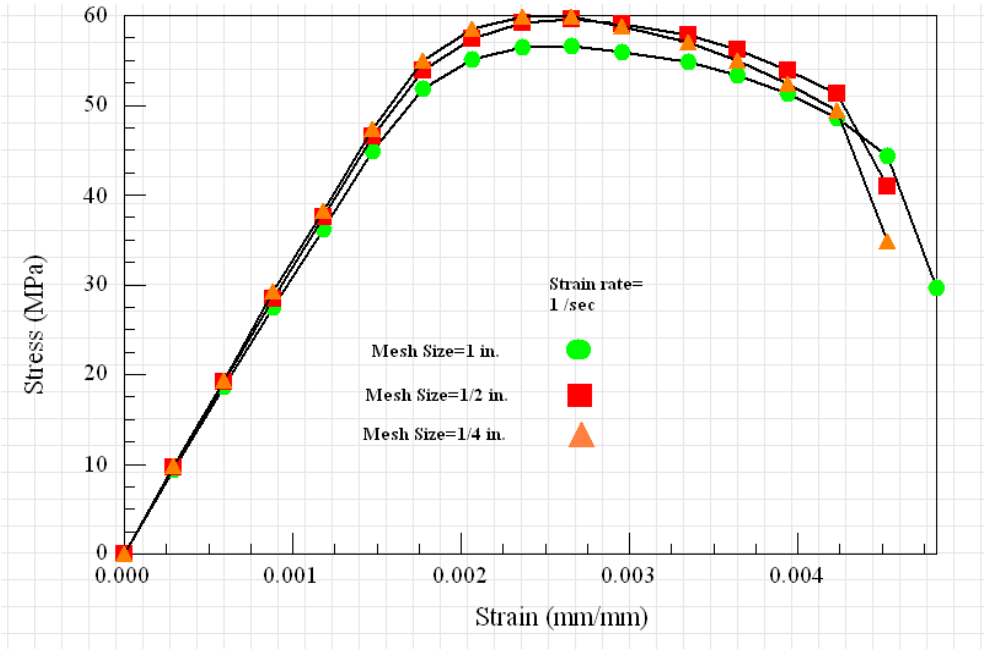

Figure 2-34: Mesh size effect on the response of 101.6 x 203.2 mm (4 x 8 in.) cylinders made of Concrete Damage REL3 material model subjected to strain rate of 1/sec

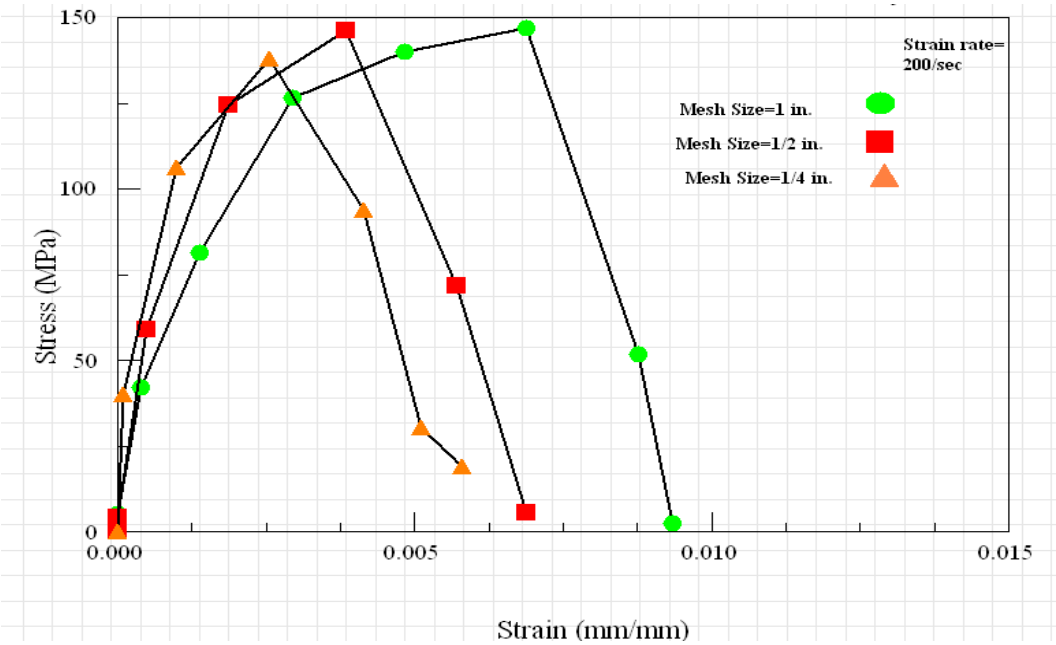

Figure 2-35: Mesh size effect on the response of 101.6 x 203.2 mm (4 x 8 in.) cylinders made of Concrete Damage REL3 material model subjected to strain rate of 200/sec

2.7. Discussion

2.7.1. Dynamic Increase Factor (DIF)

According to experimental and numerical studies performed by Ross et al. (1995), the ratios of dynamic strength to static strength for concrete subjected to dynamic loads with rates of 100 and 200 s^{-1} are approximately 1.8 and 2.0 respectively as read from the graphs presented in Ross et al.(1995). CEB equations yield the Dynamic Increase Factors (DIF) of 2.0 and 2.6 for rates of loading of 100 and 200 s^{-1}.

Tables 2-19 through 2-24 show the DIF values calculated based on the result of simulation done in this research project for the three material models in the two cases of inclusion and exclusion of the strain rate effect.

Table 2-19 Dynamic increase factor for three sizes of cylinders made of CSCM Concrete material model when Strain Rate Effect is included

	101.6 x 203.2 mm (4 x 8 in.) Cylinders		203.2 x 406.4 mm (8 x 16 in.) Cylinders		406.4 x 812.8 mm (16 x 32 in.) Cylinders		CEB	Ross et al. (1995)
Rate of loading (1/sec)	Peak Stress (MPa)	DIF	Peak Stress (MPa)	DIF	Peak Stress (MPa)	DIF	DIF	DIF
100	81.3	1.77	107.5	2.34	134.4	2.92	2.0	1.8
200	91.6	1.99	134.6	2.93	194.1	4.22	2.6	2.0

Table 2-20 Dynamic increase factor for three sizes of cylinders made of CSCM Concrete material model when Strain Rate Effect is excluded

	101.6 x 203.2 mm (4 x 8 in.) Cylinders		203.2 x 406.4 mm (8 x 16 in.) Cylinders		406.4 x 812.8 mm (16 x 32 in.) Cylinders		CEB	Ross et al. (1995)
Rate of loading (1/sec)	Peak Stress (MPa)	DIF	Peak Stress (MPa)	DIF	Peak Stress (MPa)	DIF	DIF	DIF
100	51.5	1.12	63.5	1.38	84.5	1.84	2.0	1.8
200	55.2	1.20	88.7	1.93	128	2.78	2.6	2.0

The specimen size that Ross et al. (1995) used to study the strength enhancement of concrete was about 50 mm (Ross et al. 1995). As Table 2-19 shows, for models made of CSCM Concrete material model, when strain rate effect is included in the simulations, the DIF values of 101.6 x 203.2 mm (4 x 8 in.) cylinders is very close to DIF values proposed by Ross et al. (1995). As the structure size increases while the strain rate effect is included, the DIF values exceed both the CEB and Ross et al. (1995) values. On the other hand, as observed from Table 2-20, when the strain rate effect is excluded from the simulations, the DIF values of 101.6 x 203.2 mm (4 x 8 in.) and 406.4 x 812.8 mm (16 x 32 in.) cylinders become close to the DIF values proposed by CEB equations and Ross et al. (1995).

Table 2-21 Dynamic increase factor for three sizes of cylinders made of Winfrith Concrete material model when Strain Rate Effect is included

	101.6 x 203.2 mm (4 x 8 in.) Cylinders		203.2 x 406.4 mm (8 x 16 in.) Cylinders		406.4 x 812.8 mm (16 x 32 in.) Cylinders		CEB	Ross et al. (195)
Rate of loading (1/sec)	Peak Stress (MPa)	DIF	Peak Stress (MPa)	DIF	Peak Stress (MPa)	DIF	DIF	DIF
100	134.3	2.92	106.1	2.31	205.3	4.46	2.0	1.8
200	153.4	3.33	128.3	2.79	299.2	6.50	2.6	2.0

Table 2-22 Dynamic increase factor for three sizes of cylinders made of Winfrith Concrete material model when Strain Rate Effect is excluded

	101.6 x 203.2 mm (4 x 8 in.) Cylinders		203.2 x 406.4 mm (8 x 16 in.) Cylinders		406.4 x 812.8 mm (16 x 32 in.) Cylinders		CEB	Ross et al. (1995)
Rate of loading (1/sec)	Peak Stress (MPa)	DIF	Peak Stress (MPa)	DIF	Peak Stress (MPa)	DIF	DIF	DIF
100	52.7	1.15	52.1	1.13	119.1	2.59	2.0	1.8
200	58.5	1.27	51	1.11	153.9	3.35	2.6	2.0

As seen in Table 2-21, the DIF values obtained for models made of Winfrith Concrete when the strain rate effect is included in the simulations exceed the DIF values proposed by CEB equations and Ross et al. (1995). The exclusion of strain rate effects causes the DIF values to plummet significantly for all the three sizes as observed in Table 2-22. But still none of the values for the three cylinder sizes are in the range proposed by CEB equations and Ross et al. (1995).

Table 2-23 Dynamic increase factor for three sizes of cylinders made of Concrete Damage REL3 material model when Strain Rate Effect is included

	101.6 x 203.2 mm (4 x 8 in.) Cylinders		203.2 x 406.4 mm (8 x 16 in.) Cylinders		406.4 x 812.8 mm (16 x 32 in.) Cylinders		CEB	Ross et al. (1995)
Rate of loading (1/sec)	Peak Stress (MPa)	DIF	Peak Stress (MPa)	DIF	Peak Stress (MPa)	DIF	DIF	DIF
100	123.2	2.68	130.5	2.84	118.5	2.58	2	1.8
200	149	3.24	119.9	2.61	110.2	2.40	2.6	2.0

Table 2-24 Dynamic increase factor for three sizes of cylinders made of Concrete Damage REL3 material model when Strain Rate Effect is excluded

	101.6 x 203.2 mm (4 x 8 in.) Cylinders		203.2 x 406.4 mm (8 x 16 in.) Cylinders		406.4 x 812.8 mm (16 x 32 in.) Cylinders		CEB	Ross et al. (1995)
Rate of loading (1/sec)	Peak Stress (MPa)	DIF	Peak Stress (MPa)	DIF	Peak Stress (MPa)	DIF	DIF	DIF
100	77.4	1.70	89.7	1.98	90.2	1.99	2	1.8
200	91.9	2.02	87.3	1.92	92.4	2.04	2.6	2.0

The DIF values of models made of Concrete Damage REL 3 material model when the strain rate effect is included in the model are higher than the DIF values proposed by CEB equations and Ross et al. (1995) as observed from Table 2-23. However, the exclusion of the strain rate effect decreases the DIF values, as seen in Table 2-24. For all the three cylinder sizes, the DIF values are very close to the values proposed by CEB equations and Ross et al. (1995).

2.7.2. Comparison of Strength Enhancement

The strain rate threshold that the effect of lateral inertia confinement becomes significant is 10 s^{-1} according to Rossi (1997), and 100 s^{-1} based on the study performed by Malvern et al. (1985). As observed and discussed in 2.3, the effect of lateral inertia confinement was negligible for rates of loading of 10 s^{-1} and lower. The inertia confinement effect, however, significantly affects the strength enhancement for rates of loading of 100 and 200 s^{-1} in all the three material models studied in this project.

The lateral inertia confinement is a direct function of both the models size and the rate of loading. The strength enhancement due to the lateral inertia confinement in various sizes of models made of CSCM Concrete material model is between 12 to 84 percent for rate of loading of 100/sec, and 20 to 178 percent for rate of loading of 200 /sec while the lower strength enhancement values are for 101.6 x 203.2 mm (4 x 8 in.) cylinders and the higher values are for 406.4 x 812.8 mm (16 x 32 in.) cylinders. So the effect of lateral inertia confinement in CSCM Concrete models increases as the model size and the rate of loading increases. The same trend also is observed for models made of Winfrith Concrete as the strength enhancement rises from 15 to 159 percent and 27 to 235 percent for 100 and 200 s^{-1} rates of loading respectively in 101.6 x 203.2 mm (4 x 8 in.) and 203.2 x 406.4 mm (8 x 16 in.) cylinders. However, for cylinders made of Concrete Damage REL3 material model, only the effect of rate of loading on the lateral inertia confinement was noticeable as it caused between 68 to 96 percent and 92 to 102 percent strength enhancement at rates of loading of 100 and 200 /sec. For this material model, the effect of model size on strength enhancement was not significant in 100/sec rate of loading and very little in 200/sec rate of loading.

The strain rate effect is a direct function of the rate of loading. When the strain rate effect is included in the simulations in which the effect of lateral inertia confinement is not significant, the strength enhancement is between 50 to 74 percent in cylinders made of CSCM Concrete material models. The lower and upper limits are associated with 0.0125 and 5 /sec rates of loading. Cylinders made of Winfirth Concrete and Concrete Damage REL3 also show the same trend as the strength enhancement increases from 17 to 43 percent and from 18 to 36 percent respectively as the rate of loading rises from 0.0125 to 5 /sec.

At high rates of loading of 100 and 200 /sec, both the inertial confinement and the strain rate effects can be included in the material models. As a result, cylinders made of CSCM Concrete, Winfrith Concrete, and Concrete Damage REL3 show maximum of 322, 550, and 184 percent strength enhancement respectively.

2.8. Conclusions

The following conclusions can be drawn from the simulations done on the response of CSCM Concrete, Winfrith Concrete, and Concrete Damage REL3 material models of LS-DYNA:

- The strength enhancement of concrete due to the rate of loading is affected by two different phenomena: the strain rate and the lateral inertia confinement. The three material models studied in this project provide a means to either include or exclude the effect of strain rate. However, the effect of lateral inertia confinement which is a function of both the structure size and the rate of loading cannot be excluded from the simulations.

- The strain rate effect is a direct function of the rate of loading. On the other hand, the size of structure has not noticeable effect on the strength enhancement due to the strain rate effect. In all the three material models studied in this project, an increase in the rate of loading enhanced the maximum stress observed in the models. The enhancement values are close for all the three models.
- The lateral inertia confinement is a direct function of both the models size and the rate of loading. The effect of lateral inertia confinement in CSCM Concrete and Winfrith Concrete models increases as the model size and the rate of loading increases. However, for cylinders made of Concrete Damage REL3 material model, only the effect of rate of loading on the lateral inertia confinement is noticeable as the change in the cylinder size does not significantly affect the strength enhancement.
- The effect of lateral inertia confinement on the strength enhancement of materials is not noticeable at rates of loading of 10/sec and lower. However, it causes significant strength enhancement at 100 and 200 /sec rates of loading.
- If the Dynamic Increase Factors (DIF) proposed by CEB equations and Rose et al. (1995) are considered as the baseline, the calculated DIF values for cylinders using CSCM Concrete model subjected to dynamic loads with loading rates of 100 and 200 s^{-1} are close to the baseline values when the cylinder size is close to the specimen size used by Ross et al. (1995) (101.6 x 203.2 mm (4 x 8 in.)) and the strain rate effect is included in the simulations.

However for larger cylinder sizes of 203.2 x 406.4 mm (8 x 16 in.) and 406.4 x 812.8 mm (16 x 32 in.), the calculated DIF values are close to the baseline only if the strain rate effect is excluded from the simulations.

- The DIF values calculated for the models made of Winfrith Concrete and subjected to loads with loading rates of 100 and 200 s^{-1} are not in the range of DIF values proposed by CEB equations and Ross et al. (1995) in both cases at which the strain rate effect is included in or excluded from the simulations.
- The DIF values for models made of Concrete Damage REL 3 are in close approximation with the values proposed by CEB equations and Ross et al. (1995) only if the strain rate effect is excluded from the simulations. The inclusion of the strain rate effect increases the DIF beyond the baseline values.
- In reinforced concrete structures, the size of real structures is closer to the largest cylinder studied in this research project. If the DIF values proposed by CEB equations and Ross et al. (1995) are intended to be followed to study the response of structures to impact and blast loading, both CSCM Concrete and Concrete Damage REL3 material models can be used while the strain rate effect is excluded from the simulations.
- All the material models studied in this project showed different levels of mesh sensitivity for different rates of loading. CSCM Concrete models are more mesh sensitive at low strain rates while Concrete Damage REL3 is more mesh sensitive at high strain rates. Winfrith Concrete models show mesh sensitivity at both low and high strain rates.

CHAPTER 3

DEVELOPMENT OF PRESSURE-IMPULSE DIAGRAMS FOR REINFORCED CONCRETE COLUMNS AND EFFECT OF CONFINEMENT ON THE DAMAGE LEVEL

Explosion is a sudden release of energy as a result of physical, nuclear, or chemical events. Regardless of explosion source, an explosion generates shock pressure in solid materials or blast waves in the surrounding air. A blast wave consists of a near instantaneous rise to the peak pressure followed by a gradual return to atmospheric pressure during a time period called the positive phase duration. The area under the pressure-time curve represents the impulse that is imparted to a structure during blast loading.

Pressure and impulse, as the two normalized parameters of a blast load, can be used to represent any blast condition. For structures subjected to blast loading, Pressure-Impulse diagrams are isobar curves consist of structural damage levels for each combination of pressure and impulse. Since Pressure-Impulse diagrams illustrate the damage level of structures at various blast loading conditions, they are invaluable tools in the preliminary design and assessment of protective structures the same way that the response spectrum plots are essential tools in the analysis and design of structures for seismic events (Krauthammer et al. 2008). In addition, they are also useful in the evaluation of the blast mitigation modifications made in structures.

Traditionally, Pressure-Impulse diagrams for structural components are developed using Single Degree of Freedom (SDOF) models. In SDOF models, the equivalent mass and stiffness of the structure are calculated. The equivalent mass and

stiffness are then used to model the structure as a mass and a spring system having one degree of freedom. This simplified numerical method of structural analysis has several limitations described in the next section.

This chapter describes the research conducted to develop Pressure-Impulse diagrams for reinforced concrete columns by using finite element modeling. The use of finite element modeling has many advantages over using SDOF modeling. First, it allows using different elastic-plastic material models for concrete. The sophisticated concrete material models that have been developed for different applications provide more accurate representation of the actual response of concrete. Second, finite element modeling allows that steel reinforcements be modeled as discrete elements using separate material models while coupled with concrete elements. This type of modeling improves the accuracy of the results. In addition, it provides a means for modeling several arrangements of reinforcement and studying the effect of change in the ratio and form of reinforcement as well as the effect of confinement provided by various types and spacing of transverse reinforcement. Third, finite element modeling by using LS-DYNA allows that the blast loads are applied to the structure in two methods. One method is calculating the pressure-time history of a blast event and then, applying the blast pressure directly on the surfaces of the structure. Another method is using the Load_Blast feature of LS-DYNA, defining the blast parameters, and allowing the program to apply the blast pressure on the surfaces of the structure.

Once the maximum response and consequently the damage level of a structure subjected to a specific pressure and impulse is calculated by using finite element analysis, it is shown as a point on the Pressure-Impulse diagram. The curve passing

through the points that have a similar damage level constitute an iso-bar that is the Pressure-Impulse curve for the specific structure and damage level. The Pressure-Impulse curve is subsequently used for the blast resistance evaluation of the structure.

3.1. Literature Review

A Pressure-Impulse diagram is an iso-damage curve that represents a specific structural damage level for each combination of pressure and impulse that falls on the curve. Figure 3-1 shows the primary features that define a Pressure-Impulse diagram. As observed, each Pressure-Impulse diagram has two asymptotes: impulsive asymptote and pressure asymptote. The impulsive asymptote is associated with the loads with very short duration relative to the structure's natural frequency. It represents the minimum impulse required to reach a particular level of damage. In the impulsive region, the structure response is sensitive only to the associated impulse and not to the peak pressure. On the other hand, pressure asymptote is associated with the loading that its duration is longer than the natural frequency of the structure, thus, subjects the structure to quasi-static loading. In the quasi-static region of a Pressure-Impulse diagram, the structure's response becomes insensitive to impulse, but very sensitive to peak pressure. Hence, the horizontal asymptote represents the minimum level of peak pressure required to reach that particular damage level (Shi et al. 2008).

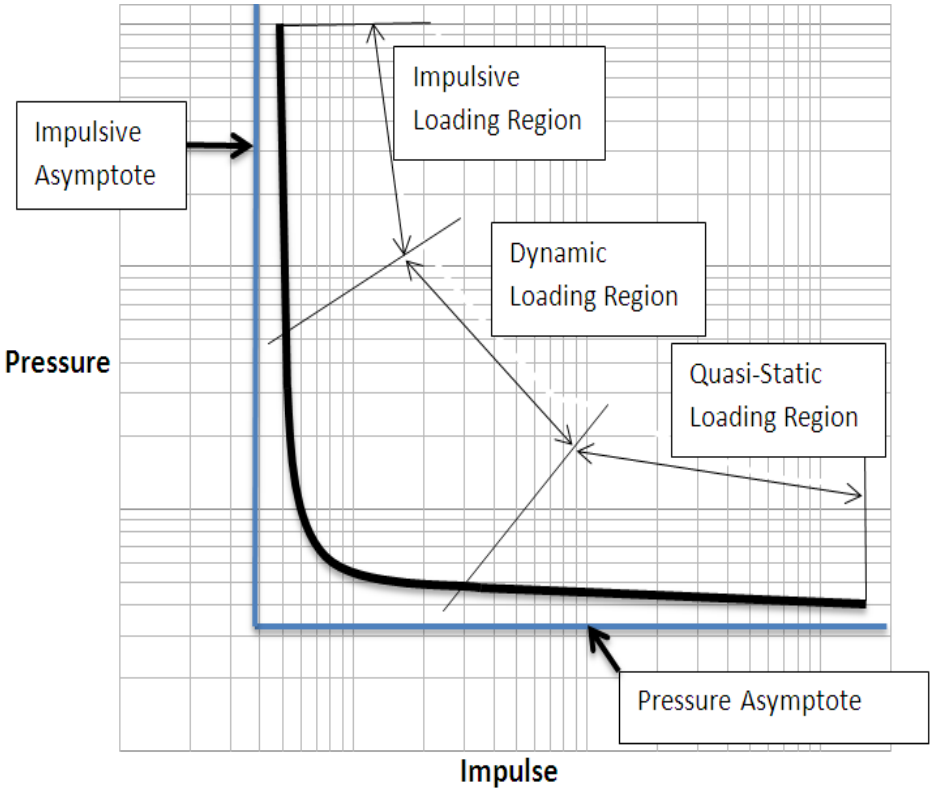

Figure 3-1: A typical Pressure-Impulse diagram

As observed in Figure 3-1, the pressure impulse curve itself divides the Pressure-Impulse space into two regions: the region above and to the right of the curve where the damage level of the structure component is exceeded, and that below and to the left where the level is lower. The pressure impulse diagrams usually contain a group of pressure impulse curves with different degrees of freedom. These curves divide the Pressure-Impulse space into several regions, each corresponding to a particular level of damage, and the curves represent the boundaries between different damage levels (Shi et al. 2008).

In order to develop Pressure-Impulse diagrams for a structure, the calculation of the final state of the structure rather than a detailed knowledge of its displacement time-

history is the principal requirement. The principles of this analysis can be established based on 1) response of a single degree of freedom (SDOF) elastic structure and 2) the link between the duration of the blast load and the natural period of the vibration of the structure (Mays and Smith 1995). A SDOF model of a structure is constructed based on the dominant response mode of a structure which is normally responsible for the overall structural failure. Equivalent mass, damping, and stiffness are the parameters used to describe a SDOF model. They are calculated based on the structure's actual mass, damping, stiffness, and the frequency of the fundamental vibration mode of the structure (Krauthammer 1998). Because SDOF model is simple, efficient and realistically represent the structural behavior based on the anticipated mode of response, it is a useful tool to predict the overall response of a structure, which determines the damage level of a structural system or structural element (Li and Meng 2002). However, SDOF analysis of a structure subjected to blast loading has its own disadvantages. The use of SDOF model may not be suitable for structure damage analysis to blast loads because the structure damage may be governed by the local modes of the structure, especially when the loading is impulsive (Karthaus and Leussink 1983). Shi et al. (2008) explain that the SDOF model is not suitable to model multi-failure modes of a structural component like a column that might initially damage because the shear failure may precede the flexural failure. In addition, because of the rigid plastic material idealization and the negligence of strain hardening and strain rate effects in the analysis, the theoretical prediction of structure response and damage to blast loads may not very accurately reflect the true behavior of the structure (Shi et al. 2008).

In their research, Shi et al. (2008) developed Pressure-Impulse diagrams for reinforced concrete columns by using numerical analysis performed using LS-DYNA. The residual axial load carrying capacity of columns was selected as the damage criterion for development of Pressure-Impulse diagrams. Effect of different parameters including column depth, height, and width, concrete strength, transverse reinforcement ratio, and longitudinal reinforcement ratio was investigated by comparing the Pressure-Impulse diagrams developed for each case.

Bao and Li (2010) used numerical modeling performed using LS_DYNA to study the effect of transverse reinforcement ratio, axial load, longitudinal reinforcement ratio, and column aspect ratio on the damage level of reinforced concrete columns subjected to blast loading. Although they did not construct Pressure-Impulse diagrams, they used impulse to study and compare the effect of each parameter on the residual lateral displacement and residual axial capacity of columns (Bao and Li 2010).

3.2. Column Models and Methods

3.2.1 Column Size, reinforcement Configuration, Boundary Conditions, and Element Formulation

Four types of columns are used in this study. The size of all the columns is selected as the same size as Bao and Li (2010) used in their research. Since no experiments are planned to be performed as part of this research project, the same column sizes as Bao and Li (2010) used are selected in order to make it possible to calibrate the model and validate the results if the columns studied by Bao and Li (2010) are planned to be constructed and

tested in the future. The columns are 355 x 355 mm square with the height of 3480 mm. The columns are modeled and meshed using eight-node hexahedral constant stress solid elements. The size of a solid element is 35.5 x 35.5 mm for column cross section and 22.16 mm for column height. These element sizes result in models consists of 19,118 nodes and 15,700 solid elements.

Eight T 25 (d=25 mm) are used as longitudinal reinforcement for all types of columns. However the configuration of transverse reinforced is different for the columns although their size is T10 (d=10 mm). Based on the transverse reinforcement configuration, columns are grouped as follows:

Type A: Square stirrups of T10 (d=10 mm) spaced at 355 mm along the height of the column

Type B: Square stirrups of T10 (d=10 mm) spaced at 175mm for the full column height except at distances less than 620 mm from the supports. Those regions have T10 (d=10 mm) at 88 mm.

Type C: Spiral stirrups of T10 (d=10 mm) spaced at 175mm for the full column height except at distances less than 620 mm from the supports. Those regions have T10 (d=10 mm) at 88 mm.

Type D: Square and diamond stirrups of T10 (d=10 mm) spaced at 175mm for the full column height except at distances less than 620 mm from the supports. Those regions have T10 (d=10 mm) at 88 mm.

The element used to model the rebar is beam element with truss formulation. The size of a beam element is 35.5 mm for square ties, 52.2 mm for diamonds, 74.4 mm for spirals, and 22.16 mm for longitudinal reinforcement.

In order to couple concrete and reinforcement in the model, an LS-DYNA command called *Constrained_Lagrange_In_Solid is used. The reinforcement is introduced as the slave elements and concrete as the master elements. The coupling constrains the acceleration and velocity in all the direction.

The four types of columns with their cross sections are shown in Figure 3-2.

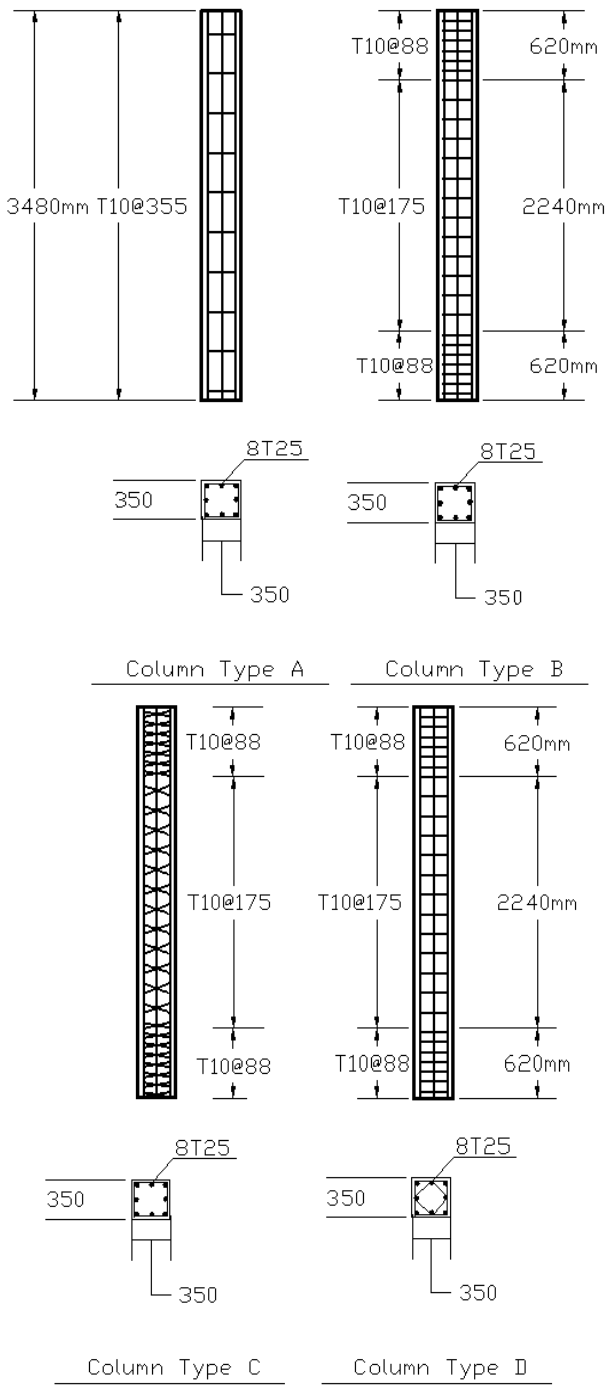

Figure 3-2: Four types of columns

The boundary condition of columns is defined as fixed at both ends. Since solid elements were used to mesh the columns, all the nodes at both support locations are restrained against translation in all direction. This boundary type represents a fixed connection and can be expected to realistically represent the column of a building

3.2.2. Concrete and Rebar Materials

LS-DYNA material Types 72R3 and 84 called as Concrete Damage REL 3 and Winfrith Concrete are used for column simulations as the concrete material models. The mass density of concrete is set to $2.32\times10^{-9}\,\frac{Mg}{mm^3}$, the Poisson's ratio to 0.15, the uniaxial compressive and tensile strength to 45.4 MPa and 4.75 MPa respectively, and the maximum aggregate size to 19 mm. For Concrete Damage REL3, the effect of strain rate in strength enhancement is considered by assigning a predefined strength enhancement curve for LcRate parameter of this material model. As concrete with unconfined compressive strength of 45.4 MPa is used, the corresponding strength enhancement due to strain rate data from LS-DYNA manual keyword is used. Tables 3-1 and 3-2 shows the curves used for tensile and compressive strength enhancement respectively. For Winfrith Concrete, the effect of strength enhancement due to the strain rate is considered by activating the associated parameter in the material model.

Table 3-1 Tensile strength enhancement versus strain rate for Concrete Damage REL3 (LS-DYNA 2007)

Strain Rate (1/sec)	-3.E+04	-3.E+02	-1.E+02	-3.E+01	-1.E+01	-3.E+00	-1.E+00	-1.E-01	-1.E-02	-1.E-03	-1.E-04	-1.E-05	0.E+00
Strength Enhancement	9.7	9.7	6.72	4.5	3.12	2.09	1.45	1.36	1.28	1.2	1.13	1.06	1

Table 3-2 Compressive strength enhancement versus strain rate for Concrete Damage REL3 (LS-DYNA 2007)

Strain Rate (1/sec)	0.E+00	3.E-05	1.E-04	1.E-03	1.E-02	1.E-01	1.E+00	3.E+00	1.E+01	3.E+01	1.E+02	3.E+02	3.E+04
Strength Enhancement	1	1	1.03	1.08	1.14	1.2	1.26	1.29	1.33	1.36	2.04	2.94	2.94

Steel is modeled by using LS-DYNA material model Type 003, Material Plastic Kinematic. For this material, the Mass density is $7.85\times10^{-9}\ \frac{Mg}{mm^3}$, Modulus of Elasticity is 200,000 MPa, Poisson's ratio is 0.30, Yield Stress is 420 MPa and Tangent Modulus is 20,000 MPa.

3.2.3 Natural Time Period and Frequency of Columns

The fundamental period of the columns is calculated using this equation:

$$T = 2\pi\sqrt{\frac{m}{k}}$$

For a column fixed at both support and subjected to a uniformly distributed force *f*, the maximum displacement at the mid-height of the column can be calculated by using this equation:

$$\Delta_{max} = \frac{fl^4}{384EI}$$

The modulus of elasticity of concrete with compressive strength of 45.4 MPa is

$$E_c = 4700\sqrt{f_c'} = 4700 * \sqrt{45.4} = 31{,}668\ MPa$$

The effective moment of inertia of the column is considered to be 35 percent of its gross moment of inertia. So, the effective moment of inertia is

$$I_{eff} = 35\% * \frac{1}{12} * 355^4 = 4.632 * 10^8\ mm^4$$

Therefore, the maximum displacement of the column when subjected to uniformly distributed force of 1 N/mm is

$$\Delta_{max} = \frac{fl^4}{384E_cI_{eff}} = 1 * \frac{3480^4}{384 * 31668 * 4.632 * 10^8} = 0.02604\ mm$$

The column stiffness is the ratio of the total applied force to the maximum displacement. So, the column stiffness is

$$K = 1 * \frac{3{,}480}{0.02604} = 133{,}641\ N/mm$$

The total mass of the column is

$$M = 2.32 * 10^{-9} * 355 * 355 * 3480 = 1.0174\ Mg$$

Therefore, the fundamental period of the structure is

$$T = 2\pi\sqrt{\frac{M}{K}} = 2\pi\sqrt{\frac{1.0174}{133{,}641}} = 0.0173\ sec$$

$$f = \frac{1}{T} = 57.8\ Hz$$

3.2.4. Development of Pressure-Impulse Diagrams

Li and Meng (2002) define pressure impulse diagrams as isodamage curves which include three regimes of structural loading and response: impulse-controlled, peak load and impulse-controlled, and peak load-controlled regimes. These regimes are illustrated in Figure 3-3 as regimes I, II, and III respectively (Li and Meng 2002).

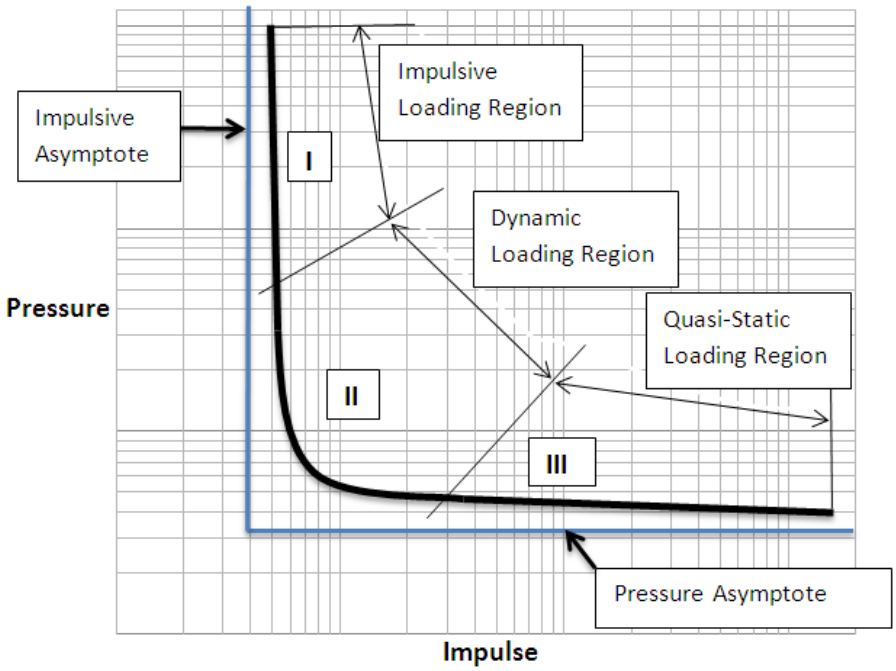

Figure 3-3: Three regimes of a Pressure-Impulse curve

To identify blast loading conditions that fall in each regime, Smith et al. (2009) give an informal criterion. Based on this criterion, the scaled distance, Z, which is defined as the ratio of the standoff distance to the cubic root of the charge weight, may

determine the loading regime. The response regime is categorized as follows (Smith et al. 2009):

Close in: $Z < 3$ ft./lb$^{1/3}$ ($Z < 1190$ mm/kg$^{1/3}$)

Near Field: $3 < Z < 10$ ft./lb$^{1/3}$ ($1190 < Z < 3967$ mm/kg$^{1/3}$)

Far Field: $Z > 10$ ft./lb$^{1/3}$ ($Z > 3967$ mm/kg$^{1/3}$)

The close-in regime is associated with the type of loading where the explosive is very close to the structure. In this case, the duration of loading is much lower than the natural period of the structure. Hence, the loading is impulsive and it generates points in the impulsive-control region (region I) of the Pressure-Impulse diagram.

The far field regime includes the loading cases in which the standoff distance is very high. According to Smith et al. (2009), as a blast wave propagates through air, the peak pressure attenuates and the duration of the positive phase of the blast wave increases. As these alterations progress, the positive pressure region of the blast wave approaches a shape closer to a half sinusoid than a triangular pulse, and is referred to as a pressure wave (Smith et al. 2009). Thus, as the blast wave is propagated in the space, its pressure drops but its duration increases. Since impulse is the area under the pressure-time curve, the impulse increases significantly as a result of wave duration increase due to large standoff distances. Consequently, the loading becomes quasi-static and the peak load-controlled region (region III) of the Pressure-Impulse diagram is developed.

In the near field regime, the standoff distance is high enough to generate the blast wave with duration close to the natural period of the structure. In this type of loading,

both the pressure and impulse affect the response of the structure. Thus, the points associated with the region II of the Pressure-Impulse diagram are generated.

Damage Criterion: Each pressure impulse curve represents a damage level that a structure experiences due to the various blast loading conditions. The damage level is calculated based on the defined damage criterion. For this study, the ratio of the mid-height displacement to the height of the columns is considered as the damage criterion.

For each simulation, the maximum displacement of the central node at the mid-height cross section of the column is read from LS-DYNA's output. Subsequently, the damage level is calculated as the ratio of the maximum displacement to the column height. The maximum reflected pressure and impulse for each blast loading condition is extracted from A.T. Blast and ConWep 2.1.08 by specifying the standoff distance, charge weight, and angle of incidence as zero degree. The combination of pressure, impulse, and damage level constitute a point in the Pressure-Impulse diagram. After running multiple simulations and following the procedure described above, the points whose damage levels are the same are connected to form a damage level curve. This curve is called the pressure impulse diagram for the specific level of structural damage.

For reinforced concrete columns, the level of damage is quantified as the degree of rotation of the support. The damage level is low, medium, and high when the support rotates 1, 2, and 4 degrees respectively (ASCE 1997). In this research, the 2 percent damage level which represents about 2 degrees rotation of the support is a medium level of damage. The 4 and 6 percent damage levels are associated with more than 4 degrees of support rotation which are high levels of damage.

3.2.5. Blast Loads

LS-DYNA provides different ways to apply the pressure from a blast load to a structure. The blast load can be generated by using the Load_Blast command of LS-DYNA. This command provides two cards for the information input. The charge weight, location of the center of the explosives, time of explosion, and the type of explosion, whether it is a surface burst or an air burst, are entered for the first card. The second card is about the conversion factors used in the simulations. Another important point in using Load_Blast command of LS-DYNA is that two load curves even if they are unreferenced need to be included in the model. In this research, the Load_Blast command is used for close-in and near field explosions. However, it is not used for the far field explosion because the far field explosions require too heavy charge weights and too long standoff distances, and consequently, the duration of simulation increases significantly.

Another method to apply the blast load is to define a pressure-time history and apply the pressure to the structure's surface. This method of load application is used for the far field explosions.

The location of explosives is an important factor in the amount of energy that is imparted to a structure. According to Mays et al. (1995), the amount of energy form a surface blast is 1.8 times the energy produced in the free air explosion (Mays and Smith 1995). For this study, all the blast loads are considered surface burst.

3.3. Development of Pressure-Impulse Diagrams for Reinforced Columns

As discussed, a Pressure-Impulse curve has three regions: Impulsive, dynamic, and quasi-static. Each region is generated based on the scaled standoff distance associated with that region as discussed in 3.2.3. The three proceeding sections discuss the point generation for each region.

3.3.1 Development of the Impulsive Region of Pressure-Impulse Diagrams

The impulsive region of the Pressure-Impulse diagrams is developed by subjecting the RC columns to close-in explosions. As discussed in section 3.3, the scaled standoff distance (Z) need to be less than 1190 mm/kg$^{1/3}$ in order to cause a close-in explosion. Table 3-3 presents the standoff and charge weight combinations that were used to generate close-in explosions. As observed, all except one of the scaled standoff distances (Z) are less than 1190 mm/kg$^{1/3}$. The blast case in which the scaled standoff distance is slightly higher will produce a point which is shifted towards the dynamic region of the Pressure-Impulse curve.

Table3-3 Standoff distance and charge weight combinations for Close-in explosion

Standoff Distance (mm)	Charge Weight (kg)	Z (mm/kg $^{1/3}$)	Standoff Distance (mm)	Charge Weight (kg)	Z (mm/kg $^{1/3}$)
1427	16	566	8560	300	1279
	28	470		380	1182
	33	445		500	1078
	39	421		700	964
	50	387		780	930
	60	365		900	887
	70	346		980	862
	80	331		1060	840
	90	318		1140	819
	100	307		1260	793
	110	298		1350	775
	120	289		1500	748
	130	282		1600	732
	140	275		1700	717
	150	269		1900	691

Figure 3-4 shows the displacement history of the central node of the four types of columns made from Damage REL3 material model when subjected to a close-in explosion with 1427mm standoff distance and 50 kg charge weight. As observed, column A which has the maximum stirrups spacing experiences the highest displacement compared to the other three types of columns. Columns B and C have the same stirrups spacing but the type of transverse reinforcement has changed from square stirrups to spiral stirrups. The modification has caused a slightly lower maximum deflection in column Type C. Column D has diamond stirrups in addition to square stirrups compared to column Type B. The addition of diamond stirrups has caused the deflection to decrease.

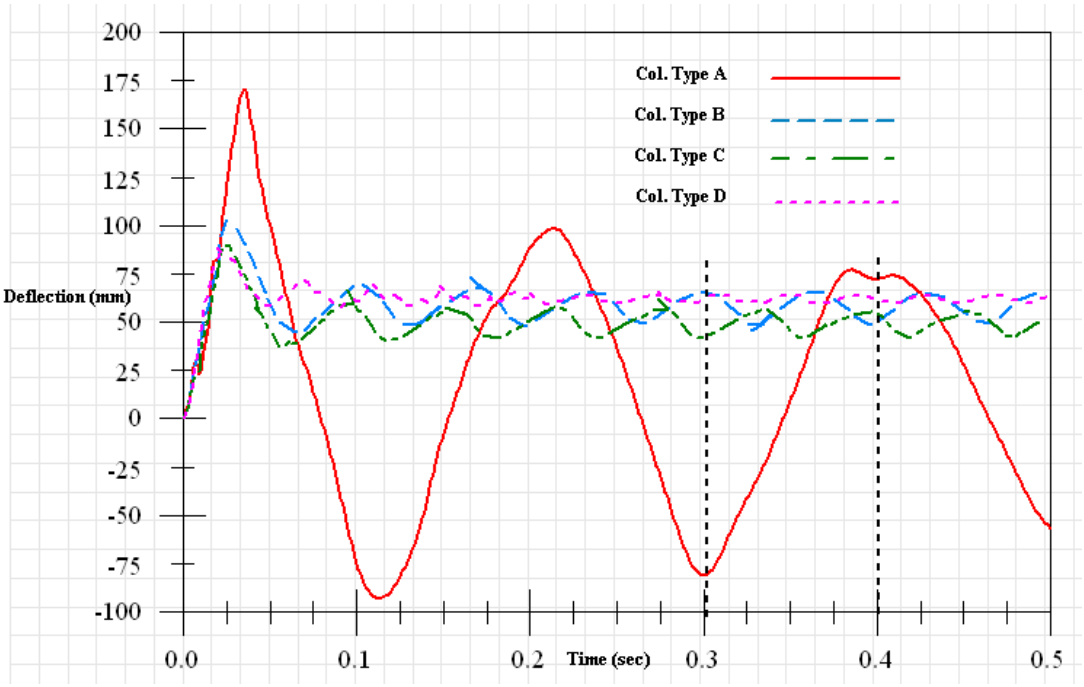

Figure 3-4: Displacement history of the four columns subjected to a close-in explosion for 1427 mm standoff distance and 50 kg charge weight

Figure 3-4 also shows the change in the stiffness of columns after damage. Since the entire column types are identical in dimension, their stiffness and mass before the damage is the same. So, they all have the same natural time period of 0.0173 sec and natural frequency of 57.8 Hz as calculated in Section 3.2.3. However, after the damage the natural frequency has changed. From the free motion of the columns between time 0.3 and 0.4 second, it is observed that column Types A, B, C, And D experience approximately 0.5, 1.5, 1.6, and 2.5 motion cycles in 0.1 second respectively. Since the natural frequency of a structure is directly proportional to the square root of the stiffness, it is observed that the stiffness of the damaged columns is in increasing order for Types

A, B, C, and D as shown in Table 3-4. In other words, the damage level is lowest in column D and is highest in column A.

Table 3-4. Decrease in frequency and stiffness of the four types of columns after damage

Before Damage	After Damage											
All Types	Type A			Type B			Type C			Type D		
f (Hz)	f (Hz)	% Decrease in f	% Decrease in K	f (Hz)	% Decrease in f	% Decrease in K	f (Hz)	% Decrease in f	% Decrease in K	f (Hz)	% Decrease in f	% Decrease in K
57.8	5	91%	71%	15	74%	49%	16	72%	47%	25	57%	34%

The impulsive region of Pressure-Impulse diagrams is developed by subjecting the four types of columns to blast loads generated based on the standoff distances and charge weights of table 3-3. The maximum displacement of the central node at the mid-height cross section of the columns is recorded for all the simulations. The ratio of this displacement to the column height constitutes the damage level for Pressure-Impulse diagram development. The pressure and impulse associated with each blast condition is calculated by using AT Blast software program. Tables 3-5, 3-6, and 3-7 show the pressure and impulse of each blast case and the damage level that the columns, using the two material models, experience at close-in explosions. According to these tables, the change in the form and spacing of the transverse reinforcement affects the level of damage. Column Type A, that has the minimum transverse reinforcement, experiences the highest damage levels. Although the change from square stirrups to spiral stirrups has lowered the damage level in column Type C, the difference in damage level for Types B and C is not significant. Addition of diamond stirrups to column Type B which makes column Type D, however, has decreased the damage level.

Table 3-5 Damage levels of columns using Concrete Damage REL3 material model subjected to Close-in blast with 1427 mm standoff distance

					Column Type A		Column Type B		Column Type C		Column Type D	
Stand Off Distance (mm)	Charge Weight (kg)	Z (mm/kg$^{1/3}$)	Impulse (kPa.msec)	Pressure (kPa)	Displ. at node #9554 (mm)	Damage Level	Displ. at node #9554 (mm)	Damage Level	Displ. at node #9554 (mm)	Damage Level	Displ. at node #9554 (mm)	Damage Level
1,427	16	566	4,957	30,919	61	1.74%	-	-	-	-	-	-
	28	470	7,895	44,339	103	2.95%	57	1.65%	54	1.55%	39	1.12%
	33	445	9,066	49,034	122	3.49%	67	1.91%	74	2.14%	50	1.44%
	39	421	10,443	54,212	136	3.92%	81	2.32%	75	2.16%	65	1.86%
	50	387	12,906	62,742	171	4.91%	104	2.98%	90	2.59%	86	2.47%
	60	365	15,095	69,712	194	5.58%	129	3.71%	111	3.19%	108	3.09%
	70	346	17,245	76,125	212	6.08%	148	4.25%	125	3.60%	127	3.64%
	80	331	19,367	82,092	236	6.77%	166	4.76%	150	4.30%	143	4.10%
	90	318	21,463	87,701	256	7.34%	182	5.23%	163	4.69%	164	4.71%
	100	307	23,523	92,964	-	-	199	5.71%	186	5.35%	179	5.14%
	110	298	25,577	98,016	-	-	237	6.82%	198	5.68%	185	5.32%
	120	289	27,616	102,844	-	-	234	6.71%	224	6.43%	207	5.94%
	140	275	31,655	111,936	-	-	269	7.72%	265	7.63%	241	6.92%
	150	269	33,657	116,238	-	-	330	9.48%	320	9.20%	270	7.77%

Table 3-6 Damage levels of columns using Concrete Damage REL3 material model subjected to Close-in blast with 8560 mm standoff distance

					Column Type A		Column Type B		Column Type C		Column Type D	
Stand Off Distance (mm)	Charge Weight (kg)	Z (mm/kg$^{1/3}$)	Impulse (kPa.msec)	Pressure (kPa)	Displ. at node #9554 (mm)	Damage Level	Displ. at node #9554 (mm)	Damage Level	Displ. at node #9554 (mm)	Damage Level	Displ. at node #9554 (mm)	Damage Level
8,560	220	1,418	3,372	2,991	-	-	-	-	-	-	-	-
	300	1,279	4,273	4,065	57	1.63%	-	-	-	-	-	-
	380	1,182	5,125	5,109	84	2.42%	-	-	-	-	-	-
	500	1,078	6,338	6,612	115	3.31%	-	-	-	-	-	-
	700	964	8,246	8,970	153	4.41%	53	1.51%	49	1.41%	36	1.03%
	780	930	8,977	9,866	171	4.93%	77	2.21%	74	2.13%	54	1.54%
	900	887	10,046	11,113	189	5.42%	115	3.32%	109	3.13%	89	2.56%
	980	862	10,742	11,983	201	5.78%	133	3.83%	128	3.69%	110	3.17%
	1,060	840	11,399	12,755	213	6.11%	159	4.58%	149	4.28%	127	3.65%
	1,140	819	12,121	13,590	248	7.11%	179	5.15%	165	4.75%	143	4.11%
	1,260	793	13,128	14,734	250	7.18%	190	5.46%	188	5.41%	163	4.70%
	1,350	775	13,872	15,568	247	7.10%	209	6.01%	205	5.89%	174	4.99%
	1,500	748	15,093	16,913	263	7.57%	235	6.75%	230	6.60%	196	5.63%
	1,600	732	15,892	17,782	282	8.11%	249	7.15%	242	6.96%	205	5.89%
	1,700	717	16,692	18,623	308	8.86%	264	7.58%	257	7.40%	221	6.35%
	1,900	691	18,257	20,250	403	11.57%	280	8.03%	284	8.17%	247	7.10%

Table 3-7 Damage levels of columns using Winfrith Concrete material model subjected to Close-in blast with 1427 and 8560 mm standoff distances

					Column Type A		Column Type B		Column Type C		Column Type D	
Stand Off Distance (mm)	Charge Weight (kg)	Z (mm/kg$^{1/3}$)	Impulse (kPa.msec)	Pressure (kPa)	Displ. at node #9554 (mm)	Damage Level	Displ. at node #9554 (mm)	Damage Level	Displ. at node #9554 (mm)	Damage Level	Displ. at node #9554 (mm)	Damage Level
1,427	80	331	19,367	82,092	66	1.90%	-	-	-	-	-	-
	90	318	21,463	87,701	81	2.33%	62	1.77%	62	1.78%	58	1.67%
	100	307	23,523	92,964	97	2.79%	75	2.16%	75	2.15%	71	2.05%
8,560	1,600	732	15,892	17,782	68	1.96%	66	1.89%	66	1.89%	65	1.87%
	1,700	717	16,692	18,623	76	2.18%	73	2.11%	73	2.10%	73	2.08%

2%, 4%, and 6% damage levels are selected to develop the Pressure-Impulse diagrams for columns using Concrete Damage REL3 material model. The pressure and impulse for the target damage levels are linearly interpolated from the data of Tables 3-5 and 3-6. The results of interpolation are given in Tables 3-8 and 3-9. These points constitute the impulsive portion of the Pressure-Impulse diagrams.

Table 3-8 Points for the impulsive region of the Pressure-Impulse diagrams for standoff distance of 1427 mm for columns using Concrete Damage REL3 model

		Col. Type A	Col. Type B	Col. Type C	Col. Type D
2% Damage	Impulse (kPa.msec)	5,588	9,368	8,788	11,008
	Pressure (kPa)	33,803	50,170	47,920	56,170
4% Damage	Impulse (kPa.msec)	10,642	16,250	18,457	18,906
	Pressure (kPa)	54,901	73,156	79,534	80,795
6% Damage	Impulse (kPa.msec)	16,901	24,060	26,447	27,849
	Pressure (kPa)	75,099	94,284	100,076	103,379

Table 3-9 Points for the impulsive region of the Pressure-Impulse for standoff distance of 8560 mm for columns using Winfrith Concrete model

		Col. Type A	Col. Type B	Col. Type C	Col. Type D
2% Damage	Impulse (kPa.msec)	4672	8758	8845	9459
	Pressure (kPa)	4554	9597	9704	10428
4% Damage	Impulse (kPa.msec)	7535	10891	11087	11948
	Pressure (kPa)	8091	12158	12389	13390
6% Damage	Impulse (kPa.msec)	11180	13872	14061	16083
	Pressure (kPa)	12498	15568	15776	17983

For columns using Winfrith Concrete material model, only the 2% damage level is selected to develop the Pressure-Impulse diagrams. The result of linear interpolation is given in Tables 3-10 and 3-11.

Table 3-10 Points of the impulsive region of the Pressure-Impulse diagrams for standoff distance of 1427 mm for columns using Winfrith Concrete model

		Col. Type A	Col. Type B	Col. Type C	Col. Type D
2% Damage	Impulse (kPa.msec)	19,854	22,678	22,688	23,252
	Pressure (kPa)	83,396	90,805	90,830	92,272

Table 3-11 Points of the impulsive region of the Pressure-Impulse diagrams for standoff distance of 8560 mm for columns using Winfrith Concrete model

		Col. Type A	Col. Type B	Col. Type C	Col. Type D
2% Damage	Impulse (kPa.msec)	16,037	16,292	16,311	16,387
	Pressure (kPa)	17,935	18,203	18,223	18,303

3.3.2. Development of the Dynamic Region of the Pressure-Impulse Diagrams

When the RC columns are subjected to near field explosions, both the peak pressure and the peak impulse are important components in the structural response. The damage level that a structure experiences in this type of blast loading, are used to develop the dynamic region of a Pressure-Impulse diagram. As discussed in section 3.2.3, the near field explosion occurs when the scaled standoff distance, Z, is between 1190 and 3967 mm/kg$^{1/3}$. Table 3.12 gives the standoff distance and charge weight combinations that were used to generate near field explosion.

Table 3-12 Standoff distance and charge weight combinations for near field explosion

Stand Off Distance (mm)	Charge Weight (kg)	Z (mm/kg$^{1/3}$)
171,200	350,000	2,429
	450,000	2,234
	500,000	2,157
	600,000	2,030
	700,000	1,928
	800,000	1,844
	950,000	1,742
	1,100,000	1,658
	1,300,000	1,569
	1,700,000	1,434
	2,000,000	1,359

Stand Off Distance (mm)	Charge Weight (kg)	Z (mm/kg$^{1/3}$)
256,800	1,000,000	2,568
	1,200,000	2,417
	1,400,000	2,296
	1,700,000	2,152
	2,000,000	2,038
	2,300,000	1,945
	2,700,000	1,844
	3,200,000	1,743
	3,500,000	1,691
	4,000,000	1,618
	5,000,000	1,502
	5,600,000	1,446

The standoff distance for the near field explosion is more than 100 times longer than the close-in explosion. In order to obtain the same damage level range as of the close-in

explosion, the charge weight needs to be very high. As the charge weight increases, the duration of the positive phase of the blast wave increases as well because it takes more time for all the explosives to undergo the chemical reaction. In addition, the peak pressure drops and the wave duration increases as the wave propagates in the air. Consequently, the near field explosions have lower peak pressure and higher peak impulse compared to the close-in explosions.

Figures 3-5 and 3-6 compare the reflected pressure and reflected impulse for two specific close-in and near field explosion events. The close-in explosion has 1140 kg TNT located at 8560 mm from the structure. The near field explosion has 3,200,000 kg TNT at 256,800 mm standoff. As observed, the duration of the near field explosion is about 40 times the duration of the close-in explosion. The peak pressure of the close-in explosion is about 8 times of the near field explosion. Thus, as the standoff distance increases, the peak pressure drops and the duration rises. As a result of blast wave elongation, the peak impulse increases significantly. For these blast events, the impulse of the near field explosion is about five times the impulse of the close-in explosion.

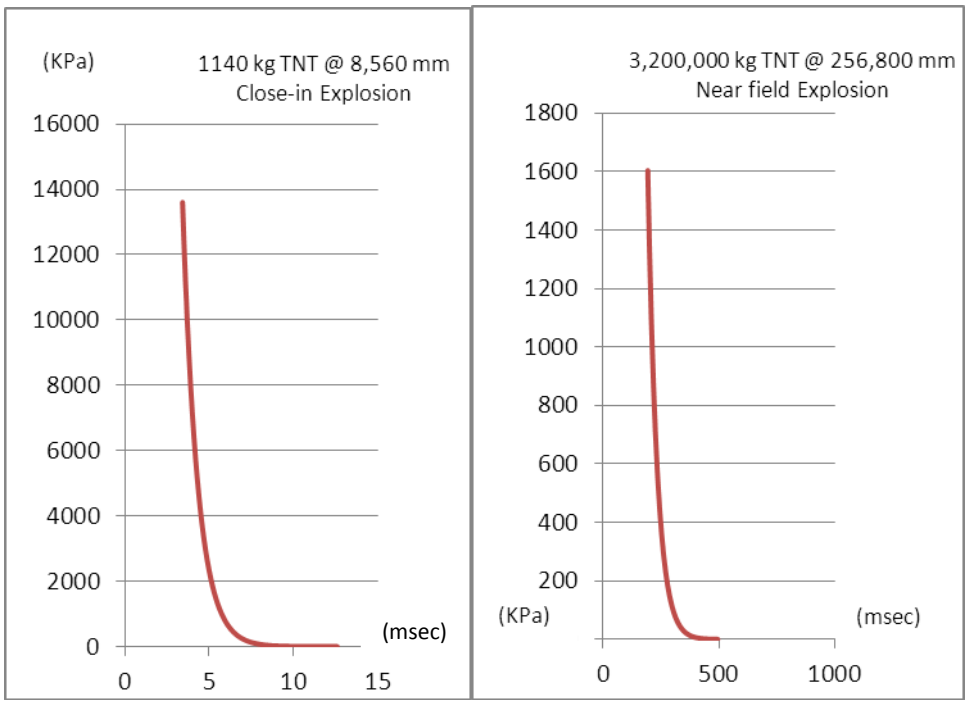

Figure 3-5: Displacement history of the four columns subjected to a close-in explosion for 1427 mm standoff distance and 50 kg charge weight

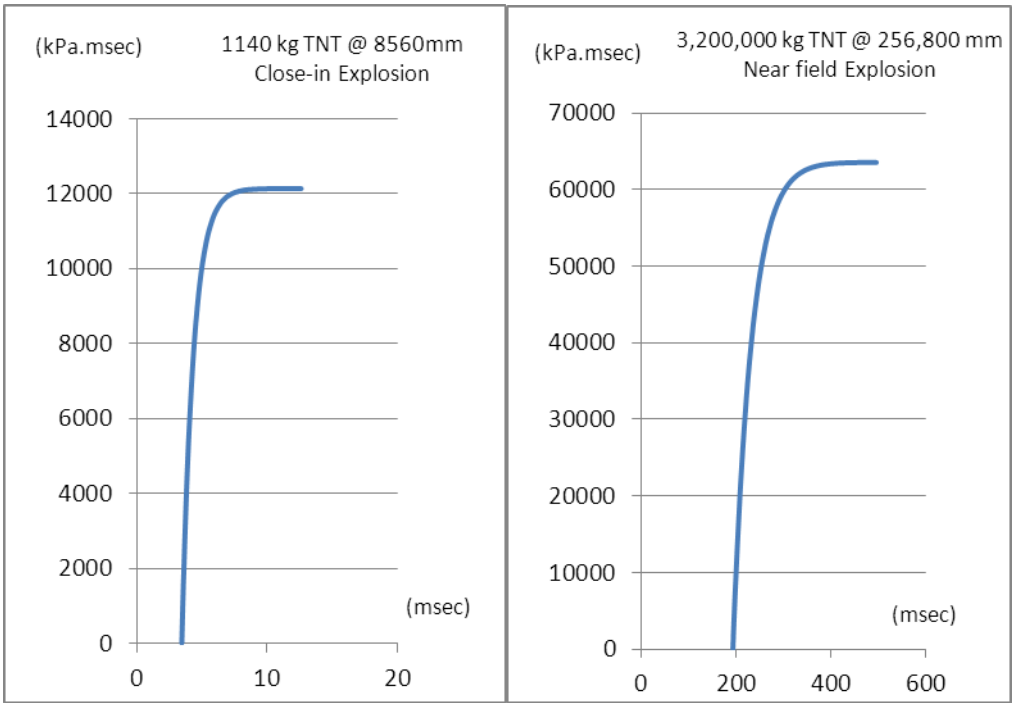

Figure 3-6: Reflected impulse-time history of the close-in and near field explosions

Figure 3-7 compares the displacement history of the four types of columns using Concrete Damage REL3 material model subjected to an explosion with 171,200 mm standoff distance and 1,100,000 kg equivalent TNT charge weight. As observed, the arrival time of the blast wave is approximately 125 milliseconds as a result of long standoff distance. Similar to the close-in explosions, column Type A which has the minimum transverse reinforcement undergoes the most severe damage as it deflects 320 mm at its mid-height. The decrease in the spacing of the transverse reinforcement decreases the maximum deflection and the damage level for column Type B. The change in the shape of transverse reinforcement from square to spiral does not have a significant effect on the reduction of the damage level as the deflection of column Type C is very close to the deflection of column Type B. However, adding the diamond stirrups to column Type B results in significantly lower damage level as column Type D deflects approximately half of column Type B.

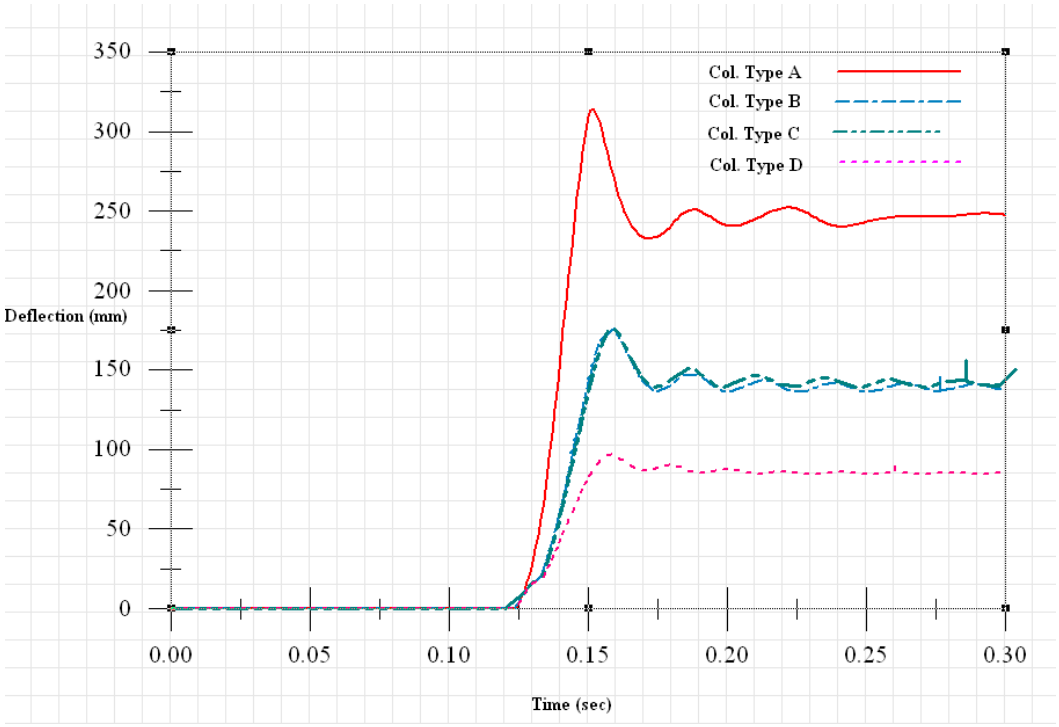

Figure 3-7: Displacement history of the four columns subjected to a near field explosion for 171,200 mm standoff distance and 1,100,000 kg charge weight

The dynamic region of the Pressure-Impulse diagrams is developed by subjecting the four types of columns to blast waves generated based on the standoff distances and charge weights of Table 3.13. The ratio of the maximum displacement of the central node at the mid-height cross section of columns to the column height is recorded as the damage level. Tables 3.13 through 3.15 give the pressure and impulse of each blast event in addition to the damage level of the columns using Concrete Damage REL3 and Winfrith Concrete models.

Table 3-13 Damage levels of the columns using Concrete Damage REL3 model subjected to near field blast with 171,200 mm standoff distance

					Column Type A		Column Type B		Column Type C		Column Type D	
Stand Off Distance (mm)	Charge Weight (kg)	Z (mm/kg$^{1/3}$)	Impulse (kPa.msec)	Pressure (kPa)	Displ. at node #9554 (mm)	Damage Level	Displ. at node #9554 (mm)	Damage Level	Displ. at node #9554 (mm)	Damage Level	Displ. at node #9554 (mm)	Damage Level
171,200	350,000	2,429	20,270	594	80	2.30%	-	-	-	-	-	-
	450,000	2,234	24,373	759	126	3.61%	-	-	-	-	-	-
	500,000	2,157	26,338	842	145	4.15%	-	-	-	-	-	-
	600,000	2,030	30,137	1,010	185	5.30%	-	-	-	-	-	-
	700,000	1,928	33,784	1,180	219	6.28%	8	0.24%	8	0.24%	-	-
	800,000	1,844	37,314	1,350	-	-	83	2.38%	79	2.27%	-	-
	950,000	1,742	42,423	1,607	-	-	140	4.02%	133	3.82%	37	1.05%
	1,100,000	1,658	47,353	1,865	-	-	176	5.06%	177	5.08%	97	2.78%
	1,300,000	1,569	53,969	2,208	-	-	229	6.58%	223	6.42%	162	4.67%
	2,000,000	1,359	74,463	3,401	-	-	-	-	-	-	327	9.40%

Table 3-14 Damage level of the columns using Concrete Damage REL3 model subjected to near field blast with 256,800 mm standoff distance

					Column Type A		Column Type B		Column Type C		Column Type D	
Stand Off Distance (mm)	Charge Weight (kg)	Z (mm/kg$^{1/3}$)	Impulse (kPa.msec)	Pressure (kPa)	Displ. at node #9554 (mm)	Damage Level	Displ. at node #9554 (mm)	Damage Level	Displ. at node #9554 (mm)	Damage Level	Displ. at node #9554 (mm)	Damage Level
256,800	1,000,000	2,568	26,924	507	74	2.13%	-	-	-	-	-	-
	1,200,000	2,417	30,764	604	111	3.18%	-	-	-	-	-	-
	1,400,000	2,296	34,439	701	141	4.06%	-	-	-	-	-	-
	1,700,000	2,152	39,728	849	178	5.11%	-	-	-	-	-	-
	2,000,000	2,038	44,795	998	213	6.13%	-	-	-	-	-	-
	2,300,000	1,945	49,684	1,149	-	-	8	0.24%	8	0.24%	-	-
	2,700,000	1,844	55,972	1,350	-	-	110	3.16%	104	2.98%	11	0.30%
	3,200,000	1,743	63,549	1,604	-	-	187	5.38%	187	5.37%	103	2.97%
	3,500,000	1,691	67,962	1,757	-	-	213	6.14%	208	5.99%	125	3.60%
	5,000,000	1,502	88,873	2,520	-	-	-	-	-	-	276	7.93%

Table 3-15 Damage level of the columns using Winfrith Concrete model subjected to near field blast with 171,200 and 256,800 mm standoff distances

					Column Type A		Column Type B		Column Type C		Column Type D	
Stand Off Distance (mm)	Charge Weight (Kg)	Z (mm/Kg$^{1/3}$)	Impulse (KPa.msec)	Pressure (KPa)	Displ. at node #9554	Damage Level	Displ. at node #9554	Damage Level	Displ. at node #9554	Damage Level	Displ. at node #9554	Damage Level
171,200	1,100,000	1,658	47,353	1,865	38	1.08%	-	-	-	-	-	-
	1,300,000	1,569	53,969	2,208	81	2.32%	-	-	-	-	-	-
	1,700,000	1,434	65,783	2,893	-	-	52	1.51%	54	1.55%	54	1.55%
	2,000,000	1,359	74,463	3,401	-	-	111	3.18%	109	3.12%	103	2.95%
256,800	3,500,000	1,691	67,962	1,757	47	1.34%	-	-	-	-	-	-
	4,000,000	1,618	75,153	2,011	88.1027	2.53%	-	-	-	-	-	-
	5,000,000	1,502	88873	2520	-	-	47	1.35%	43.2	1.24%	40.9	1.18%
	5,600,000	1,446	96871	2824	-	-	84.3	2.42%	87.2	2.51%	76.4	2.20%

Using linear interpolation, the pressure and impulse associated with 2%, 4%, and 6% damage levels are calculated for columns using Concrete Damage REL3 model. For Winfrith Concrete model, only the 2% damage level is considered for Pressure-Impulse curves development. The results of interpolation are given in Tables 3.16 through 3.19.

Table 3-16 Points for the dynamic region of the Pressure-Impulse diagrams for standoff distance of 171,200 mm for columns using Concrete Damage REL3 model

		Col. Type A	Col. Type B	Col. Type C	Col. Type D
2% Damage	Impulse (kPa.msec)	19,330	36,687	36,844	45,130
	Pressure (kPa)	556	1,320	1,327	1,749
4% Damage	Impulse (kPa.msec)	25,792	42,361	43,127	51,624
	Pressure (kPa)	819	1,604	1,849	2,086
6% Damage	Impulse (kPa.msec)	32,742	51,444	51,895	59,732
	Pressure (kPa)	1,131	2,077	2,100	2,543

Table 3-17 Points for the dynamic region of the Pressure-Impulse diagrams for standoff distance of 256,800 mm for columns using Concrete Damage REL3 model

		Col. Type A	Col. Type B	Col. Type C	Col. Type D
2% Damage	Impulse (kPa.msec)	26,449	53,474	53,723	60,796
	Pressure (kPa)	495	1,270	1,278	1,512
4% Damage	Impulse (kPa.msec)	34,188	58,826	59,206	69,893
	Pressure (kPa)	694	1,446	1,458	1,827
6% Damage	Impulse (kPa.msec)	44,149	67,149	67,962	79,552
	Pressure (kPa)	979	1,729	1,757	2,180

Table 3-18 Points for the dynamic region of the Pressure-Impulse diagrams for standoff distance of 171,200 mm for columns using Winfrith Concrete model

		Col. Type A	Col. Type B	Col. Type C	Col. Type D
2% Damage	Impulse (kPa.msec)	52,261	68,330	68,271	68,573
	Pressure (kPa)	2,119	3,042	3,039	3,056

Table 3-19 Points for the dynamic region of the Pressure-Impulse diagrams for standoff distance of 256,800 mm for columns using Winfrith Concrete model

		Col. Type A	Col. Type B	Col. Type C	Col. Type D
2% Damage	Impulse (kPa.msec)	71,950	93,732	93,659	95,303
	Pressure (kPa)	1,898	2,705	2,702	2,764

3.3.3. Development of the Quasi-Static Region of the Pressure-Impulse Diagrams

Far field explosions subject structures to pressure waves with duration longer than the natural time period of the structure, and therefore, impose quasi-static loading on the structures. The damage level that a structure experiences at this type of loading can be used to develop the quasi-static region of the Pressure-Impulse diagram. In this region, the damage level is sensitive to the maximum applied pressure rather than the duration of loading as long as the loading duration is longer than the natural time period of the structure.

As discussed in section 3.2.3, the scaled standoff distance should be greater than 3967 mm/kg $^{1/3}$ in order for the loading to be quasi-static. Providing this scaled standoff distance for the damage levels considered in this research requires too heavy charge weights and long standoff distances. As a result of high standoff distances, the duration of simulations increases significantly. Considering the number of required simulations, the computational cost will be very high.

As a result, instead of using the Load_Blast command of LS_DYNA, the reflected pressure is applied directly to the structure by defining a triangular pressure curve and the

surfaces that it applies to. For the triangular pressure curves used, the maximum applied pressure varies for different types of columns and damage levels. However, the duration of the pressure load which should be greater than the natural time period of the structure is kept constant.

The loading can be considered quasi-static if the duration of loading is greater than 6.4 times the natural time period of the structure (Mays and Smith 1995). The natural time period of the columns was calculated as 0.0173 sec in Section 3.2.3. The duration of the blast load is considered to be 0.8 sec to make sure that the simulations generate points in the quasi-static region. Moreover, the rise time for all the pressure curves is at 0.001 sec. Figure 3-8 shows a typical pressure wave time history that is used for the quasi-static loading of the structure.

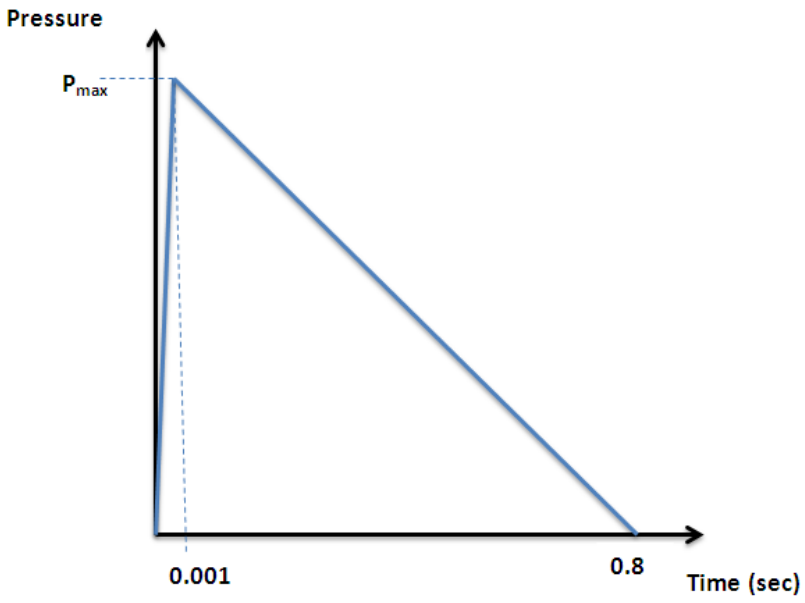

Figure 3-8: Pressure wave time history used for the quasi-static loading of columns

Table 3.20 gives the applied pressure and impulse and the associated damage level for columns using Concrete Damage REL3 material model. As observed, the response of columns using this material model is unexpected because a slight change in the maximum pressure causes a sharp increase in the maximum deflection and the damage level. Since logarithmic scaling is used to draw the Pressure-Impulse diagrams, all the points associated with the desired damage levels of 2%, 4%, and 6% will be too close to be separated on the logarithmic scale.

Table3-20 Damage level of the columns using Concrete Damage REL3 model subjected to pressure loads of far field explosions

					Column Type A		Column Type B		Column Type C		Column Type D	
Shape of Pressure Wave	Max Pressure (MPa)	Load Duration (sec)	Impulse (kPa.msec)	Pressure (kPa)	Displ. at node #9554 (mm)	Damage Level	Displ. at node #9554 (mm)	Damage Level	Displ. at node #9554 (mm)	Damage Level	Displ. at node #9554 (mm)	Damage Level
Triangular	0.57	0.8	228,000	570	5.4	0.16%	-	-	-	-	-	-
Triangular	0.58	0.8	232,000	580	222.4	6.39%	-	-	-	-	-	-
Triangular	0.75	0.8	300,000	750	-	-	-	-	7.82	0.22%	-	-
Triangular	0.78	0.8	312,000	780	-	-	8.25	0.24%	-	-	-	-
Triangular	0.79	0.8	316,000	790	-	-	-	-	-	-	8.34	0.24%
Triangular	0.8	0.8	320,000	800	-	-	253.1	7.27%	230.9	6.64%	176.8	5.08%
Triangular	0.9	0.8	360,000	900	-	-	-	-	-	-	223.6	6.43%

The response of column models using Winfrith Concrete model subjected to pressure loading with duration of 0.8sec and 2.4 sec covers a spectrum of damage levels for different maximum pressures. The unexpected response observed in Concrete Damage RE3 models is not observed in Winfrith Concrete models. Table 3-21 gives damage levels of four types of columns subjected to the pressure waves of far field explosions.

Table 3-21 Damage level of the columns using Winfrith Concrete model subjected to pressure loads of far field explosions

					Column Type A		Column Type B		Column Type C		Column Type D	
Shape of Pressure Wave	Max Pressure (MPa)	Load Duration (sec)	Impulse (kPa.msec)	Pressure (kPa)	Displ. at node #9554 (mm)	Damage Level	Displ. at node #9554 (mm)	Damage Level	Displ. at node #9554 (mm)	Damage Level	Displ. at node #9554 (mm)	Damage Level
Triangular	1.1	0.8	440,000	1,100	68.5	1.97%	-	-	-	-	-	-
Triangular	1.2	0.8	480,000	1,200	85.1	2.45%	-	-	-	-	-	-
Triangular	1.3	0.8	520,000	1,300	-	-	55	1.58%	54.7	1.57%	51.9	1.49%
Triangular	1.4	0.8	560,000	1,400	-	-	86.6	2.49%	78.6	2.26%	70	2.01%
Triangular	1	2.4	1,200,000	1,000	64.1	1.84%	-		-	-	-	-
Triangular	1.1	2.4	1,320,000	1,100	82.8	2.38%	-	-	-	-	-	-
Triangular	1.2	2.4	1,440,000	1,200	-	-	57.2	1.64%	59.2	1.70%	54.2	1.56%
Triangular	1.3	2.4	1,560,000	1,300	-	-	76.1	2.19%	80.8	2.32%	69.6	2.00%

In spite of the unexpected behavior of the Concrete Damage REL3 models, the damage levels of 2%, 4%, and 6% are interpolated using data of Table 3-19. As observed in Table 3-22, the values of pressure and impulse are too close to be drawn on a logarithmic scale. For Winfrith Concrete models, the target damage level of 2% is interpolated. The interpolation results for both material models are given in Tables 3-22 and 3-23.

Table 3-22. Points for the quasi-static region of the Pressure-Impulse diagrams for columns using Concrete Damage REL3 model for pressure loading of 0.8 sec duration

		Col. Type A	Col. Type B	Col. Type C	Col. Type D
2% Damage	Impulse (kPa.msec)	229,181	314,003	305,545	317,454
	Pressure (kPa)	572	785	764	793
4% Damage	Impulse (kPa.msec)	230,465	316,279	311,776	319,107
	Pressure (kPa)	576	791	779	798
6% Damage	Impulse (kPa.msec)	231,749	318,555	318,006	347,259
	Pressure (kPa)	579	796	795	868

Table 3-23. Points for the quasi-static region of the Pressure-Impulse diagrams for columns using Winfrith Concrete model for pressure loading of 0.8 sec duration

		Col. Type A	Col. Type B	Col. Type C	Col. Type D
2% Damage	Impulse (kPa.msec)	442,500	538,462	544,927	559,231
	Pressure (kPa)	1,106	1,346	1,362	1,398

Table 3-24. Points for the quasi-static region of the Pressure-Impulse diagrams for columns using Winfrith Concrete model for pressure loading of 2.4 sec duration

		Col. Type A	Col. Type B	Col. Type C	Col. Type D
2% Damage	Impulse (kPa.msec)	1,235,556	1,518,545	1,498,065	1,560,000
	Pressure (kPa)	1,030	1,265	1,248	1,300

3.3.4. Pressure-Impulse Diagrams

Pressure-Impulse diagrams are generated by combining the results of simulations performed for the impulsive, dynamic, and quasi-static regions. Since models using Concrete Damage REL3 model does not provide a spectrum of damage levels for the quasi-static loading, the results of simulations for the quasi-static loading are not incorporated in the Pressure-Impulse diagrams developed for this type of material model. Figures 3-9 through 3.12 show the Pressure-Impulse diagrams for the four types of columns using Concrete Damage REL3 model.

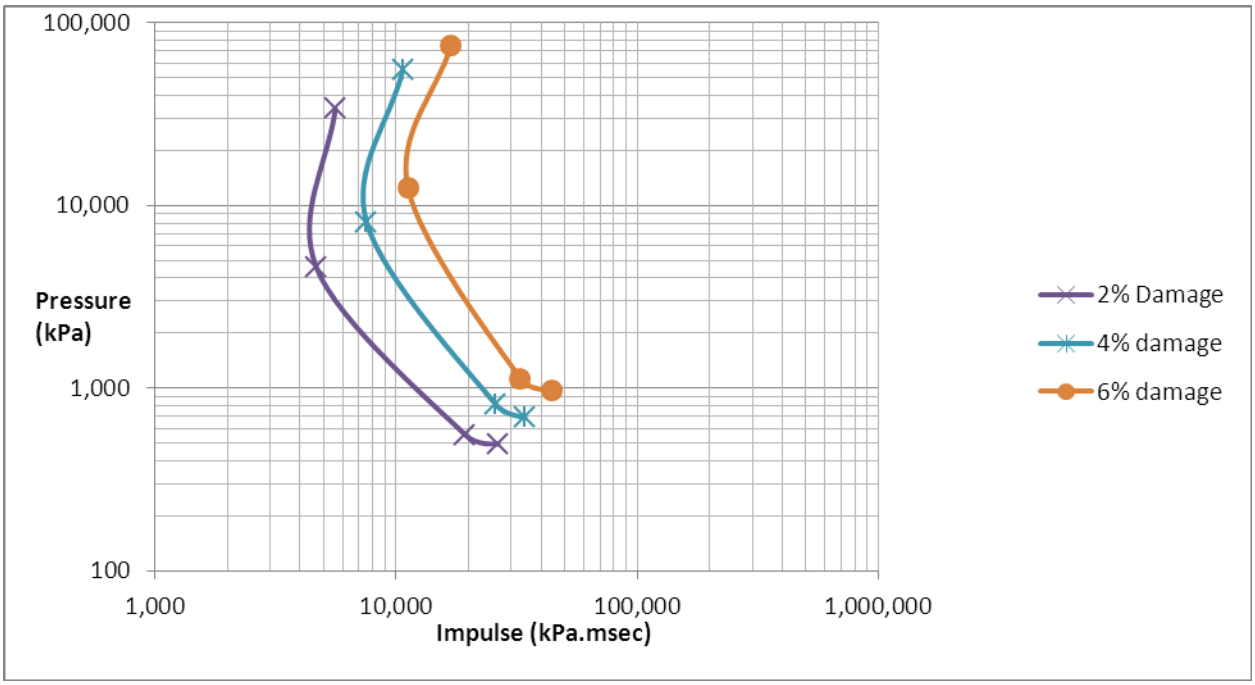

Figure 3-9: Pressure-Impulse diagram for three damage levels of column Type A using Concrete Damage REl3 model

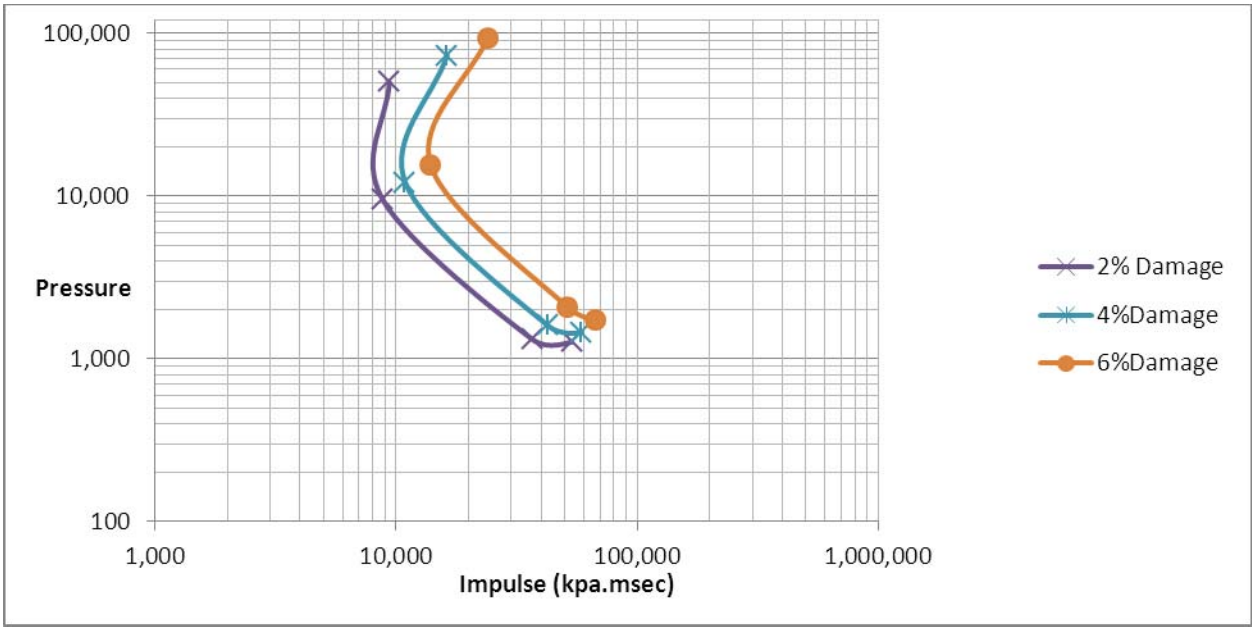

Figure 3-10: Pressure-Impulse diagram for three damage levels of column Type B using Concrete Damage REl3 model

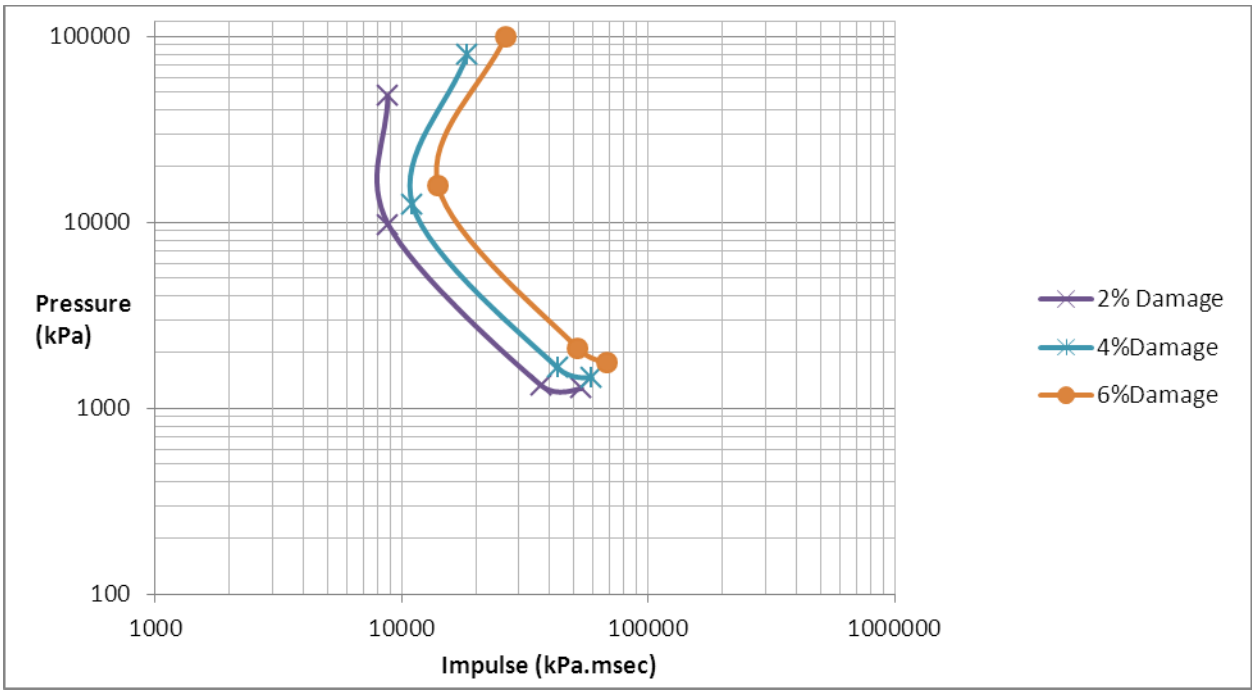

Figure 3-11: Pressure-Impulse diagram for three damage levels of column Type C using Concrete Damage REl3 model

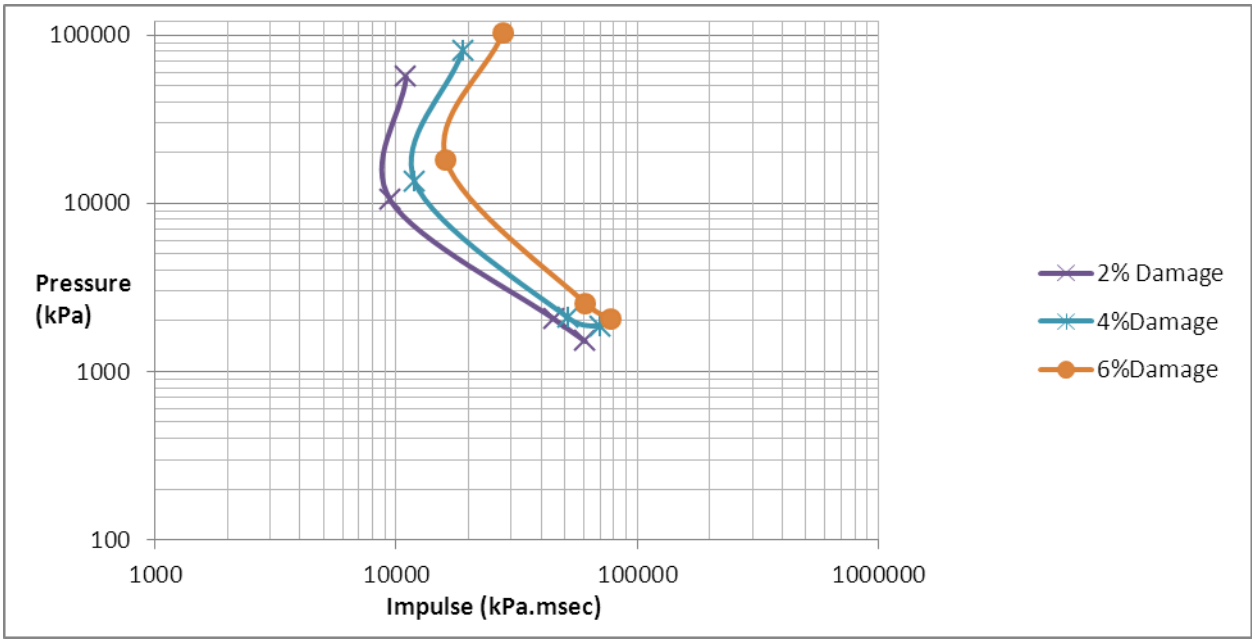

Figure 3-12: Pressure-Impulse diagram for three damage levels of column Type D using Concrete Damage REl3 model

One of the applications of the Pressure-Impulse diagrams is to assess the damage level of a structure under a given explosion. The pressure and impulse of an explosion can be calculated by knowing the standoff distance, the equivalent TNT, and the type of burst, whether it is a surface or an air burst. Once the pressure and impulse are known, the damage level of the structure can be estimated by locating the damage isobar that passes through the point whose coordinate in the Pressure-Impulse diagram is the impulse and pressure of the explosion.

Another application of Pressure-Impulse diagrams is the evaluation of the structural modifications. In this research, the dimension, material, and longitudinal reinforcement of the columns are kept constant while the spacing and the shape of the transverse reinforcement is changed. The performance of different types of columns under various types of loading can be evaluated and compared by generating Pressure-Impulse curves for a specific damage level for all the column types. Figures 3-13 through 3-15 compare the performance of the four types of columns subjected to loading that causes damage levels of 2%, 4%, and 6%. As observed, the Pressure-Impulse curve for column Type A, which has the minimum stirrups compared to other types, falls at the left side of the other types of column. This signifies that column Type A is weaker as it reaches the same damage level as the other types of columns at the lower pressure and impulse values. The change in the shape of stirrups from square to spiral does not have a significant effect on the reduction of damage level as the Pressure-Impulse curves of columns Type B and C are very close. Although the addition of diamond stirrups in column Type D slightly improves the performance in the dynamic and quasi-static regions, the improvement in the impulsive

region is not very significant because the Pressure-Impulse curves of columns Types B and D are very close.

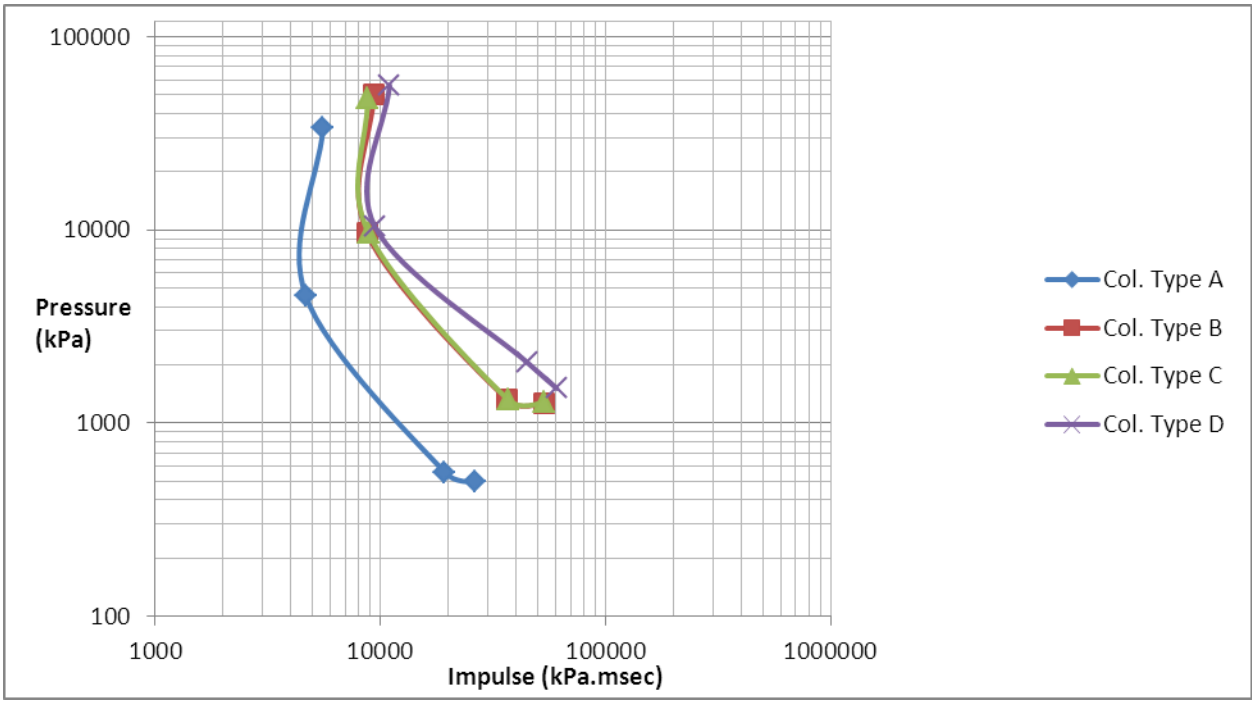

Figure 3-13: 2% damage level Pressure-Impulse curves for the four types of columns using Concrete Damage REL3 model

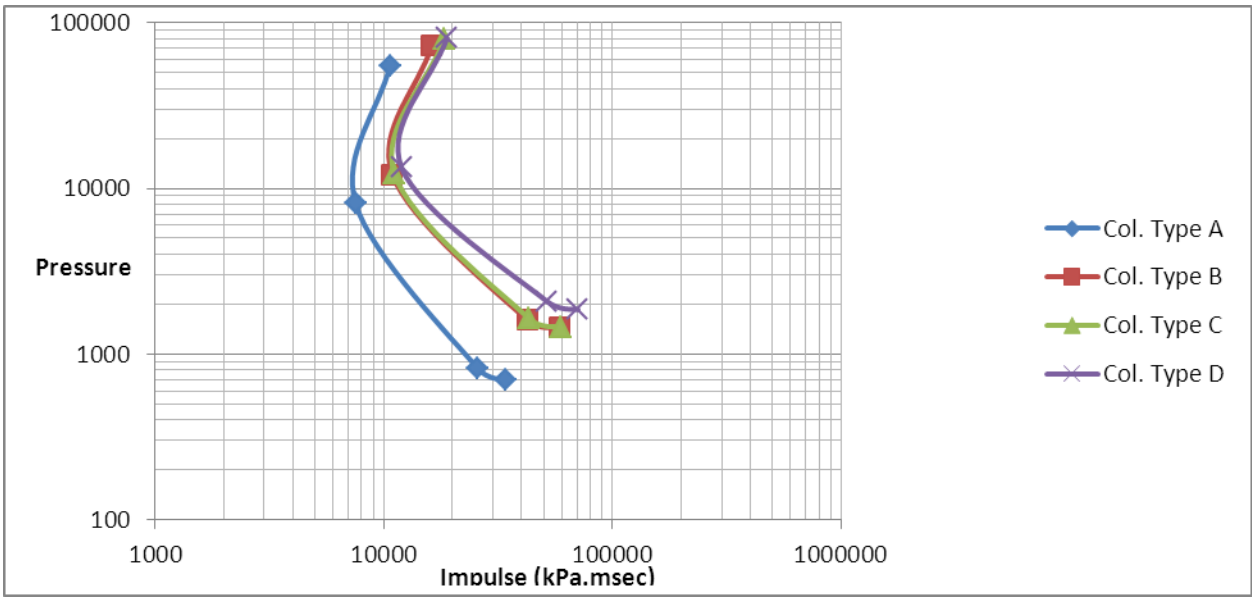

Figure 3-14: 4% damage level Pressure-Impulse curves for the four types of columns using Concrete Damage REL3 model

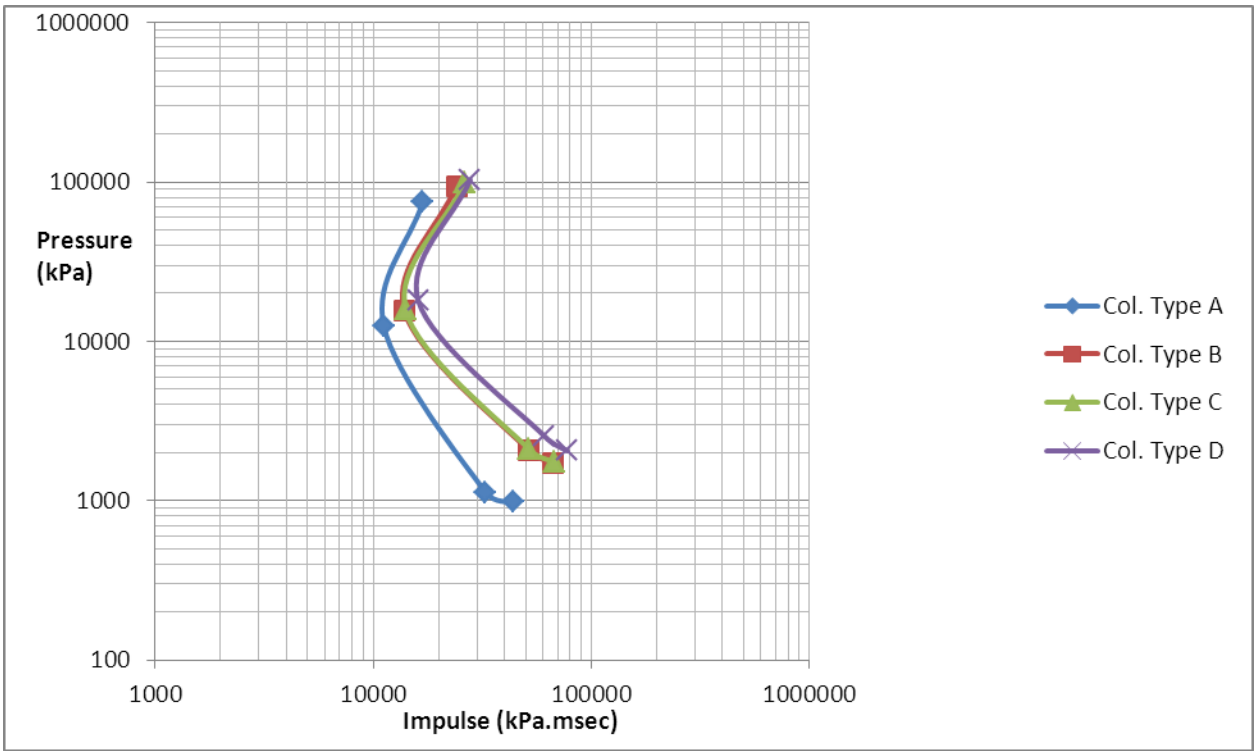

Figure 3-15: 6% damage level Pressure-Impulse curves for the four types of columns using Concrete Damage REL3 model

The Winfrith Concrete material model responded well in the quasi-static region. So, the Pressure-Impulse diagrams for columns using this material model include the quasi-static region as observed in Figure 3-16. However, the pressure and impulse at which the 2% damage is reached is different in models using Winfrith Concrete and Concrete Damage REL3 models although the material properties used in the models are the same. As seen in Figure 3-17, models using Concrete Damage REL3 reach the 2% damage level at lower combinations of pressure and impulse compared to models using Winfrith Concrete model. In addition, models using Concrete Damage REL3 show improvement in structural response as the column type changes from A to D. However,

for models using Winfrith Concrete model, the improvement is not significant at the dynamic and quasi-static regions, and no improvement is observed at the impulsive region.

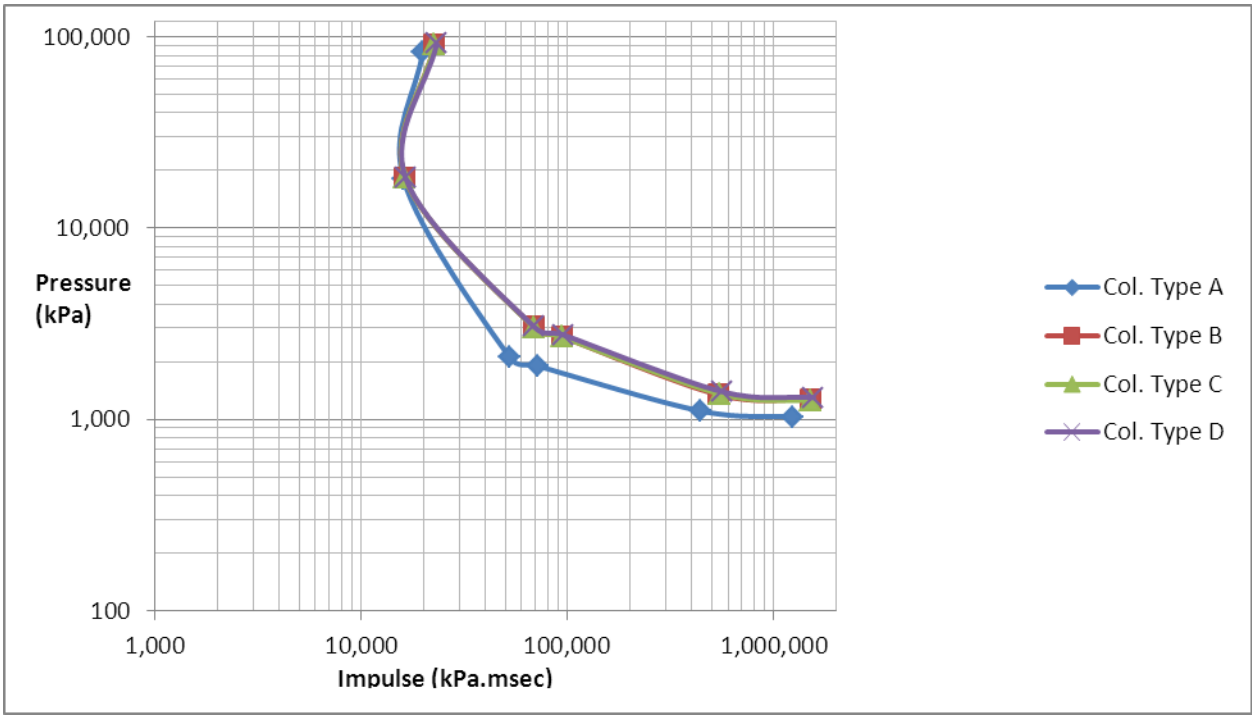

Figure 3-16: 2% damage level Pressure-Impulse curves for the four types of columns using Winfrith Concrete model

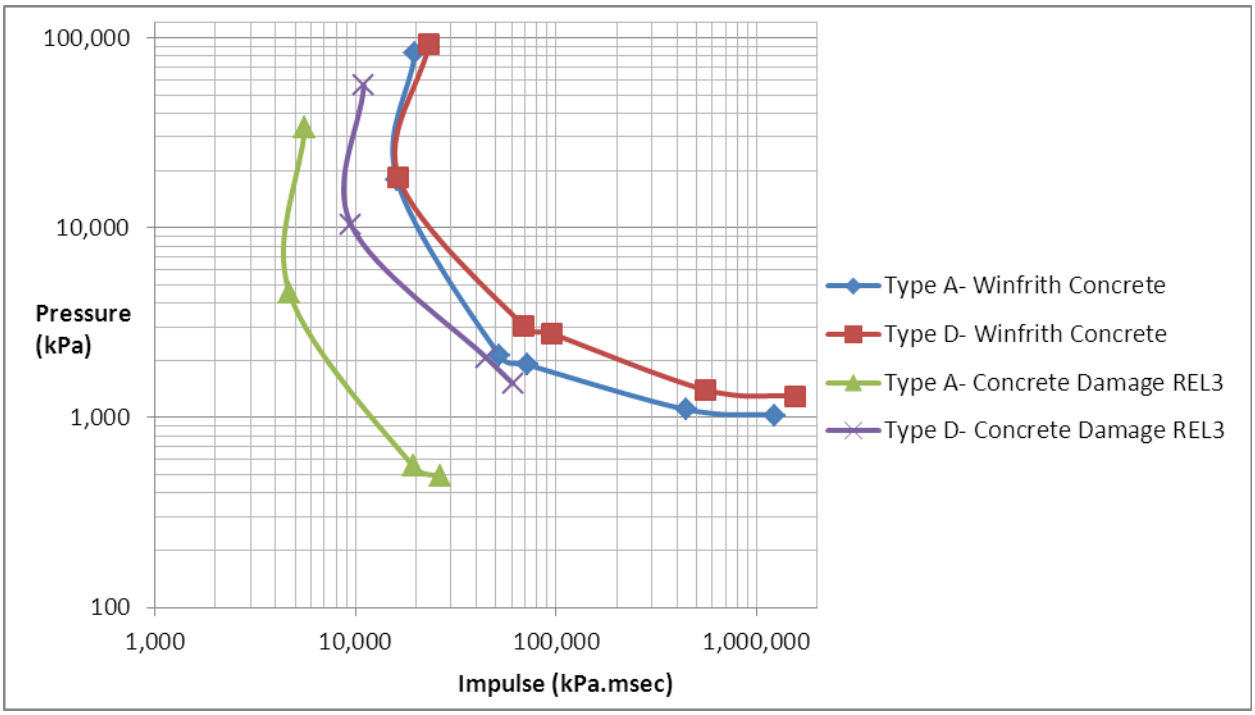

Figure 3-17: A comparison of Pressure-Impulse diagrams developed for models using Winfrith Concrete and Concrete Damage REL3 material models

3.4. Discussion

The impulsive region of the Pressure-Impulse diagrams can be developed by subjecting the columns to close-in explosions. The standoff distances used to generate the impulsive loadings are 1427 mm and 8560 mm and charge weight ranges from 16 to 1900 kg equivalent TNT. Since the explosives are very close to the structure, no wave elongation occurs as the wave travels in the air. This leads to the duration of loading of about 15 milliseconds and consequently, low impulse values. High pressure and low impulse are of characteristics of close-in explosions. For instance, to have 2% damage in near surface close-in explosion with 1427 mm standoff distance in the seismically-detailed column (Type D) using Concrete Damage REL3 material model, the pressure and impulse should be 56,170 kPa and 11,008 kPa.msec respectively. The same column

needs 10,428 kPa and 9459 kPa.msec to experience the same damage level when the standoff distance is 5680 mm, 5 times more than 1427 mm. Although both the pressure and the impulse have decreased in the second standoff distance, the damage level has remained the same. This is an important reason that a Pressure-Impulse diagram is needed to correctly predict the structural response. Another important observation is that at the impulsive region, the damage level is more sensitive to the peak impulse than to the peak pressure. A comparison between the mentioned two blast events shows that while the change in the peak pressure is more significant than the change in the impulse, the column still experiences the same damage level.

The data from near field explosions are used to develop the dynamic region of the Pressure-Impulse diagrams. To have near field explosion, the standoff distances need to be greater than the standoff distances used for the close-in explosion. As a result, the charge weight need to be high enough to cause the same range of damage level experienced in the close-in explosion. The standoff distances used in this research for the near field explosion are 171,200 and 256,800 mm. The charge weight ranges from 350,000 to 5,600,000 kg equivalent TNT. The high amount of charge weight and the standoff distance causes the blast wave to have higher duration and elongates as travels in the air. As a result of high standoff distance, the peak pressure drops significantly; however, the peak impulse increases due to the increased positive phase duration of the blast wave. In this type of loading, the pressure and impulse that causes 2% damage in the column Type need to be 1,749 kPa and 45,130 kPa.msec when the standoff distance is 171,200 mm, and 1512 kPa and 60,796 kPa.msec when the standoff distance increases 1.5 times to 256,800 mm. For 171,200 mm standoff distance, the columns reach 4%

damage level as the pressure and impulse increase to 2,086 kPa and 51,624 kPa.msec. Comparing the pressure and impulse values for the 2% and 4% damage level shows that at the dynamic region, the structure response is sensitive to both the peak pressure and the peak impulse.

To develop the quasi-static part of the Pressure-Impulse diagrams, the structure need to be subjected to the pressure and impulse associated with the far field explosion. In the far field explosion, the duration of the pressure wave increases significantly while the peak pressure drops. The Concrete Damage REL3 material did not responded well to the quasi-static loading. So, this part of the Pressure-Impulse diagram developed for only the models using the Winfrith Concrete model. The two loading cases that caused the 2% damage in column Type D have pressure and impulse values of 1,398 kPa and 559,231 kPa.msec for one loading case and 1,300 kPa and 1,560,000 kPa.msec for the other. A comparison between the two blast loading cases shows that in the quasi-static region of the Pressure-Impulse diagram, the response of the structure is more sensitive to the peak pressure than to the peak impulse because the significant increase in the impulse was counteracted by a very small decrease in the peak pressure for the two blast loading cases which cause 2% damage level.

In addition to the development of the Pressure-Impulse diagrams, the Pressure-Impulse diagrams of four types of columns were also studied to compare the effect of transverse reinforcement ratio and shape on the maximum structural response. Bao and Li (2010) used finite element analysis to study the effect of transverse reinforcement ratio on the damage level of reinforced concrete columns under blast loading. They

showed that the seismically-detailed columns which had more transverse reinforcement experienced less damage compared to conventional columns.

In this research, column Type A represents a conventionally-designed column, and column Type D represents a seismically-detailed column. As seen in Figures 3-18 and 3.19, column Type D is more resistant to explosion than column Type A because the pressure and impulse values at which column Type D reaches each damage level is higher than those for column Type A. This can be explained by considering the fact that the ductility capacity of a column depends on the ratio and distribution of transverse reinforcement within the plastic hinge region. The transverse reinforcement provides confinement for the core concrete and prevents the longitudinal reinforcement from buckling. The combination of providing confinement for core concrete and lateral support for longitudinal reinforcement causes the seismically-detailed columns to withstand higher loads.

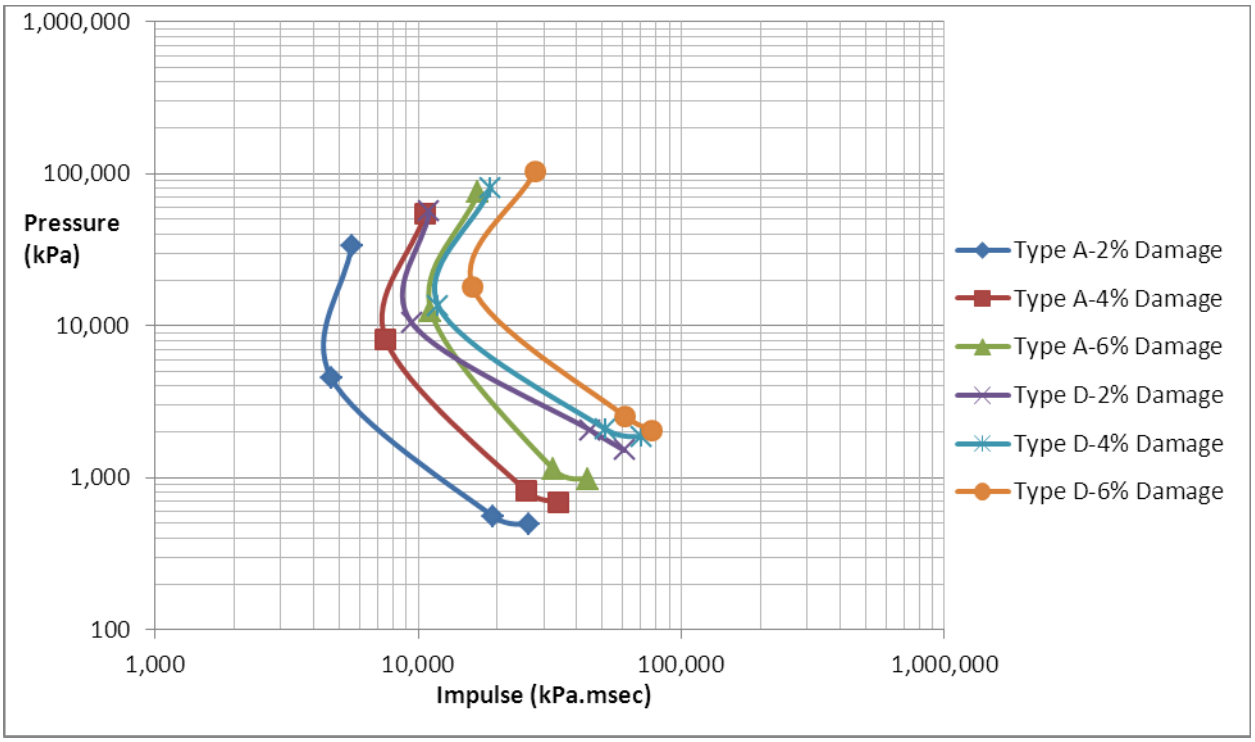

Figure 3-18: Effect of increase in the transverse reinforcement ratio on the damage level of models using Concrete Damage REL3 model

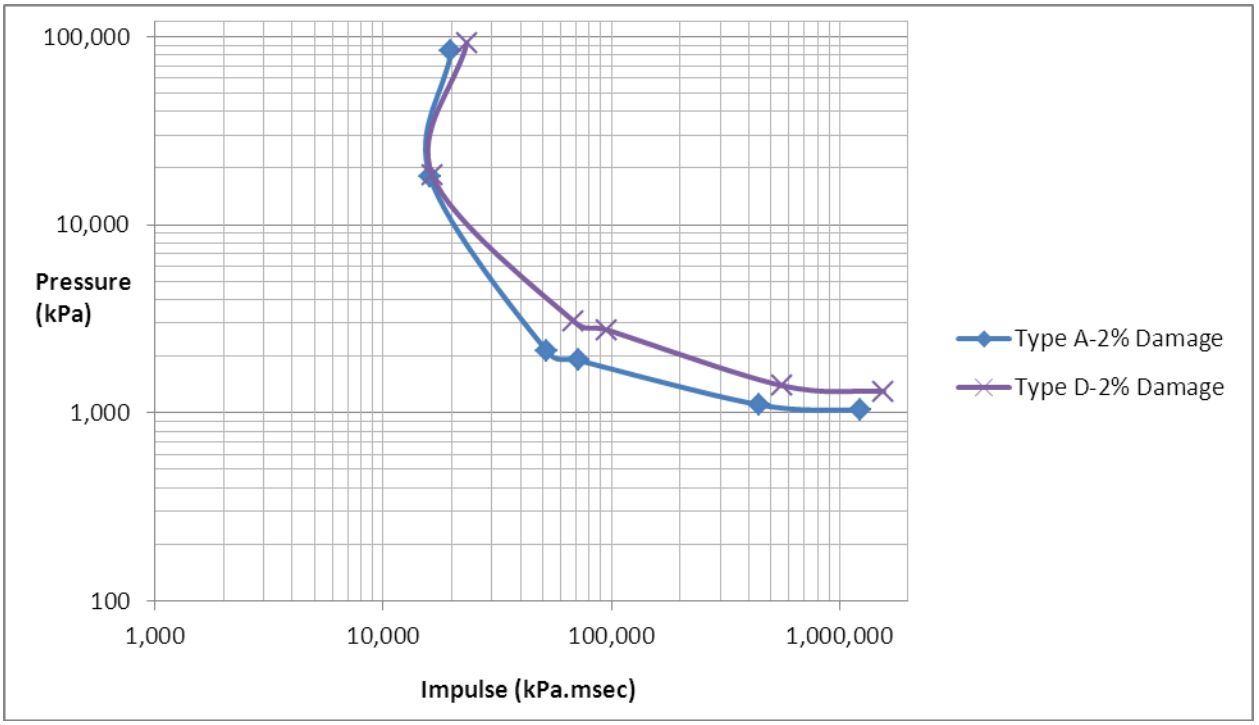

Figure 3-19: Effect of increase in the transverse reinforcement ratio on the damage level of models using Concrete Damage REL3 model

Another observation that can be made from Figures 3-18 and 3-19 is that the difference in performance of column Types A and D is not uniform among the dynamic, impulsive, and quasi-static regions. As observed, the difference in the damage level is lower at the impulsive region. For instance, for models using Concrete Damage REL3 material model, although there is a significant difference between the Pressure-Impulse plots of column Types D for 2% damage and column Type A for 4% damage at the dynamic region, the plots become tangent at the impulsive region. In addition, for models using Winfrith Concrete model, the 2% damage Pressure-Impulse plots of both types of column are very close at the impulsive region. This shows that the change in the transverse reinforcement ratio has improved the performance of columns at both the dynamic and the impulsive regions but the improvement is lower at the impulsive region. This can be explained by considering the fact that the impulsive region is associated with close-in explosions. When the explosives are very close to the structure, the pressure concentration is higher at the location on the structure that has the minimum distance with the explosives. Consequently, in addition to the structural global damage, the structural experiences local damage which adds to the global damage. For this reason, the column with higher transverse reinforcement ratio shows less improvement in the impulsive region.

As observed in Fig 3.17 and discussed in 3.3.4, for the same pressure and impulse values, the damage level experienced by models using Winfrith Concrete material model is lower than those of Concrete Damage REL 3 model. This can be explained by considering the conclusions of Chapter two that Winfrith Concrete material

model generates higher level of strength enhancement when subjected to high strain rates. As a result of strength enhancement, the damage level decreases.

3.5. Conclusions

The following conclusions can be drawn from the study performed on the response of the four types of reinforced concrete columns subjected to blast loading

- Pressure-Impulse diagrams developed by using numerical simulations can be utilized to compare the resistance of different structures to blast loading. Four types of columns whose difference is the ratio and shape of transverse reinforcement are compared. The significant improvement as a result of increasing the ratio of transverse reinforcement is seen through a comparison between columns Type A and D. Column Type A is a conventionally-designed column and column Type D is a seismically-detailed column. The comparison showed that column Type D experienced lower damage level than column Type A. This study illustrates that pressure-impulse diagrams developed by using the results of finite element analysis are capable of capturing the reduction of damage level caused by changes in the ratio and form of transverse reinforcement.
- The improvement in the Pressure-Impulse diagram of the seismically-detailed column is not uniform in the impulsive, dynamic, and quasi-static regions. The change in the transverse reinforcement causes lesser

improvement in the impulsive region. This is explained by considering the fact that in the impulsive region, the column is subjected to close-in explosion and localized very high pressure. As a result, the localized damage in addition to the global damage is experienced by the columns, and consequently, the global damage increases.

CHAPTER 4

CONCLUSIONS AND FUTURE WORK

This research is an attempt to understanding the response of reinforced concrete structures subjected to high strain rates experienced during blast and impact loading. It studies the response of reinforced concrete structures at both the material and structural levels.

4.1. Non-Linear Response of Three Concrete Material Models of LS-DYNA

At the material level, the non-linear response of three concrete material models of LS-DYNA is studied for cylinder structures subjected to intermediate and high strain rates. The concrete material models studied for this project are 1) material type 159 called CSCM Concrete, 2) material type 84 called Winfrith Concrete, and 3) material type 72R3 called Concrete Damage REL3.

4.1.1. Conclusions

Based on the work presented in the second chapter, at intermediate and high strain rates, concrete material models demonstrate strength enhancement. The strength enhancement is affected by two phenomena: the strain rate effect and the lateral inertia confinement effect. The strain rate effect can be either included or excluded from the models

by using the corresponding parameter in the material models. However, the effect of lateral inertia confinement which is a function of the size of the structure cannot be excluded from the simulations.

The strength enhancement due to the strain rate effect depends on the rate of loading. The size of the structure does not affect this type of strength enhancement. The three material models studied in this project generated strength enhancement due to the strain rate effect. The enhancement values are very close for the three material models.

The strength enhancement due to the lateral inertia confinement is a function of both the size of the structure and the rate of loading. The effect of lateral inertia confinement in CSCM Concrete and Winfrith Concrete models increases as the model size and the rate of loading increases. However, for cylinders made of Concrete Damage REL3 material model, only the effect of rate of loading on the lateral inertia confinement is noticeable as the change in the cylinder size does not significantly affect the strength enhancement.

At the intermediate rates of loading of 0.0125, 1, 5, and 10 s^{-1}, the strength enhancement was mainly due to the strain rate effect, and the effect of lateral inertia confinement was not noticeable. The effect of lateral inertia on strength enhancement, as well as the effect of strain rate, was significant at high strain rates of 100, and 200 s^{-1} for all the three material models.

Two references are used in this research for the DIF values of concrete: CEB equations and the values published by Ross et al. (1995). For the smallest cylinder size that used in this research (101.6 x 203.2 mm (4 x 8 in.)), the calculated DIF values for cylinders using CSCM Concrete model are very close to those proposed by the two references. However, for the two other larger cylinders (203.2 x 406.4 mm (8 x 16 in.) and 406.4 x

812.8 mm (16 x 32 in.)) using CSCM Concrete model, the calculated DIF values are close to those proposed by the references only if the strain rate effect is excluded from the simulation.

The calculated DIF values for models using Winfrith Concrete are not in the range of values proposed by the references neither when the strain rate effect is excluded nor when it is included.

The DIF values for models using Concrete Damage REL 3 model are in close approximation with the values proposed by CEB equations and Ross et al. (1995) only if the strain rate effect is excluded from the simulations. The inclusion of the strain rate effect increases the DIF beyond the baseline values.

In reinforced concrete structures, the size of real structures is closer to the largest cylinder studied in this research project. If the DIF values proposed by CEB equations and Ross et al. (1995) are intended to be followed to study the response of structures to impact and blast loading, both CSCM Concrete and Concrete Damage REL3 material models can be used while the strain rate effect is excluded from the simulations.

In addition to strength enhancement, the mesh sensitivity is also studied for the three material models. CSCM Concrete models are more mesh sensitive at low strain rates while Concrete Damage REL3 is mesh sensitive at high strain rates. Winfrith Concrete models show mesh sensitivity at both low and high strain rates.

4.1.2. Future Work

The difference observed in the response of the three concrete material models of LS-DYNA signifies the need for more precise numerical and experimental studies. In this research, for all the three material models, the option of automatic parameter generation of material models was used. For future work, the concentration of study can be on specific material parameters for calibration of the material models with respect to the data from experiments.

4.2 Development of Pressure-Impulse Diagrams for reinforced Concrete Columns and Effect of Confinement on the Damage Level

At the structural level, the non-linear response of reinforced concrete columns subjected to blast is studied by using pressure-impulse diagrams. In this study, by using the result from finite element analysis, the three parts of a pressure-impulse diagram are studied and developed for reinforced concrete columns with four configurations of transverse reinforcement. The effect of confinement is then studied by comparison of the pressure-impulse diagrams developed for the four types of columns.

4.2.1. Conclusions

In the third chapter, Pressure-Impulse diagrams for four types of columns whose distinction is the ratio and form of the transverse reinforcement are developed by using finite element analysis. Based on this study, column Type D which is a seismically-detailed column and has the highest ratio of transverse reinforcement experienced lower damage levels compared to column Type A which is a conventionally-designed column. This study shows that Pressure-Impulse diagrams developed by using finite element analysis are capable of capturing the reduction of damage level caused by changes in the ratio and form of transverse reinforcement.

Each Pressure-Impulse diagram has three regions: impulsive, dynamic, and quasi-static. Although column Type D showed lower damage levels compared to column Type A, the improvement in structural response is not uniform in the all regions of the Pressure-Impulse diagrams. The improvement in the impulsive region is lower than the improvement in the dynamic and quasi-static regions. This is explained by considering the fact that in the impulsive region, the column is subjected to close-in explosion and localized very high pressure. As a result, the localized damage in addition to the global damage is experienced by the columns, and consequently, the global damage increases.

4.2.2. Future Work

The material model used in blast simulations is one of the areas that require more investigation. As discussed in 4.1.2, the calibration of the material model should be

performed using experimental data. In addition to material model parameters, the erosion of material can be included in the models by using an additional command. Inclusion of erosion criterion may increase the accuracy of the results. The criterion and its numerical value need to be selected based on experimental data.

As observed in this research, pressure-impulse diagrams developed based on the results of finite element simulations can illustrate structural improvements due to modifications. In this research, the effect of transverse reinforcement ratio was studied. For future research studies, the effect of aspect ratio, number and area of longitudinal reinforcement, compressive strength of concrete, and axial service loads can be investigated.

REFERENCES

ASCE (1997). Design of Blast Resistant Buildings in Petrochemical Facilities. New York, American Society of Civil Engineers (ASCE).

Bao, X. and Li, B. (2010). "Residual Strength of Blast Damaged Reinforced Concrete Columns." International Journal of Impact Engineering **37**(3): 295-308.

Bischoff, P. and Perry, S. (1991). "Compressive Behaviour of Concrete at High Strain Rates." Materials and Structures **24**(6): 425-450.

Grote, D., Park, S. and Zhou, M. (2001). "Dynamic Behavior of Concrete at High Strain Rates and Pressures: I. Experimental Characterization." International Journal of Impact Engineering **25**(9): 869-886.

Hentz, S., Donze´, F. V. and Daudeville, L. (2004). "Discrete Element Modelling of Concrete Submitted to Dynamic Loading at High Strain Rates." Computers & Structures **82**(29-30): 2509-2524.

Karthaus, W. and Leussink, J. (1983). Dynamic Loading: More Than Just a Dynamic Load Factor. Proceeding of the First International Symposium on the Interaction of Non-Nuclear Munitions with Structures,. Colorado, Prins Maurits Laboratorium Tno Rijswijk (Netherlands)**:** 10-14.

Kotsovos, M. D. (1987). "Consideration of Triaxial Stress Conditions in Design: a Necessity." ACI **84**(3): 8.

Krauthammer, T. (1998). Blast Mitigation Technologies: Developments and Numerical Considerations for Behavior Assessment and Design. International Conference on Structures Under Shock and Impact, SUSI, Computational Mechanics Inc.

Krauthammer, T., Astarlioglu, S., Blasko, J., Soh, T. and Ng, P. (2008). "Pressure-Impulse Diagrams for the Behavior Assessment of Structural Components." International Journal of Impact Engineering **35**(8): 771-783.

Li, Q. and Meng, H. (2002). "Pressure-Impulse Diagram for Blast Loads Based on Dimensional Analysis and Single-Degree-of-Freedom Model." Journal of Engineering Mechanics **128**: 87.

LS-DYNA (2007). LS-DYNA Keyword User's Manual Volume I. California, Livermore Software Technology Corporation**:** 369.

Malvar, L. J. and Crawford, J. E. (1998). Dynamic Increase Factors for Concrete, DTIC Document.

Malvar, L. J., Crawford, J. E., Wesevich, J. W. and Simons, D. (1997). "A Plasticity Concrete Material Model for DYNA 3D." International Journal of Impact Engineering **19**(9-10): 847-873.

Malvern, L., Tang, T., Jenkins, D. and Gong, J. C. (1985). Dynamic Compressive Testing of Concrete. 2'nd Symposium on the Interaction of Non Nuclear Munitions with Structures. Florida, US Department of Defence**:** 194-199.

Mays, G. C. and Smith, P. D., Eds. (1995). Blast Effects on Buildings. London, Thomas Teford.

Murray, Y. D. (2007). Users Manual for LS-DYNA Concrete Material Model 159. Springfield, VA, U.S Department of Transportation**:** 89.

Murray, Y. D., Odeh, A. A. and Bligh, R. (2007). Evaluation of LS-DYNA Concrete Material Model 159, U.S Department of Transportation**:** 206.

Ross, C. A., Tedesco, J. W. and Kuennen, S. T. (1995). "Effects of Strain Rate on Concrete Strength " ACI Material Journal **92**(1): 9.

Rossi, P. (1997). "Strain Rate Effects in Concrete Structures: the LCPC Experience." Materials and structures **30**: 54-62.

Shi, Y., Hao, H. and Li, Z. (2008). "Numerical Derivation of Pressure-Impulse Diagrams for Prediction of RC Column Damage to Blast Loads." International Journal of Impact Engineering **35**(11): 1213-1227.

Smith, S. J., McCann, D. M. and Kamara, M. E. (2009). Blast Resistant Design Guide for Reinforced Concrete Structures. Skokie,Illinois, Portland Cement Association.

Yaramada, V. K. R. (2010). Numerical Response of Steel Reinforced Concrete Slab Subjected to Blast and Pressure Loadings in LSDYNA. M.S, University of Missouri Kansas City.

VITA

Rasekh Rahim Zadeh was born in Booshehr, Iran in 1980. He attended Dr. Shariati high school in Booshehr till the eleventh grade and continued the Pre-university at the private classes of the Baha'i community in Shiraz. He was admitted to the Baha'i Institute for Higher Education (BIHE) for his Bachelor's degree in Civil Engineering. Following graduation in 2002, he joined the oil and gas industry and worked in the civil engineering field for five years.

He joined the University of Missouri-Kansas City in 2009 to pursue his Masters in Civil Engineering with a concentration on Structural Engineering. He was awarded graduate research assistantship from the Civil Engineering Department to study the Non-linear response of reinforced concrete structures subjected to blast loading. In addition to the research assistantship position, he was also awarded graduate teaching assistantship for Reinforced Concrete and Steel Structures Design courses. He is the co-author of a presentation titled *Size and Strain Rate Effect Comparison of Three Concrete Material Models in LS-DYNA* at the ACI conference in Pittsburg, PA in 2010. He also attended the ACI Missouri Chapter seminar in Rolla, MO in 2011 with a poster titled *Non-Linear Response of Reinforced Concrete Structures Subjected to Blast and Impact Loading*.

He is a student member of American Society of Civil Engineers, American Concrete Institute, and the Design Build Institute of America. He holds accreditation as an E.I.T and LEED GA. He plans to utilize his research and educational knowledge and past professional experience in pursuing a career in Structural Engineering.